Development of Supplemental Resistance Method for the Design of Drilled Shaft Rock Sockets

Thomas C. Sandford, Ph.D, P.E - PI
James McCarthy, B.S. E.I.T
Jonathan Bussiere, B.S. E.I.T

Prepared for
The New England Transportation Consortium
March 31, 2011
NETCR83 **Project No. 05-1**

ACKNOWLEDGEMENTS

The following are the members of the Technical Committee that developed the scope of work for the project and provided technical oversight throughout the course of the research:

Michael McDonnell, Connecticut Department of Transportation, Chairperson

Chris Benda, Vermont Agency of Transportation

Robert Burnett, New York State Department of Transportation

Thomas Cleary, New Hampshire Department of Transportation

Peter Connors, Massachusetts Department of Transportation

Leo Fontaine, Connecticut Department of Transportation

Laura Krusinski, Maine Department of Transportation

Michael Sherrill, Rhode Island Department of Transportation

Technical Report Documentation Page

1. Report No.	2. Government Accession No.	3. Recipient's Catalog No.
NETCR83	N/A	N/A

4. Title and Subtitle	5. Report Date
Development of Supplemental Resistance Method for the Design of Drilled Shaft Rock Sockets	March 31, 2011
	6. Performing Organization Code N/A
7. Author(s) Thomas C. Sandford, Ph.D, P.E James McCarthy, E.I.T Jonathan Bussiere, E.I.T	8. Performing Organization Report No. NETCR83
9. Performing Organization Name and Address University of Maine Department of Civil and Environmental Engineering 5711 Boardman Hall Orono, ME 04469	10 Work Unit No. (TRAIS) N/A 11. Contract or Grant No. N/A
12. Sponsoring Agency Name and Address New England Transportation Consortium C/O Advanced Technology & Manufacturing Center University of Massachusetts Dartmouth 151 Martine Street Fall River, MA 02723	13. Type of Report and Period Covered Final Report 14. Sponsoring Agency Code NETC 05-1 A study conducted in cooperation with the U.S. DOT

15 Supplementary Notes

N/A

16. Abstract

Rock Socketed Drilled Shafts have been used on a variety of projects, especially bridges, in areas with bedrock close to the surface. The large loads that these foundation structures can resist make them more practical than alternatives, such as pile groups, in certain situations. However, the current conservative design practices are based on the performance of Rock Socketed Drilled Shafts in soft rock formations. The current design practice often neglects one of the two resisting forces, usually end bearing. In areas, such as New England, with good quality hard rock, Rock Socketed Drilled Shafts have been found to have ultimate capacities 7-25 times the predicted value. The goal of this research is to develop a design method that utilizes the full potential of Rock Socketed Drilled Shafts in hard rock.

A finite element model using constitutive relationships and surface interactions was created to replicate Rock Socketed Drilled Shafts in hard rock. The model was calibrated by duplicating results from five Osterberg load tests on shafts in hard rock. For the purpose of this research hard rock is classified as having an unconfined strength greater than 30 MPa. After calibrating the model, the model was used to show performance of shafts of various sizes founded in rock of two different qualities. The performance results were used to develop a design method for Rock Socketed Drilled Shafts based on allowable top of shaft displacement under loading.

This research revealed that portions of both resistance forces, end bearing and side shear, can be used together in the design of Rock Socketed Drilled Shafts if top of shaft tolerable displacements are considered. This method applies to well cleaned sockets and primarily hard rock. This method can be used with limit equations as well as Osterberg tests.

17. Key Words	18. Distribution Statement
Drilled Shaft, Rock Socket, Service Limit, Finite Element Model	No restrictions. This document is available to the public through the National Technical Information Service, Springfield, Virginia 22161.

19. Security Classif. (of this report)	20. Security Classif. (of this page)	21. No. of Pages	22. Price
Unclassified	Unclassified	186	N/A

Form DOT F 1700.7 (8-72) Reproduction of completed page authorized

SI* (MODERN METRIC) CONVERSION FACTORS

APPROXIMATE CONVERSIONS TO SI UNITS

Symbol	When You Know	Multiply By	To Find	Symbol
		LENGTH		
in	inches	25.4	millimetres	mm
ft	feet	0.305	metres	m
yd	yards	0.914	metres	m
mi	miles	1.61	kilometres	km
		AREA		
in^2	square inches	645.2	millimetres squared	mm^2
ft^2	square feet	0.093	metres squared	m^2
yd^2	square yards	0.836	metres squared	m^2
ac	acres	0.405	hectares	ha
mi^2	square miles	2.59	kilometres squared	km^2
		VOLUME		
fl oz	fluid ounces	29.57	mililitres	mL
gal	gallons	3.785	Litres	L
ft^3	cubic feet	0.028	metres cubed	m^3
yd^3	cubic yards	0.765	metres cubed	m^3

NOTE: Volumes greater than 1000 L shall be shown in m^3

Symbol	When You Know	Multiply By	To Find	Symbol
		MASS		
oz	ounces	28.35	grams	g
lb	pounds	0.454	kilograms	kg
T	short tons (2000 lb)	0.907	megagrams	Mg
		TEMPERATURE (exact)		
°F	Fahrenheit temperature	5(F-32)/9	Celcius temperature	°C

* SI is the symbol for the International System of Measurement

APPROXIMATE CONVERSIONS TO SI UNITS

Symbol	When You Know	Multiply By	To Find	Symbol
		LENGTH		
mm	millimetres	0.039	inches	in
m	metres	3.28	feet	ft
m	metres	1.09	yards	yd
km	kilometres	0.621	miles	mi
		AREA		
mm^2	millimetres squared	0.0016	square inches	in^2
m^2	metres squared	10.764	square feet	ft^2
ha	hectares	2.47	acres	ac
km^2	kilometres squared	0.386	square miles	mi^2
		VOLUME		
mL	millilitres	0.034	fluid ounces	fl oz
L	litres	0.264	gallons	gal
m^3	metres cubed	35.315	cubic feet	ft^3
m^3	metres cubed	1.308	cubic yards	yd^3
		MASS		
g	grams	0.035	ounces	oz
kg	kilograms	2.205	pounds	lb
Mg	megagrams	1.102	short tons (2000 lb)	T
		TEMPERATURE (exact)		
°C	Celcius temperature	1.8C+32	Fahrenheit temperature	°F

°F

°F 32 98.6 212

-40 0 40 80 120 180 200

-40 -20 0 20 40 60 80 100

°C 37 °C

ABSTRACT

Rock Socketed Drilled Shafts have been used on a variety of projects, especially bridges, in areas with bedrock close to the surface. The large loads that these foundation structures can resist make them more practical than alternatives, such as pile groups, in certain situations. However, the current conservative design practices are based on the performance of Rock Socketed Drilled Shafts in soft rock formations. The current design practice for axial capacity often neglects one of the two resisting forces, usually end bearing. In areas, such as New England, with good quality hard rock, Rock Socketed Drilled Shafts have been found to have ultimate axial capacities 7-25 times the predicted value. The goal of this research is to develop a design method that utilizes the full potential of Rock Socketed Drilled Shafts in hard rock.

A finite element model using constitutive relationships and surface interactions was created to replicate Rock Socketed Drilled Shafts in hard rock. The model was calibrated by duplicating results from five Osterberg load tests on shafts in hard rock. For the purpose of this research hard rock is classified as having an unconfined strength greater than 30 MPa. After calibrating the model, the model was used to show performance of shafts of various sizes founded in rock of two different qualities. The performance results were used to develop a design method for Rock Socketed Drilled Shafts based on service limit criteria.

This research revealed that portions of both resistance forces, end bearing and side shear, can be used together in the design of Rock Socketed Drilled Shafts if service limit state criteria are considered. This method applies to well cleaned sockets and primarily hard rock. This method can be used with equations for nominal resistance as well as Osterberg tests.

TABLE OF CONTENTS

List of Tables

List of Figures

List of Symbols and Abbreviations

Symbol	Meaning
AASHTO	American Association of State Highway and Transportation Officials
A_g	Gross Area of Section
A_p	Area of Shaft Tip
A_s	Area of Shaft Side Surface
ASD	Allowable Stress Design
A_{st}	Total Area of Longitudinal Reinforcement
CAX4R	Four Sided Four Node Bilinear Axisymmetric Stress Elements
COHAX4	Four Node Axisymmetric Interface Elements
c	Cohesion
c_r	Mass Cohesion of the Rock
c_s	Spacing of Discontinuities
D	Shaft Diameter
d	Shaft Depth
E	Elastic Modulus
E_i	Intact Young's Modulus
E_m	Mass Young's Modulus
f	Sides Shear
f'_c	Concrete Compressive Strength
FHWA	Federal Highway Administration

f_y	Specific Yield Strength of Reinforcement
LRFD	Load Resistance Factor Design
L_s	Length of Shaft
m	Fractured Rock Mass Parameter
NETC	New England Transportation Consortium
O-Cell	Osterberg Cell
P	Load
p_a	Atmospheric Pressure
P_n	Nominal Axial Resistance
RMR	Rock Mass Rating
R_n	Nominal Resistance of Shaft
R_p	Nominal Shaft Tip Resistance
RQD	Rock Quality Designation
R_R	Nominal Factored Resistance of Shaft
R_s	Nominal Shaft Side Resistance
s	Fractured Rock Mass Parameter
s_u	Undrained Shear Strength
t	Thickness of Discontinuities
q_m	Mass Uniaxial Strength
q_p	Unit Tip Resistance
q_s	Unit Side Resistance

q_u	Uniaxial Compressive Strength
q_{ult}	Ultimate Bearing Capacity
q_{ui}	Intact Uniaxial Strength
w	Settlement
α_E	Reduction Factor to Account for Jointing in Rock
ϕ	Friction Angle
ϕ_{qp}	Resistance Factor for Tip Resistance
ϕ_{qs}	Resistance Factor for Shaft Side Resistance
υ	Poisson's Ratio
ρ	Density
Ψ	Dilation Angle

Chapter One

Introduction

1.1 Background

Rock Socketed Drilled Shafts are a foundation type that are created by boring out a vertical hole into bedrock and the overlying soil and then backfilling the opening with concrete and rebar for the purpose of resisting loads. Rock Socketed Drilled Shafts rely on two resistance forces, side shear and end bearing, to oppose axial loads (Turner, 2006). When the shaft is loaded, side shear is then enabled immediately along the rock-concrete interface from the top down. Side shear increases rapidly until it reaches a maximum which is believed to occur around deformations of 5-10 mm (0.2 -0.4 inches). End bearing is not enabled until sufficient loads have been applied to constitute deformations in lower reaches of the shaft. Because ultimate side shear and end bearing resistances are mobilized at different deformations the two components cannot be simply summed to obtain the shaft's capacity (Sagong et al, 2007). For this reason the estimated amount of either side shear or end bearing that is activated at certain loads is hard to quantify because it depends on different shaft dimensions and rock properties.

The current design procedures for Rock Socketed Drilled Shafts depend on values obtained during routine subsurface explorations. Drilling is performed, and rock cores are taken to determine the depth of bedrock at that particular site and the properties of the rock, such as uniaxial compressive strength (q_u), Elastic Modulus (E), Poisson's Ratio (υ), jointing, and degree of weathering (Turner, 2006). Presently, Rock Socketed Drilled Shafts are designed conservatively. Full scale load test results have shown that the axial capacity of Drilled Shafts is often much higher than anticipated, especially in hard rock. Hard rock will be characterized as rock that has a uniaxial unconfined compressive strength of 30 MPa (4,340 psi). When the surrounding rock is stronger than the concrete, the failure at the rock-concrete interface is controlled by the concrete or by the strength along the interface.

Full scale tests on Rock Socketed Drilled Shafts can be performed with the use of Osterberg cells or O-Cells. O-Cells are loading devices that allow full scale load tests to be performed on shafts without compromising the structural integrity of the shaft (Osterberg, 1998). To perform an O-Cell test, a hydraulic loading piston is placed at the base of the shaft along with proper instrumentation to monitor deformations and loading pressures. The concrete shaft is then cast, and proper time is allotted for the concrete to set. When the O-Cell piston is pressurized, it applies load to both the shaft and the underlying rock. With deformation and load results for both the side shear and the end bearing of the socket, nominal resistances can be estimated that depend on the dimensions of the socket. The O-Cell test is useful because it eliminates the need for an excessive overhead reaction system that would load from the top. O-Cell tests also provide separate results for both side shear and end bearing which can be valuable when designing production shafts (Turner, 2006; Osterberg, 1998).

There are a number of reasons why Rock Socketed Drilled Shafts have been conservatively designed. One of these is uncertainty regarding construction of the shafts. Most of the drilled shafts that have been constructed in the past were done properly; however, a select few have been constructed poorly. This resulted in shafts that failed during load tests, and thus failures have forced engineers to become more conservative in their design (O'Neill & Hassan, 1994; O'Neill, 1999; O'Neill, 2005; Osterberg, 1999; Schmertmann & Hayes, 1997; and Schmertmann et al, 1988). The AASHTO code recommends that engineers use only one resistance force (side shear or end bearing) in calculating the nominal resistances of a Rock

Socketed Drilled Shaft. This method completely ignores the other contributing resistance and results in much larger and more costly Rock Socketed Drilled Shafts.

The common practices used today for Rock Socketed Drilled Shaft design result in resistance factors much lower than 0.50. Many load tests, most notable O-Cell tests, have shown that Rock Socketed Drilled Shafts design resistances have been underestimated by as much as 2500%. This is especially true in hard, unweathered rock where the ratio of tested ultimate capacity to predicted ultimate capacity ranges from 7 to 25 (Schmertmann & Hayes, 1997).

1.2 Research Objective

The objective of the research was to produce a robust and easy-to-use drilled shaft design method for hard rock that incorporated both end bearing and side shear. The method was to be based on O-Cell load tests and a calibrated finite element model. The model was to address rock properties and shaft geometries not covered by the load tests, as well as top-down loading not covered by the load tests. The research was to be accomplished in three phases.

Phase I:

a. Review of pertinent literature on the behavior of Rock Socketed Drilled Shafts and current modeling techniques, especially in hard rock.

Phase II:

a. Use finite element modeling software to create a model of a typical Rock Socketed Drilled Shaft. Include rock properties similar to hard rock, common shaft dimensions, and representative concrete rock interfaces.
b. Develop a method to load the model similar to that of the O-Cell.
c. Validate the model by comparing finite element results against O-Cell results from

the field.

Phase III:

a. Utilize the model calibrated in Phase II by determining response with different dimensions and rock properties that fill in gaps in available field data.

b. Using field data and finite element results, provide design recommendations for Rock Socketed Drilled Shafts in hard rock. This will include the amount of side shear and end bearing that is mobilized at service limit and strength limit states for shaft of different dimensions founded in hard rock with different properties.

1.3 Organization of this Report

Chapter Two contains a literary review of pertinent information regarding Rock Socketed Drilled Shafts. Important topics include design of shafts, full scale testing on test shafts, and the resistance mechanisms of shafts to axial loads. Chapter Three contains information on the finite element model created using the commercial program ABAQUS. Details on model construction and methods utilized are covered. Calibration is documented in Chapter Four for the model described in Chapter Three. To calibrate the model, results of the model were compared to O-Cell test results that have been completed throughout New England in hard rock. Chapter Five contains the design method incorporating side shear and end bearing. A parametric study was conducted using the calibrated model to find the responses for shafts with different lengths, widths, and rock properties A summary of all research findings, conclusions, and recommendations is provided in Chapter Six.

Chapter Two

Review of Relevant Literature

In today's world, structures are getting larger and larger. Some of these large structures have begun to push the limits of conventional foundation types, such as driven piles. Now more than ever it is the focus of engineers to match foundation types to particular job conditions, where as in the past, projects were designed more on previous experiences. This has lead engineers to experiment with drilled shafts that extend down into bedrock, allowing for more capacity than simply founding the structure on top of rock. Unfortunately, excavation in rock can be expensive compared to excavation in soil, and costs increase as the strength of the rock mass increases. Current design guidelines for Rock Socketed Drilled Shafts provide little economical relief on project investors, because they tend to be conservative especially in harder rock masses. The guidelines are based on limited resources and test data, thus they do not apply well to all drilled shaft applications (Turner, 2006).

Rock Socketed Drilled Shafts are being used as support for superstructures with large vertical and horizontal loads, such as long span bridges. These loads are transferred to the surrounding rock via side shear along the sides of the shaft and by base resistance in the form of bearing capacity at the base of the shafts (Sagong et al, 2007). Because of the limited information associated with Rock Socketed Drilled Shafts and complications involved with proper inspection of shafts, it has lead many engineers to design shafts based on either side resistance or base resistance. For example the 2006 AASHTO *LRFD Bridge Design Specifications* state "Design based on side-wall shear alone should be considered for cases in which the drilled hole cannot be cleaned and inspected or where it is determined that large movements of the shaft would be required to mobilize resistance in end bearing" (Turner, 2006).

This literature review will cover current practices involving Rock Socketed Drilled Shafts. Topics of interest consist of current design practices, construction of shafts, testing methods, nominal side resistance and bearing capacity, and current modeling of drilled shafts. This information should facilitate the construction of a finite element model that will reproduce the action of full-scale Rock Socketed Drilled Shafts in hard rock and assist in improving current design guidelines.

2.1 Current Design Guidelines

The nominal axial compression resistance of a drilled shaft comes from both side shear and end bearing. These two resistance components are the response of the shaft in coordination with foundation displacement. It is unlikely that the value of both resistance components will reach maximums at the same displacement. AASHTO (2007) indicates that the axial compression load on a shaft socketed into rock is carried solely in side shear until a total shaft movement on the order of 10 mm (4/10 inch) occurs (AASHTO, 2007). The following summarizes the current design guidelines from AASHTO (2007).

$$R_R = \phi R_n = \phi_{qp} R_p + \phi_{qs} R_s \qquad \text{(Equation 2.1)}$$

$$R_p = q_p A_p \qquad \text{(Equation 2.2)}$$

$$R_s = q_s As \qquad \text{(Equation 2.3)}$$

R_R = nominal factored resistance of shaft, N (lb)

R_n = nominal resistance of shaft, N (lb)

R_p = nominal shaft tip resistance, N (lb)

R_s = nominal shaft side resistance, N (lb)

ϕ_{qp} = resistance factor for tip resistance

ϕ_{qs} = resistance factor for shaft side resistance

q_p = unit tip resistance, MPa (psi)

q_s = unit side resistance, MPa (psi)

A_p = area of shaft tip, mm^2 ($inch^2$)

A_s = area of shaft side surface, mm^2 ($inch^2$)

(AASHTO, 2007)

Calculating the area for each contributing resistance is straight forward. The base area is generally a circle while the side area is calculated by multiplying the circumference of the shaft by the shaft depth. Determining the unit tip and side resistance in not as easy and generally depends on a number of rock properties.

2.1.1 End Bearing Resistance

Rock Socketed Drilled Shafts utilize end bearing at the base of the shaft in order to resist applied axial loads. However, end bearing is often underestimated or even overlooked completely by designers and engineers based on poor rock conditions or as a precaution towards poor construction methods. In any case the practice of underestimating or completely ignoring the end bearing of Rock Socketed Drilled Shafts often leads to over-designed shafts that are uneconomical (Turner, 2006). A method to estimate nominal end bearing capacity derived from bearing capacity theory is given in Equation 2.4.

$$q_p = 2.5q_u \qquad \text{(Equation 2.4)}$$

q_p = unit tip resistance, MPa (psi)

q_u = unconfined compressive strength of rock, MPa (psi)

Equation 2.4 only applies to intact rock. Intact rock is rarely encountered in the field and thus a reduction of the unit base resistance needs to be made for discontinuities. When the rock is jointed, Equation 2.5 applies to unit base resistance. Equation 2.5 uses the fractured rock mass parameters s and m. These parameters can be related to the rock mass rating (RMR) or Geomechanics Classification (GSI) of the rock (Turner, 2006).

$$q_p = [\sqrt{s} + (m * \sqrt{s} + s)^{1/2}] * q_u \qquad \text{(Equation 2.5)}$$

s, m = fractured rock mass parameters

q_p = unit tip resistance, MPa (psi)

q_u = uniaxial compressive strength of rock, MPa (psi)

(AASHTO, 2007)

For bearing capacity in rock masses where jointing is generally horizontal and discontinuities are spaced no closer than 0.3 m (12 in), the following equation, proposed by the Canadian Geotechnical Society (CGS, 1985), can be used to predict the nominal end bearing resistance of an axially loaded rock socket.

$$q_{ult} = 3d\left[\frac{3 + \frac{c_s}{D}}{10 * \left(1 + \frac{300t}{c_s}\right)^{0.5}}\right] q_u \qquad \text{(Equation 2.6)}$$

$d = 1 + 0.4\, L_s/D$

Where q_u is the lesser of the values of the uniaxial compressive strength of the rock or concrete, D is the base diameter; c_s is spacing of discontinuities in the same units as D; t is the thickness of discontinuities in the same units as D and c_s; L_s is the depth of the socket. It is suggested that Equation 2.6 be applied only for t < 5 mm (0.2 inch), or t < 25 mm (1 inch) if discontinuities are filled with soil or rock debris (Reese & O'Neill, 1987).

Table 2.1 Fractured Rock Mass Parameters s & m (after AASHTO, 2007)

Rock Quality	Constants	Rock Type A = Carbonate rocks with well developed crystal cleavage – *dolomite, limestone, and marble* B = Lithified argillaceous rocks – *mudstone, siltstone, shale, and slate* C = Arenaceous rocks with strong crystals and poorly developed crystal cleavage – *sandstone, and quartzite* D = Fine grained polymineralic igneous crystalline rocks – *andesite, dolerite, diabase, and rhyolite* E = Coarse grained polyminerallic igneous & metamorphic crystalline rocks – *amphibolites, gabbro gneiss, granite, norite, quartz-diorite*				
		A	B	C	D	E
Intact Rock Samples RMR =100	m s	7.00 1.00	10.00 1.00	15.00 1.00	17.00 1.00	25.00 1.00
Very Good Quality Rock Mass RMR = 85	m s	2.40 0.082	3.43 0.082	5.14 0.082	5.82 0.082	8.567 0.082
Good Quality Rock Mass RMR = 65	m s	0.575 0.00293	0.821 0.00293	1.231 0.00293	1.395 0.00293	2.052 0.00293
Fair Quality Rock Mass RMR = 44	m s	0.128 0.00009	0.183 0.00009	0.275 0.00009	0.311 0.00009	0.458 0.00009
Poor Quality Rock Mass RMR = 23	m s	0.029 3.0×10^{-6}	0.041 3.0×10^{-6}	0.061 3.0×10^{-6}	0.069 3.0×10^{-6}	0.102 3.0×10^{-6}
Very Poor Quality Rock Mass RMR = 3	m s	0.007 1.0×10^{-7}	0.010 1.0×10^{-7}	0.015 1.0×10^{-7}	0.017 1.0×10^{-7}	0.025 1.0×10^{-7}

2.1.2 Side Shear Resistance

AASHTO (2007) recommends the following expression for determining nominal side shear resistance of a Rock Socketed Drilled Shaft.

$$q_s = 0.65 * \alpha_E * p_a * (q_u / p_a)^{0.5} < 7.8 * p_a * (f'_c / p_a)^{0.5} \qquad \text{(Equation 2.7)}$$

q_s = unit shear resistance, MPa (psi)

q_u = uniaxial compressive strength of rock, MPa (psi)

p_a = atmospheric pressure (= 0.101 MPa = 14.6 psi)

α_E = reduction factor to account for jointing in rock (Table 2.2)

f'_c = concrete compressive strength, MPa (psi)

Table 2.2 Estimation of α_E (AASHTO, 2007)

E_m[1] / E_i[2]	α_E
1.00	1.00
0.50	0.80
0.30	0.70
0.10	0.55
0.05	0.45

1. Elastic Modulus of rock mass 2. Elastic Modulus of intact rock

2.1.3 Combination of Side Shear and End Bearing

When combining side shear and end bearing capacities, designers need to be careful because the two different components need to be evaluated at a common axial displacement. As has already been mentioned the two different components do not mobilize at similar displacements, and maximum resistance values for each are not generally mobilized at the same displacement. In order to evaluate combined side friction and end bearing the construction of a load-vertical deformation curve is suggested (AASHTO, 2007).

2.2 Issues with Current Design Guidelines in "Hard Rock"

When Rock Socketed Drilled Shafts are loaded, they mobilize both side shear and end bearing to resist axial loads. However, the contribution of each component at loads below the failure load is relatively unknown and varies depending on shaft geometry. For this reason the AASHTO code recommends using only one resisting force component (side shear or end bearing) when determining a nominal capacity. This approach completely ignores the contribution of the other resisting component and results in an overly conservative design. The states of Maine, Massachusetts, New Hampshire, and New Jersey all reported using only one resisting component while designing Rock Socketed Drilled shaft in their respective states (Turner, 2006). At the time of the survey the only two drilled shaft projects in Maine were the Bath-Woolwich Bridge and the Hancock-Sullivan Bridge. The Bath and Hancock projects were both in hard rock, and the design approach showed that engineers were reluctant to be less conservative with their design despite having hard rock. Both Bath and Hancock shafts were used in model calibration in Chapter Four.

Design guidelines for drilled shafts in rock are not necessarily site specific. That is to say there are not different guidelines for hard rock or weak rock. The current guidelines are based on the majority of shafts, which are constructed in areas with weaker rock formations. Thus the adoption of methods from areas with different and possible weaker rock formations to the Northeast may be misleading and costly. To completely ignore one resisting force, primarily bearing capacity, may be applicable in some areas with weak rock formations, but in areas with hard rock it appears to be conservative. A study by Schmertmann and Hayes (1997) revealed that drilled shafts in weak rock and hard soils were designed well as shown in Figure 2.1. The anticipated shaft strength was often close to the tested strength. However, hard rock shafts had 5 to 15 times more capacity than anticipated by design methods.

2.3 Construction Process

The construction process of a drilled shaft can be as important to the capacity or more important than any other procedure that takes place during the planning and design phase. If shafts are not drilled properly or if concrete is not placed correctly, the structural integrity of the shaft could be affected resulting in less than adequate capacity. To ensure that shafts are constructed properly, it requires a firm knowledge of subsurface conditions, a competent contractor with appropriate equipment, proper inspection of the socket prior to the placement of concrete, and a feasible design.

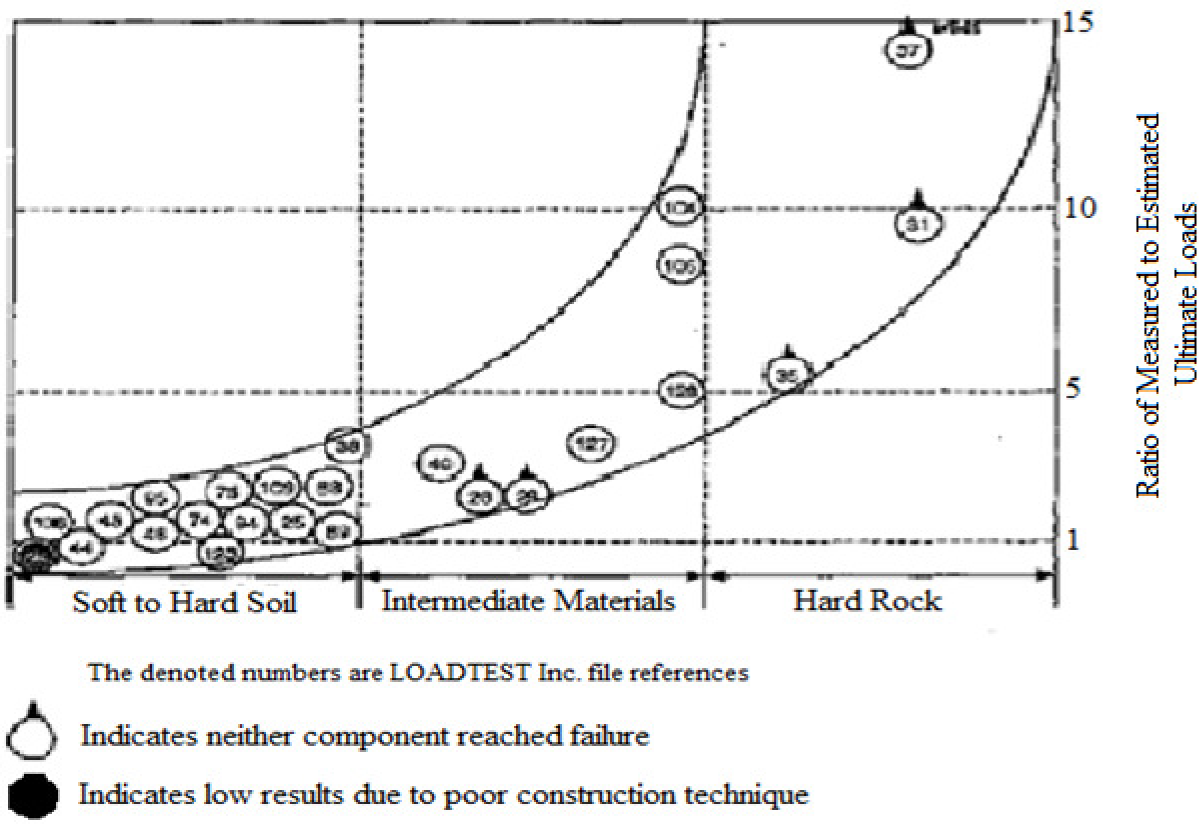

Figure 2.1 Plot of Measured vs. Estimated Ultimate Axial Capacity of Drilled Shafts in Soil and Rock (after Schmertmann & Hayes, 1997)

According to Turner (2006) the two preferred methods for rock excavation are auger type drills and core barrels as shown in Figure 2.2 (Turner, 2006). These drills need to be much more powerful and provide more torque than equipment used to excavate soil. Thanks to recent advances in machinery, rock excavation has become a far easier task than it was in years past. Auger drills are generally used in softer rocks, which have an upper compressive strength limit of about 48 MPa (7000 psi). If auger drills are used in any harder rock, drillers often come across problems with auger teeth wearing out too quickly. Augers are ineffective in harder rock because the drill chews up the entire rock mass that is excavated by means of teeth mounted on the base. However, auger drills with self-rotating bits have been reported to have penetrated rock with strength upwards of 100 MPa (15,000 psi). More commonly in hard rock, core barrels are used because only a small amount of rock needs to be cored around the sides of the rock mass. The rest of the mass is removed as a whole or in pieces. The base of the core may become free from the rest of the mass when a horizontal fracture is encountered. If no fractures are present near the anticipated base of the shaft, a rock chisel is often used to pry the rock core free. If rock is too strong for even core barrels, the alternative is often downhole hammers, which utilize individually operated button bits driven by compressed air (Turner, 2006)

Figure 2.2 Auger Drill (left) and Core Barrel (right) (Turner, 2006)

Wet excavation is also used in some cases of rock excavation. Wet excavation uses either water or a slurry during the drilling process. Wet excavation has a number of advantages that make it appealing for use in the drilling process. The water or slurry helps to stabilize the adjacent soil by counteracting the groundwater pressures and eliminates the need for casing in some situations. It also lubricates the cutting equipment and assists in removal of debris with the use of circulating pumps (O'Neill & Reese, 1999). Unfortunately wet excavation does not come without its disadvantages. There are concerns about the thin layer of mud film made up of fine rock cuttings that stick to the sides of the shaft after drilling is complete. This film can deter bonding between the concrete and rock, thus bringing down the overall capacity of the shaft (Turner, 2006). The effect a film layer has on the shaft capacity depends on the ability of the contractor to properly clean out the socket, which in turn relies on the properties of the rock. Soft sedimentary rocks can be more difficult to fully remove all debris, because the surrounding rock can be damaged and weathered once exposed to the elements. On the other hand there is no reason that shafts in strong metamorphic/igneous rock, which are less affected by weathering, cannot be properly cleaned leaving only strong sound rock. The process of inspecting rock socketed drilled shafts after drilling is complete remains somewhat of an obstacle as shafts can reach depths of 61 m (200 ft) below ground surface. Additionally, the timing of such inspection is critical because settling of suspended solids or soil infiltration through seams, joints, or around the casing can affect the cleanliness of the socket.

The placement of rebar and then concrete marks the culmination of a drilled shaft construction project. As with any process the successes of placing rebar and concrete lies in the hands of those performing the work and providing the materials. Proper rebar installation techniques need to be used and need to conform to design. During concrete placement there are a number of things that all need to happen to ensure proper concrete rock bonding. Debris needs to be removed from the socket for reasons discussed earlier and concrete needs to be properly mixed and placed (O'Neill, 2005).

2.4 Full Scale Testing Procedures

Testing procedures are considered especially important for drilled shafts due to some of the material properties and construction uncertainties. Engineers rely on full scale tests to ensure that designs are adequate and safe for use by the public. Test shafts are beneficial because they allow engineers to come up with more economical designs as well as provide information to researchers in the ongoing effort to learn more about drilled shafts. When test shafts are used, more economical designs result because high resistance factors are permitted. Tests that are conducted to failure are most useful to researchers because a better understanding of nominal resistance can be gathered. However, test shafts are not always subject to failure. From time to time these shafts are only subject to nominal loads used in design or restricted to the capability of the testing equipment. If the structural integrity of the test shaft has not been damaged, they are often used as production shafts.

Shafts can be tested in a number of ways with modern technology. New methods involve techniques that allow engineers to measure specific responses of shafts under different load scenarios. Static load tests are still run to determine the capacity of drilled shafts. Static load tests are usually conducted with a hydraulic jack that uses a reaction beam to jack against the shaft. To conduct static load tests, high capacity drilled shafts often require very large reaction beams that may consist of large bulky concrete counter weights. Other alternatives to large bulky counterweight systems are driven piles or more shafts in the vicinity of the test shaft. The extra piles or shafts are then attached to the reaction beam so that large loads can be applied to the test shaft (Turner, 2006).

A common load test that has gained popularity with the engineering community is the Osterberg Cell or O-Cell test, which will be a main focus throughout this report. The O-Cell load test can be performed on shafts without the hassle of bulky overhead set-ups, which can be seen in Figure 2.3. It can be used on shafts intended for test purposes only, or it can be used on shafts that are intended to be used as production shafts. The test is performed by placing a sacrificial hydraulic piston at the bottom of the shaft that can be pressurized and monitored from the surface. The piston exerts an equal pressure on the bottom of the concrete shaft and the base of the excavation. The capacity limits of the test are based on the size and number of cells placed at the base of the shafts (Osterberg, 1998; Osterberg, 1999).

An advantage of the O-Cell load test is that end bearing and side shear can be analyzed separately. The upward and downward load applied by the cell is the same at all times, however, the displacements of the shaft and the bottom of the excavation will generally differ. The upward movement is a function of the side shear, and the downward movement is a function of the end bearing. Although the O-Cell has advantages over the static load test, it does have some disadvantages. The main disadvantage is that only one of the resisting forces can be carried to failure (Schmertmann, 1993).

Other disadvantages are the limited movement of the O-Cells, which are generally limited to about six inches of movement, and the construction of the top-down load curve. The top-down load curve is created from O-Cell results by summing loads applied to both the side shear and bearing capacity at corresponding displacements. For example, an O-Cell test is run on a Rock Socketed Drilled Shaft, and load-displacement curves are obtained for both the upward and downward displacement of the cell. Upward displacement of the O-Cell would correspond to side shear movement and downward displacement of the O-Cell would correspond to bearing capacity movement of the shaft. If the side shear reached a displacement of 2.54 cm (1 in) at 20 MN (2,200 ton) and bearing capacity reached a displacement of 2.54 cm (1 in) at 40 MN (4,400 ton), than the equivalent top-down load for a displacement of 2.54 cm (1 in) would be 60 MN (6750 ton). This procedure can be repeated for multiple displacements and loads to obtain an entire top-down load displacement curve. There are also calculations made to account for additional compression of the shaft due to elastic compression of the concrete. Elastic compression of the shaft generally results in more top-down displacement for a given applied load. Figure 2.4 displays points chosen from a side shear and end bearing curve in order to construct the equivalent top-down curve displayed in Figure 2.5 (LOADTEST, 1998a).

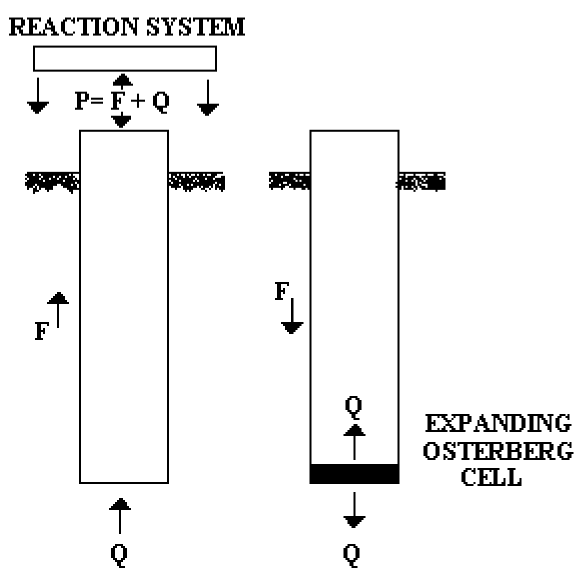

Figure 2.3 Conventional Top Load Test (left) Osterberg Cell Load Test (right)

(after Turner, 2006)

2.5 Modeling of Drilled Shafts

There have been numerous efforts to model drilled shafts in rock over the past 20 years using finite element analysis. Programmers have used ABAQUS (Zuo, 2004; Hassan, 1997), which is used for this study, and other modeling software such as ANSYS (DiGioia et al., 1998) to create their models. For the most part these models seem to use similar approaches with minor differences regarding certain parameters. Modeling has been performed in a wide variety of rock, such as limestone, schist, and soft argillite. This section will discuss the similarities and differences of previous modeling techniques along with what was successful and what was unsuccessful about these models.

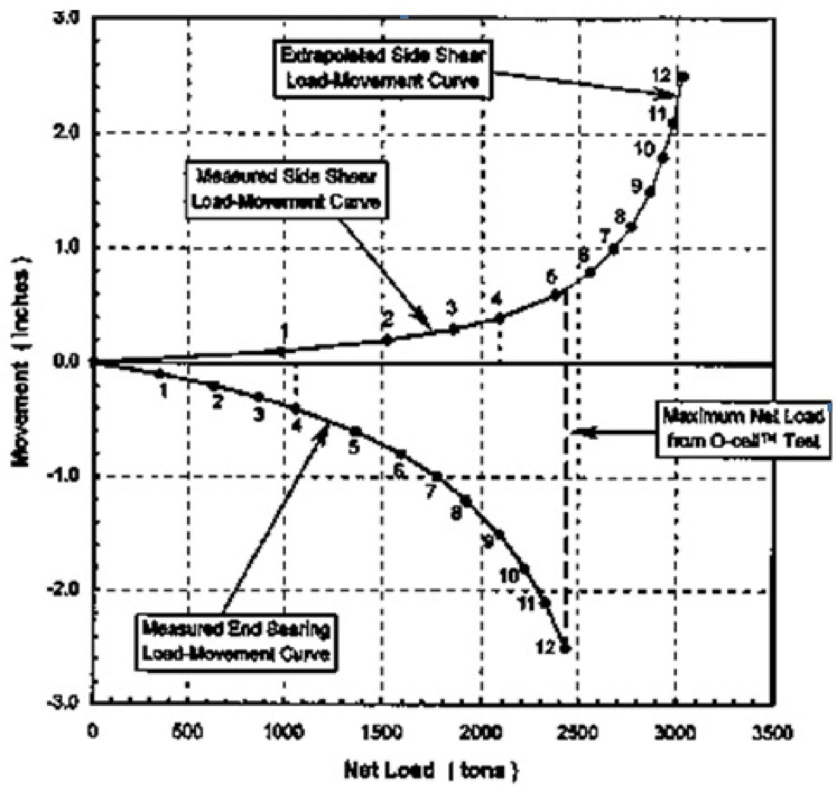

Figure 2.4 Example Upward and Downward Load-Deflection Curves for Construction of Equivalent Top-Load Curve (Loadtest, 1998a)

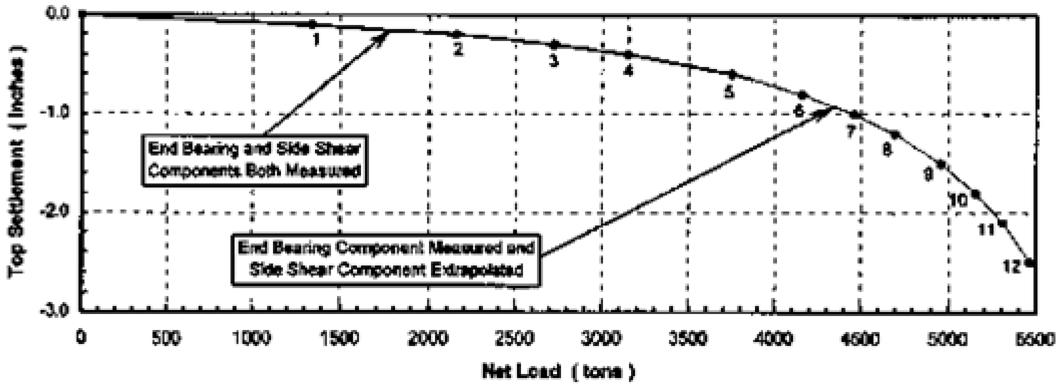

Figure 2.5 Equivalent Top-Load-Deflection Curve Obtained from Figure 2.4
(Loadtest, 1998a)

The majority of modeling has been done using an axisymmetric approach. Modeling in three dimensions creates larger files and is unnecessary because loads and displacements are equal in the radial direction. The length of rock extending out beyond the shaft is one parameter that varies from model to model. Some models used a fixed distance of rock from the shaft and others related this distance of rock to shaft diameters or shaft lengths. One particular model used to model Osterberg Cell tests simply extended the rock 12 meters (40 ft) beyond the edge of the shaft horizontally and 9 meters (30 ft) vertically beneath the base (Zuo, 2004). Another model extended the rock 20 shaft diameters horizontally and 1.5 shaft lengths vertically (Hassan, 1997). Previous work at the University of Maine on integral abutments had used infinite elements, however none of the other material reviewed for this study had used this technique. Regardless of the method used most models had the densest mesh in the vicinity of the shaft with a progressively looser mesh with increasing distance from the shaft.

The inclusion of the soil materials above the rock did not seem to be important to the majority of those modeling Rock Socketed Drilled Shafts. Their idea was that the soil did not play a significant role. The side shear capacity of the soil was negligible and so is the confinement produced by soil compared to the confinement of the rebar in concrete. However, those that did not include the overburden soil used applied loads to represent the absent soil. To represent the soil, modelers used distributed loads equal to the overburden weight of the soil. In some instances where the concrete-rock interface was the only point of interest, the concrete extending above the rock was not included either. Again the absent material was represented in the form of applied loads (Zuo, 2004). The application of the applied loads is important because rock and concrete act differently when compressive loads are applied. If soil layers are substantially thick and representative loads are not applied, then field results and modeling results may vary considerably.

Material properties and the parameters used to define the materials seem to be similar among models. All the models used elastic properties in their definitions. The elastic properties consisted of a Young's modulus and Poisson's ratio. Poisson's ratio was assumed for most models, which correlated well with one another. Concrete values were always close to 0.15, and rock values were close to 0.3. The Young's modulus was either from test results or assumed for materials such as concrete. DiGioia et al. (1998) mentions that Young's modulus for the rock mass was used instead of Young's modulus for intact rock but does not explain how mass values were determined. It is important to account for the joints and rock quality, which will be explained in more detail in later chapters. It is assumed that DiGioia et al. (1998) uses a correlation of Young's modulus for intact rock and Rock Mass Rating (RMR) to determine the Young's modulus of the rock mass since they separated all their parameters up into groups depending on RMR. Turner (2006) provides a number of different correlations using RQD and RMR to obtain mass E values given intact E values of the rock. Zuo et al. (2004) used field tests to obtain elastic properties. To do so they matched elastic portions of field Osterberg Cell tests by adjusting the Young's modulus until model results corresponded well with field results. Other parameters for failure definition were used for modeling the rock. These usually included cohesion of the material and a friction angle of the material. For those models that based materials on a rating system for the rock the values of cohesion and friction both decreased with decreasing rock quality. This is outlined in Table 2.2. Also included with Mohr Coulomb or Drucker-Prager failure criteria is the use of a dilation angle. The dilation angle can be assumed to be half of the friction angle. This is done so that unrealistic high dilation does not occur (Zuo, 2004). Other parameters, such as density, come from test results or are assumed values.

There are differences among models when it comes to modeling the contact between the rock and concrete. Hassan (1997) and Zuo et al. (2004) use a similar type of model in some ways. They both used a method of roughening the sides. The model produced by Zuo et al. (2004) used a sinusoidal profile with an elongated wavelength. This method mimics the dilation that occurs in field shafts as asperities on the rock and concrete rise up over one another. This phenomenon is explained in detail by Sangong et al. (2007) and will be discussed in later chapters. Other approaches to side shear contact used actual failure of the rock along the rock shaft interface. McVay et al. (1992) used this approach and found that the side shear capacity was a function of the unconfined compressive strength of the rock. This method assumes that the material has a constant stiffness until failure is reached and then the stiffness reduces to a minimal value.

For the most part there is little discussion in the technical papers about how these models are loaded. Hassan et al. (1997) loaded by applying velocity vectors to the surface instead of actual applied loads. A velocity vector is a pre-determined settlement rate of the surface, and the entire surface move a certain direction in unison. Loads can still be measured when using velocity vectors by monitoring the reaction force at the nodes.

Table 2.3 Rock Descriptions and Rock Strength Based on RMR (after DiGioia et al., 1998)

RMR	81-100	61-80	41-60	21-40	<20
Class No.	I	II	III	IV	V
Description	Very Good Rock	Good Rock	Fair Rock	Poor Rock	Very Poor Rock
Cohesion of Rock Mass c' MPa (ksf)	> 0.30 (>6.30)	0.20 - 0.30 (4.20 - 6.30)	0.15 - 0.20 (3.10 - 4.20)	0.10 - 0.15 (2.10 - 3.10)	< 0.10 (< 2.10)
Friction Angle of the Rock Mass ϕ'	>45	40-45	35-40	30-35	<30

The work done by Zuo et al. (2004) is of special interest to this project. They created a model to represent an Osterberg Cell test in mica schist. The shaft tested was socketed 6 meters (20 ft) into rock and had a diameter of 0.52 meters (1.7 ft). They concluded that numerical modeling was a good representation of drilled shafts and that loads were carried predominantly by side shear. In their case little stress reached the base of the drilled shaft, and the majority of displacement was caused by elastic compression in the concrete.

Chapter Three

Development of Finite Element Model

This chapter covers the development of a finite element model to simulate a typical Rock Socketed Drilled Shaft constructed in hard rock. For the purpose of this investigation hard rock is considered to be rock with a uniaxial unconfined strength greater than 30 MPa (4,350 psi). Typical shaft dimensions and typical hard rock properties were incorporated. An axisymmetric technique was used to create the model in the commercial finite element program ABAQUS (HKS Inc. 2001). The model was calibrated by replicating multiple field test results. The calibrated model was then used to study behavior of Rock Socketed Drilled Shafts for the full range of dimensions and rock characteristics to be encountered in hard rock in the Northeast. The calibration of the model and the development of a design incorporating side shear and end bearing by using the calibrated model will be covered in Chapters Four and Five respectfully.

3.1 Model Overview

Because a drilled shaft is symmetric about its vertical axis, an axisymmetric model (symmetric around the z-axis of the model) was used to simplify the construction and analysis process in ABAQUS. An axisymmetric view is limited to a two-dimensional cut of half of the model taken about the z-direction. However, when viewing results the model can be manipulated to display the entire shaft and the surrounding soil in three dimensions, which will be described in Section 3.2.1.

For the purpose of creating an initial model a test shaft in Hancock, Maine was used as a prototype, since it had a simple soil/rock profile. To begin, nodes and elements representing a large block of rock that measured 30x40 meters (98x131 ft) was placed into the model with a gravity load applied. The size of the initial rock mass varied from model to model depending on the size of the shaft and applied loads. The modeled rock mass could be much larger, however we chose to end the rock at a distance far enough from the shaft that boundary stresses and deformations due to applied loads were negligible. It was later discovered that the rock mass could be discontinued at a distance of 3 shaft diameters from the outer edge of the shaft as shown in section 3.5.1. To represent the surrounding rock outside of the rock mass itself, restraints were place on the node at the base and sides. The nodes at the base of the rock were restrained in the z-direction and the sides were restrained in the radial direction. Properties of the rock were determined by examining boring logs and laboratory test reports from the projects and applied to the rock mass. Once the rock mass properties were incorporated into the model, nodes and elements representing the overburden soil layer or layers, if present, were placed into the model. Overburden soils had the same radial dimension as the underlying bedrock. The depth of the overburden layer was determined using data provided in test reports and boring logs. If more than one layer was present, they were all given separate and appropriate soil characteristics and then added layer by layer to limit complications and confusion of applying them all at once. Gravity was also applied to the soil layers as it was to the underlying bedrock. From this point on gravity is applied to any part placed into the assembly.

To calibrate the model, an Osterberg Cell (O-Cell) configuration needed to be included. A typical O-Cell configuration has steel plates at the bottom of the excavation and at the base of the shaft. The O-Cell is sandwiched between the two steel plates. The plates have a larger diameter than the O-Cell, which distributes the load more evenly on the base of the excavation and bottom of the shaft. The O-Cell was modeled as a controlled rate input applied to each plate on the cell footprint. The dimensions of the O-Cell footprint and of the plates were obtained from reports by the testing contractor, LOADTEST, Inc.. Typical material properties for steel material properties were used for the top and bottom plates.

The final part incorporated into the model consisted of nodes and elements representing the shaft. Dimensions for the shaft were determined from test reports. Typical concrete properties were applied in most cases, however, some reports included concrete strength tests. These concrete properties were used to determine appropriate cohesion and elastic modulus values for the concrete. Material properties will be covered in more detail in Section 3.3.1. Shaft dimensions used during the calibration stage of the model were replicas of those from the field tests.

Once all the parts were placed into the model and the contact surfaces between the parts had been defined, which will be described in more detail in Section 3.4, loads could be applied. The type of loading and location at which it was applied was dependent on the situation. During the calibration stage, all of the loading was carried out from the base of the shaft to replicate the O-Cell as described in Chapter Four. The calibrated model was then used to find responses for loading on the top of the shaft as encountered in practice, which is explained in Chapter Five.

3.2 Construction of Finite Element Model

This section will discuss the sequence and the tools used while constructing a model of a typical Rock Socketed Drilled Shaft. Topics will include the type of model used to define the problem, definition of the different parts along with mesh controls that coincide with the part, and the assembly of all the different parts into the model including boundary conditions along the extremity.

3.2.1 Axisymmetric Model

Rock Socketed Drilled Shafts are almost always a circular shaft drilled vertically into the ground surface. The axial loads applied to the shaft are done either on top of the shaft, which could be from the superstructure above or from a static load test, or the shaft is loaded from the base as a result of an O-Cell load test. In either case it is assumed that the shaft will have stresses and strains that are symmetric about the vertical axis or z- direction. For this reason an axisymmetric model was chosen to replicate existing drilled shafts and used to create new ones.

While using an axisymmetric model in ABAQUS, there are only two dimensions that are used in the modeling viewport as opposed to the conventional three dimensions. However results can be viewed as though the model is in three dimensions. The vertical direction, which is referred to in three-dimensional models as the y-direction, is called the z-direction in an axisymmetric model. The horizontal direction is no longer the x or z direction but rather referred to as the radial dimension or r-direction.

The window used to build parts displays the part in the two-dimensional r-z plane as shown in Figure 3.1a. Parts can have an infinite z dimension but only a positive r dimension. They are only allowed to have a positive r dimension value because for a negative and positive value the model would wrap around itself. Although a part is created in the two-dimensional space ABAQUS wraps the part 360° about the z axis. While working with the model the 360° wrap is not seen, however, when viewing results the r dimension can be swept about the z-axis from 0° to 360°. An example of the window used to build parts in two dimensions can be seen in Figure 3.1(a) and a finished model with results displayed using a 180° and a 360° sweep of the r-dimension about the z-axis can be seen in Figures 3.1(b) and 3.1(c) respectively.

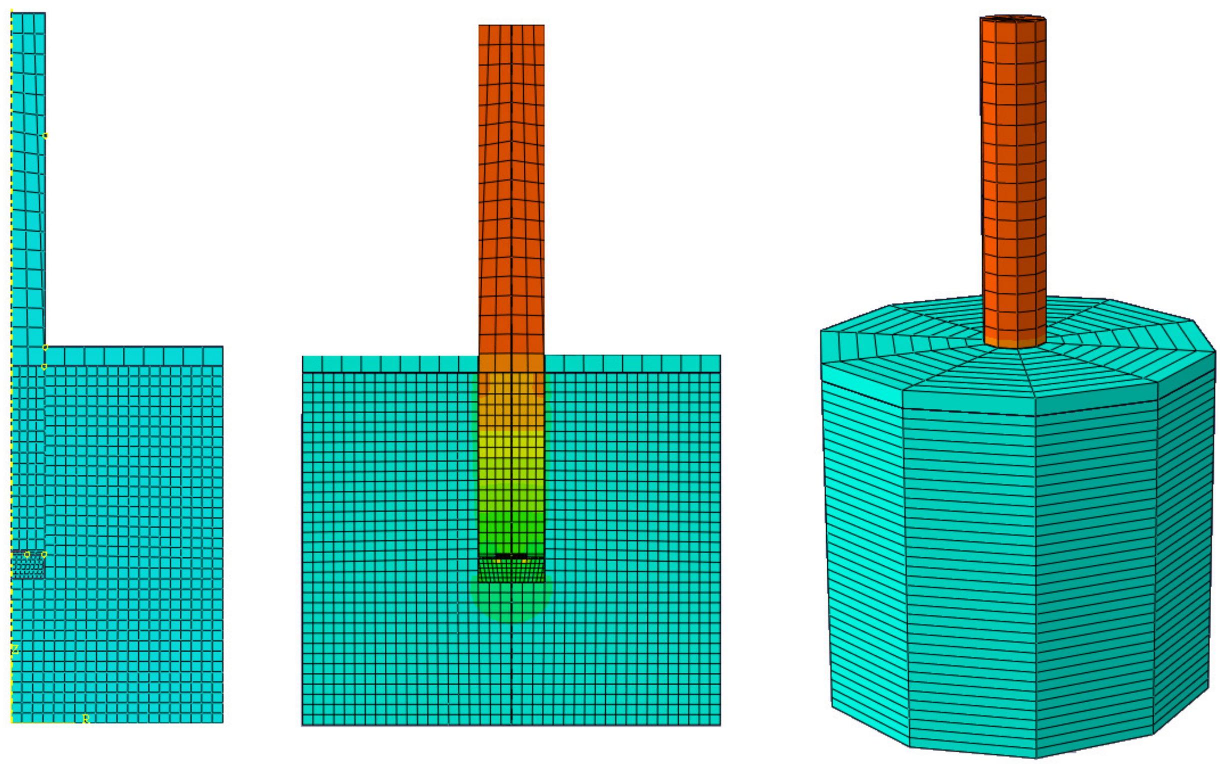

a. b. c.

Figure 3.1 ABAQUS Viewport (a): Construction of Model (b): Results with 180° Sweep (c): Results with 360° Sweep

The advantage of the axisymmetric model is that it is a simpler mesh, and thus the user does not need to create a large complex three-dimensional model. The axisymmetric method reduces errors and provides more consistent results in all directions.

3.2.2 Creation of Parts and the Assembly

To create the physical parts of the model, such as the rock or shaft, every part needed to be modeled individually. The parts are then assigned material and mesh properties before being applied to an assembly. Once in the assembly the finishing touches, such as contact properties, boundary conditions, and loading conditions, can be applied.

The first step is to create the two-dimensional parts individually that will be assembled to create the model. The most common parts that were used in this study were the surrounding rock, concrete shaft, overburden soil, and when necessary O-Cell test loading plates. During the calibration stage, dimensions for the subsurface parts, such as rock and soil, were determined using boring logs from the site. Dimensions of Osterberg loading equipment, such as plates, were obtained from reports acquired from the testing firm, LOADTEST, Inc.. The rock and soil layers were broken into separate parts that interact with one another once they were placed into the assembly. Mesh controls for the parts, such as element type and mesh densities, were assigned to the part along with material properties prior to placement in the assembly.

The different parts are placed into an assembly and then arranged in order to represent the Drilled Rock Socket profile. In order to have an assembly that can have loads applied, there needed to be proper interaction between the different parts in the assembly. Contact was established using two different methods in the creation of this model. The first was through tied surfaces, which was often between two parts that were created to model one solid instance. The most common occurrence of this was within the rock. Mesh densities needed to be a much tighter knit in the immediate area of the shaft than at a distance of multiple shaft diameters. To accomplish this, two parts were made with different mesh densities and then tied together in the assembly. Tied pairs act as one solid part and actually share nodes at their interacting surfaces, and thus the surfaces cannot penetrate one another, separate, or slide relative to the other. The second type of contact utilized in the creation of this model was a contact where sliding, penetration or separation can occur. To accomplish this, tangential and normal behavior was established between a master and a slave surface using frictional parameters that were set to specific shear or normal stresses. The use of a master surface and slave surface is an approach applied by ABAQUS to model intermingling surfaces. The subject of master and slave surfaces can be further researched, however, there are a number of guidelines to follow, such as slave surfaces are tighter meshed surfaces and slave surfaces should be the harder of the two materials when possible (Hibbitt et al., 2001).

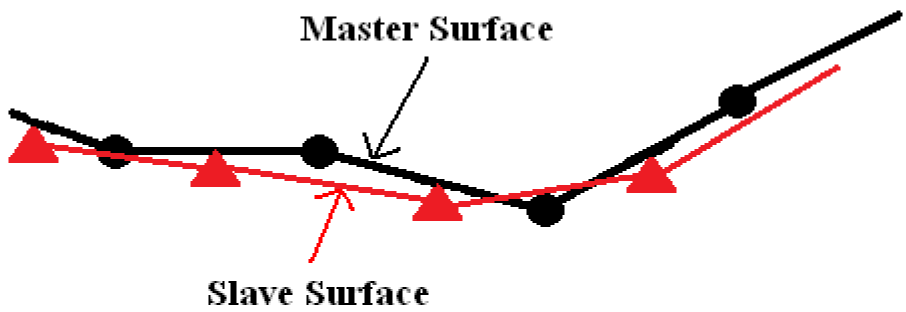

Figure 3.2 Master and Slave Surface Interaction

3.3 Part Module

The process of building a model began in the part module where the different parts were created and then assigned specific properties before being placed into the assembly. Within the part module each part was assigned material definitions, element types and mesh controls. This section is intended to outline how each part was assigned properties along with typical values used to create our model.

3.3.1 Material Selection

Material selection was the first of the three major variables that can be adjusted in the part module and assigned to specific parts. In this section common material properties for the different parts will be classified into three main categories, geotechnical materials, structural materials, and an interface material that was utilized to mimic the side shear response of different shafts during loading.

3.3.1.1 Geotechnical Materials

The first category of interest comprised geotechnical materials. For our model the geotechnical materials included the rock and overlying soil. Both of these were modeled using elastic properties, densities, and a Mohr-Coulomb failure criterion. Rock was always considered to be uniform throughout the mass; however, in some cases there were a number of different overlying soil layers. When different soil layers were encountered, a part was made for each, and different material definition assigned to the appropriate layers. Below in Table 3.1 are some typical ranges for the geotechnical materials.

Table 3.1 Summary of Geotechnical Properties

Element Type	Rock	Soil (Clay – Gravel)
Young's Modulus (E) **GPa (ksi)**	0.67 - 5.40 (97 – 783)	0.50 - 1.40 (72 - 203)
Poisson's Ratio (υ)	0.25	0.25 - 0.40
Density (ρ) **kg/m^3 (lb/ft^3)**	2,600 (162)	1,600 – 2,200 (100 - 138)
Friction Angle (ϕ)	35° - 40°	18° - 35°
Dilation Angle (Ψ)	30° – 35°	13° - 30°
Cohesion (c) **MPa (psi)**	1.0 – 9.0 (145 - 1,320)	0.0 – 0.10 (0 - 14.50)

As has been discussed earlier, material properties for geotechnical properties were determined using a combination of actual test data and estimated values when test data was not available. Any data that was available from the tests for the calibration models was incorporated; however, there were limited data available for many of these models. Values that were typically or occasionally estimated were Poisson's ratio (AASHTO, 2007; Bowles, 1977), densities (Bowles, 1977), and friction angles (Bowles, 1977). Values that were typically available from test reports included, but were not limited to, rock unconfined strength, Rock Quality Designation (RQD) values, and rock elastic modulus values.

Both rock unconfined strength (q_u) and Young's Modulus (E) test results were on intact rock specimens and thus needed to be adjusted to rock mass values before being included into the model. Intact values were lowered to account for discontinuities and other defects that were present in rock masses. Because RQD values were usually included in test data, we used RQD correlations to reduce intact Young's modulus (E_i) and unconfined strength values (q_u) in order to account for discontinuities and other impurities in the rock mass. Rock Mass Rating (RMR) gives more nuanced correlations than RQD, but descriptive information was lacking to obtain RMR.

Equations 3.1 and 3.2 as well as Table 3.2 were used to reduce intact Young's modulus values (E_i) to mass Young's modulus values (E_m). Unconfined strength values (q_u) were reduced to mass strength (q_m) using a correlation between nominal bearing capacity (q_{ult}), strength of intact rock, and rock quality. Figure 3.3 shows the correlation used to obtain mass strength (q_m) values. The alphabetical designation of lines in Figure 3.3 represents the type of rock. For hard igneous or metamorphic rock, line E in Figure 3.3 is used to calculate mass strength values (q_m). For the definition of other rock designations refer to Table 2.1.

$$(RQD < 70)\ E_m = E_i\ (RQD/350) \qquad \text{(Equation 3.1)}$$

$$(RQD > 70)\ E_m = E_i\,(0.2 + (RQD - 70) / 37.5) \qquad \text{(Equation 3.2)}$$

(Turner, 2006)

Table 3.2 Estimation of E_m Based on RQD (AASHTO, 2007)

RQD (percent)	E_m / E_i	
	Closed Joints	Open Joints
100	1.00	0.60
70	0.70	0.10
50	0.15	0.10
20	0.05	0.05

Equations 3.1 and 3.2 were used to reduce intact elastic modulus values for the calibration of the finite element model, which will be discussed in Chapter Four. During the calibration stage it was discovered that additional reduction of the elastic modulus was necessary in order to match field results. By reducing the mass modulus value (E_m) by a factor of two, more representative values were obtained from the finite element model. The reduction of mass modulus values will be discussed in more detail in Chapter Four Calibration of Finite Element Model.

Dilation angle is a material property that is not as well known as others, such as elastic modulus, friction angle, and cohesion. However, to incorporate Mohr-Coulomb failure criterion it is mandatory that a dilation angle be used. A dilation angle (Ψ) is defined as a ratio of plastic volume change to the plastic shear strain. A dilation angle can be associated, $\Psi = \phi$, or non-associated, $\Psi = 0°$. Associated flow leads to physically unrealistic volume changes when used in ABAQUS and non-associated flow lead to multiple convergence problems. Previous work done at the University of Maine using ABAQUS showed that using a dilation angle of five degrees less than that of the friction angle provided the best solution convergence (Delano, 2004). For this reason all dilation angles were set at five degrees less than the friction angle or at zero in the case of materials that had no friction, such as saturated clay.

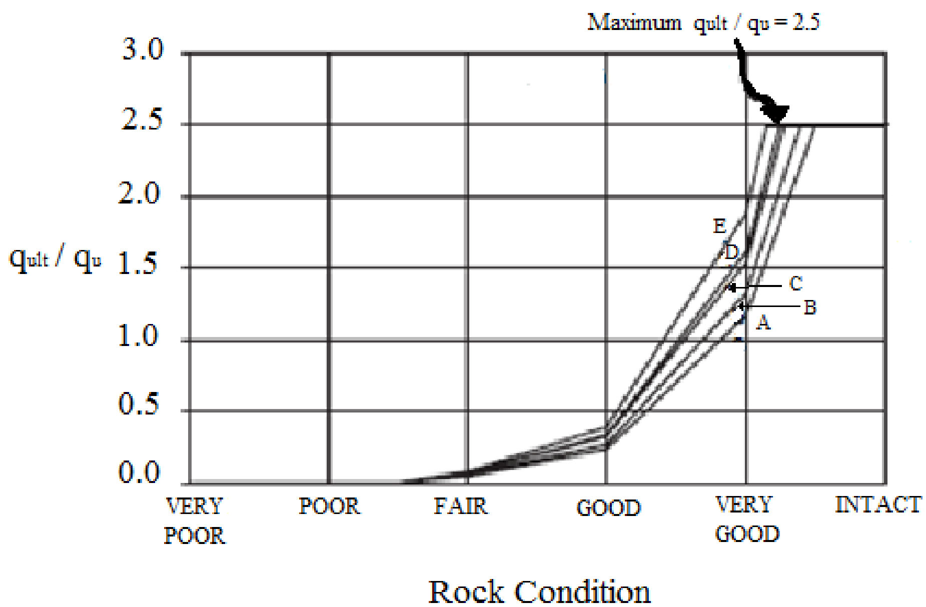

Figure 3.3 Strength Reduction Factor for Rock Mass (after Turner, 2006)

3.3.1.2 Structural Materials

The structural materials incorporated into the model included concrete and the steel used in calibration models as O-Cell plates. Structural materials were defined in the same manner as geotechnical materials, by use of elastic properties, densities, and Mohr-Coulomb failure criterion. However, Mohr-Coulomb failure criterion was not applied to the steel plates because they were restricted in all directions, thus it was assumed that failure would not occur in the plates prior to failure in the surrounding rock mass or concrete shaft. Table 3.3 provides typical values that were used in both calibration and supplemental modeling.

Table 3.3 Summary of Structural Properties

Element Type	Concrete	Steel
Young's Modulus (E) GPa (ksi)	29 (4,205)	200 (29,000)
Poisson's Ratio (υ)	0.15	0.3
Density (ρ) kg/m^3 (lb/ft^3)	2,400 (150)	7,860 (490)
Friction Angle (ϕ)	40°	N/A
Dilation Angle (Ψ)	35°	N/A
Cohesion (c) MPa (psi)	14 (2,030)	N/A

3.3.1.3 Shaft/Rock Interface Properties

One of the most challenging parts of modeling Rock Socketed Drilled Shafts was to capture the proper behavior of the socket's side shear between the concrete and the rock. Initial attempts involved adjusting friction and including actual bonding between the rock and concrete shaft. The main focus was on bonding; however this provided results not measured in the field. It was originally thought that the side shear resistance would reach a maximum value and then decline as bonding began to break until it reached a steady state that was purely friction as shown in Figure 3.4(a). However, all O-Cell test results showed that side shear reached a maximum value and seemed to level off as shown in Figure 3.4(b).

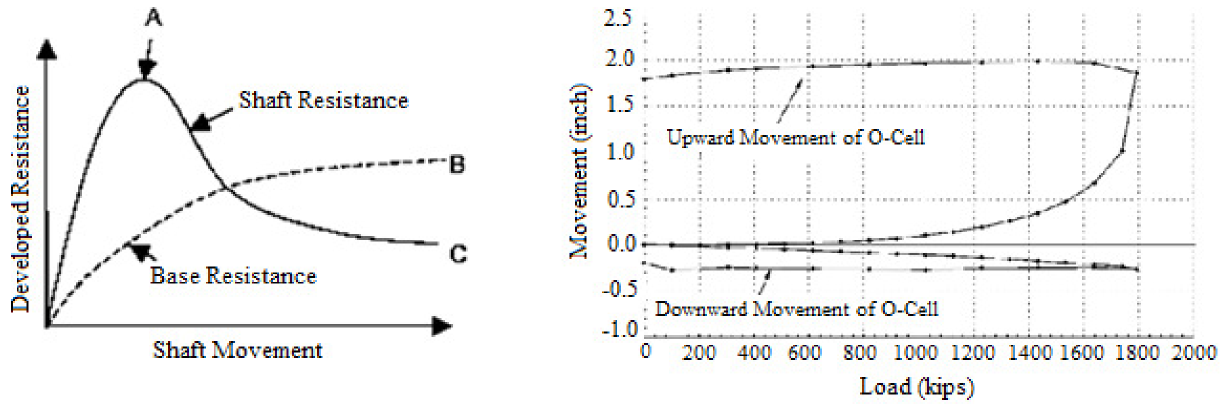

(a) **(b)**

Figure 3.4 (a): Assumed Side Shear Action (after Turner, 2006) **(b): Observed Side Shear Action** (after Loadtest, 1998b)

The measurements of the tests indicated the side shear did not decrease as expected with debonding, but instead became constant with movement. Sangong et al. (2007) explains the behavior of the side walls. The walls of drilled shafts and the sides of concrete shafts are not completely smooth, and some are even intentionally roughened. Therefore there are thousands and thousands of small asperities along the walls of the rock and sides of the shaft. As the shaft begins to move a dilation effect begins to occur along the asperities, which causes an increase in local shear stress. Thus the majority of side shear is assumed to consist of numerous asperities rising up over one another until one fails or they completely pass over each other and on to the next asperity.

In order to obtain representation of the measured behavior of side shear, where the side shear became constant with movement, the side shear was modeled with a thin finite layer of cohesive elements which would reach a maximum constant shear. These elements were placed between the rock walls and concrete shaft. In the model the layer was permanently attached to both the rock and concrete. As a result the majority of relative movement of the shaft and rock was across this layer. Just as with geotechnical and structural materials, the interface behavior was defined by elastic properties, densities, and Mohr-Coulomb failure criteria. Since the concrete was equal to or weaker than the rock, the interface was treated as part of the concrete shaft with the elastic properties and densities of the interface modeled identical to the concrete within a specific model. However, the Mohr-Coulomb properties, which would define the failure criteria of the interface, were a property characteristic only of the interface.

As previously mentioned Mohr-Coulomb failure criteria requires a friction angle, dilation angle, and a cohesion value of the material. By setting the friction angle and dilation angle equal to zero, uncertainties with confining stresses at different depths along the shaft were eliminated. Thus the failure along the concrete/rock interface was solely dependent on cohesion of the interface. The strength of the interface was variable from test to test but was within a narrow range. In calibration models the cohesion of the interface was calculated using field results from O-Cell tests. In order to properly define the failure curve, appropriate strain values needed to be assigned to maximum cohesion. It was observed in field tests that failure generally occurred around 10 mm (0.4 inch). The interface layer used for modeling purposes was 5 mm (0.2 inch) thick, which results in a strain of 2.0 or 200%. Typical values for concrete/rock interface properties are presented in Table 3.4.

3.3.2 Element Selection and Mesh Controls

The proper selection of elements and mesh controls are important in order to obtain accurate results. ABAQUS allows users to define different areas of the model with different element types and mesh controls. For the purpose of this model two different element types were utilized, while mesh controls were subject to variable change from part to part.

Table 3.4 Summary of Concrete Shaft/Rock Interface Properties

Element Type	Interface Layer
Elastic Modulus (E) **GPa (ksi)**	29 (4,210)
Poisson's Ratio (υ)	0.15
Density (ρ) **kg/m^3 (lb/ft^2)**	2,400 (150)
Friction Angle (ϕ)	0°
Dilation Angle (Ψ)	0°
Cohesion (c) **MPa (psi)**	1 .37 - 1.60 (200 – 232)

3.3.2.1 Element Selection

The majority of the model was modeled with the use of four sided four node bilinear axisymmetric stress elements (CAX4R). Originally four sided eight node biquadratic axisymmetric stress elements (CAX8R) were used because they provide more detailed images and more precise results; however, there was excessive buckling in the eight node biquadratic elements due to the large loads produced by the O-Cell. Because of the buckling associated with the biquadratic elements we settled on the use of bilinear four node elements with a tighter mesh. The four node bilinear elements were used to model all physical parts of the model, such as the socket, surrounding rock, overburden soil, and in the plates in the case of verification models.

The second element type utilized in the model was interface elements in the boundary area between the concrete shaft and the rock. The interface elements were four node axisymmetric cohesive elements (COHAX4). This area was modeled with a finite thickness and a cohesive behavior representative of the behavior observed from the LOADTEST test results. Sections are used in ABAQUS to relate material properties to element groups. When creating the cohesive section, which was used for the interface elements, it was important to select continuum response. The continuum response is recommended by ABAQUS for modeling finite thickness adhesive layers.

3.3.2.2 Mesh Controls

Mesh controls included the type of mesh and the density of the mesh used for a specific part. A mesh is the combination of nodes and elements that make up a part. ABAQUS and other finite element programs use the combination of nodes and elements to calculate how forces, stresses, temperature, etc. are transferred from one point to another. To understand the logistics of how finite element programming operates, the reader will need to do additional research as it will not be covered in extensive detail here.

Mesh type was dependent on the type of elements used. As was previously discussed in Section 3.3.2.1 there were two different element types used in the creation of drilled shaft models. Recall that a majority of the parts used four sided four node bilinear axisymmetric stress elements (CAX4R). All the parts that used CAX4R elements were meshed using a structural quad mesh. Structural mesh techniques use predefined mesh topologies and transform the mesh of a regularly shaped region onto the geometry of the part, which for a rectangular part looks just like a Rubik's cube made up of nodes and elements. When four node axisymmetric interface elements (COHAX4) are used, ABAQUS requires that sweep elements be used. A sweep element mesh creates a mesh for one layer of the object and then copies that mesh one element layer at a time until the entire part is meshed (Hibbitt et al. 2001).

If a part is more tightly meshed, more nodes and elements are needed to fill the space than if the part is loosely meshed. To assign the density of the mesh, the user applies an approximate global size to the part. The smaller the global size applied the tighter the mesh will be. When using tighter meshes, results were better defined. Results are better defined because all results including displacements, forces, etc. are given at nodes. For example if a surface had differential displacements and a loose mesh was used, the user may only be able to obtain displacements at a few points along the surface, thus limiting understanding of how that surface was moving. However, if a tight mesh was used the user may be able to obtain displacements at numerous locations along the surface and could obtain a better understanding of how the surface was moving. For this reason tight meshes were used at locations where results were needed to compare to test results, such as the base and top of the shaft, O-Cell plates, and rock within close proximity to the shaft.

3.4 Part Interactions and Contact Modeling

Interface properties are used to define the interaction or contact between two parts that have been applied to the assembly. Contact is important because the parts are allowed to move independently of one another and sometimes through one another within the assembly. This section will review the different interface properties and how they were applied to the model. The shear interface of the shaft/rock will not be covered in this section because it was covered in its entirety in Section 3.3.1.3. However, initial tied methods for modeling the shaft-rock interface will be covered in this section.

In order to model contact between two parts, it was mandatory to assign a master surface and a slave surface. This means that one part would have a surface that was either designated as the master surface or slave surface and the second part in contact would be assigned the other. For more information on this subject see Section 3.2.2 or ABAQUS handbooks and user manuals (HKS Inc. 2001).

3.4.1 Frictional Surfaces

The majority of surfaces that were modeled used frictional parameters. This required that each surface first be properly designated as either a slave surface or a master surface. There was then an interaction property designated to that contact pair. An interaction property was defined using a frictional parameter and a normal parameter. This means that normal forces are translated normal to the surfaces and shear is translated parallel to the surfaces. It is assumed that the surfaces are always parallel to one another, but Figure 3.2 shows that this is not always the case. When this occurs the normal and parallel directions refer to the master surface (Hibbitt et al., 2001).

When modeling using frictional parameters only, there was no adhesion in the normal direction, thus the normal direction was modeled with hard contact while surfaces were allowed to separate. The shear forces were translated along the parallel direction using coefficients of friction. A limiting shear stress was never applied because of uncertainty with the magnitude of the normal forces between the two surfaces. Table 3.5 provides typical values of friction that were used while assembling models of drilled shafts.

Table 3.5 Frictional Values

Contact Materials		Coefficient of Friction
Soil	**Concrete**	tan(ϕ)[1], 0.3 - 0.6[2]
Soil	**Rock**	tan(ϕ)[1], 0.3 – 0.6[2]
Rock	**Concrete**	0.7[2]
Steel	**Rock**	0.5[2]
Steel	**Concrete**	0.5[2]

[1](Liu & Evett 2000), [2](NAVFAC 1982)

3.4.2 Tied Surfaces

While creating and using our drilled socket model there were a number of different surfaces that needed to be modeled with the use of ties. A tied pair is created by selecting the two surfaces involved and applying a tied constraint. By applying a tied constraint the tied pair cannot move apart from one another in any direction. The slave nodes are not allowed to penetrate, separate, or slide relative to the master surface. This is a very powerful technique to connect two parts with incompatible meshes (Hibbitt et al., 2001).

This technique was used when different mesh densities were desired within the same part. For example, it was not as important to have a dense mesh at the perimeter of the rock mass; however, it was important to have a tight mesh for rock that was in the immediate vicinity of the shaft. To accomplish this, two different parts were created. One with a tight mesh placed close to the shaft and the other with a looser mesh placed at a distance from the shaft. The two parts were joined to make one part with the use of a tied surface. This technique was also employed for other parts such as the shaft and occasionally on different soil layers within the model.

3.4.3 Bonded Surfaces

Bonded surfaces were only applicable to the interaction between the sides of the shaft and the side walls of the rock. This was a technique used to simulate the bonding of concrete to rock, but was eventually deemed inadequate. Extensive work was performed on bonded surfaces and because of this was included into this investigation. The idea of a bonded surface corresponds well with conventional side shear mechanics, but after investigation both conventional side shear mechanics and bonded surfaces were found to not correspond well with field results. For more information on conventional side shear mechanics and the solution to modeling drilled shaft side shear see Section 3.3.1.3.

The bonded surfaces command was not supported by ABAQUS CAE, the program used to model the majority of ABAQUS models. Instead bonded surface commands needed to be manually entered into the input file. ABAQUS CAE creates the input file when the user draws parts and applies different properties to them. When a command is not supported by CAE the input file can be opened and manually edited in order to obtain desired results. The input file that has been created using CAE and user edits is what is actually submitted in order to obtain results.

In order to create the bonded surface that will debond under certain criteria, the user has to follow a number of steps. First a slave and master surface along with a node set corresponding to the proper surface need to be created and named in ABAQUS CAE. After entering the input file, the user next needs to enter the initial conditions command prior to the beginning of any steps. Next the user needs to determine the step in which the surface needs to begin debonding. Within that step the user needs to apply the debond and fracture criterion commands along with any required data. Below shows the command lines that need to be added to the CAE created input file in order to construct a bonded surface. These command lines tell the program to debond the shaft/rock interface (Asurf & Bsurf) at certain stresses (σ, τ^1, $\tau^{2)}$. These stresses were determined based on the tensile strength of the concrete, allowable movement, etc.

*Initial Conditions, Type=contact

Asurf, Bsurf, Nset

*Step (*step in which debonding will occur, line is not user added*)

*Debond, slave=Asurf, master=Bsurf

0, 1, t^1, a^1, t^2, a^2, …. t^f, 0 (*aplitude curve for magnitude of debonding with corresponding time*)

*Fracture Criterion, Type=critical stress

σ, τ^1, τ^2 (*max normal and shear stresses surface can withstand*)

3.5 Boundary Conditions and Loading

Boundary conditions and loading are as important as any other part of the modeling sequence. Without boundary conditions the parts would be allowed to free float through space. The following outline the techniques used and why they were used to model both boundary condition and applied loads.

3.5.1 Boundary Conditions

Boundary conditions were used to make sure the model was secure and not floating in empty space. These boundary conditions simulated the rock mass that was not modeled but exists in the real world. It is hard to model a rock mass that is more or less infinitely deep and wide. It is also unnecessary to model rock at more than three shaft diameters from the shaft because loads and deformations are negligible. So as a result boundary conditions were applied to the outer edges of rock masses and the outer edges of the different soil layers. Figures 3.5 and 3.6 show load-deformation curves for 7 meter (21 ft) deep shafts with diameters of 1 meter (3 ft) and 3.5 meter (11 ft) respectfully. In both cases the rock surrounding the shaft was modeled 1, 3, 5, 7, and 9 shaft diameters beyond the edge of the shaft. The distance of rock between the shaft and fixed boundary conditions on the edge of the rock was more influential on smaller diameter shafts. However, it was determined that 3 shaft diameters would be sufficient for our application. For the shaft with a diameter of 1 meter (3.3 ft) there was a 5% difference between the models that used 3 and 9 shaft diameters of rock, while for the 3.5 meter (11.5 ft) diameter shaft there was only a 3% difference between 3 and 9 shaft diameters of rock. Using smaller amounts of surrounding rock, while not significantly altering results, aided in the ease of model construction. By eliminating unnecessary rock element and nodes, the calculation process is also sped up.

The base of the rock mass was restricted in the vertical direction with allowable movement set to zero in order to imitate underlying rock. The sides of the rock and the sides of the different soil layers were restricted in the radial direction and also set to have zero movement with the intention of modeling the soil or rock that exists beyond the modeled instances. In order to assure that this approach did not give faulty results, stress at the edges were calculated in the model to make sure that ample rock and soil had been modeled. For example, if an insufficient amount of rock had been modeled underneath the shaft then lower deformations may occur than if a sufficient amount of rock had been modeled. More material would allow more compression; however, there is an effective depth beyond which compression is not important.

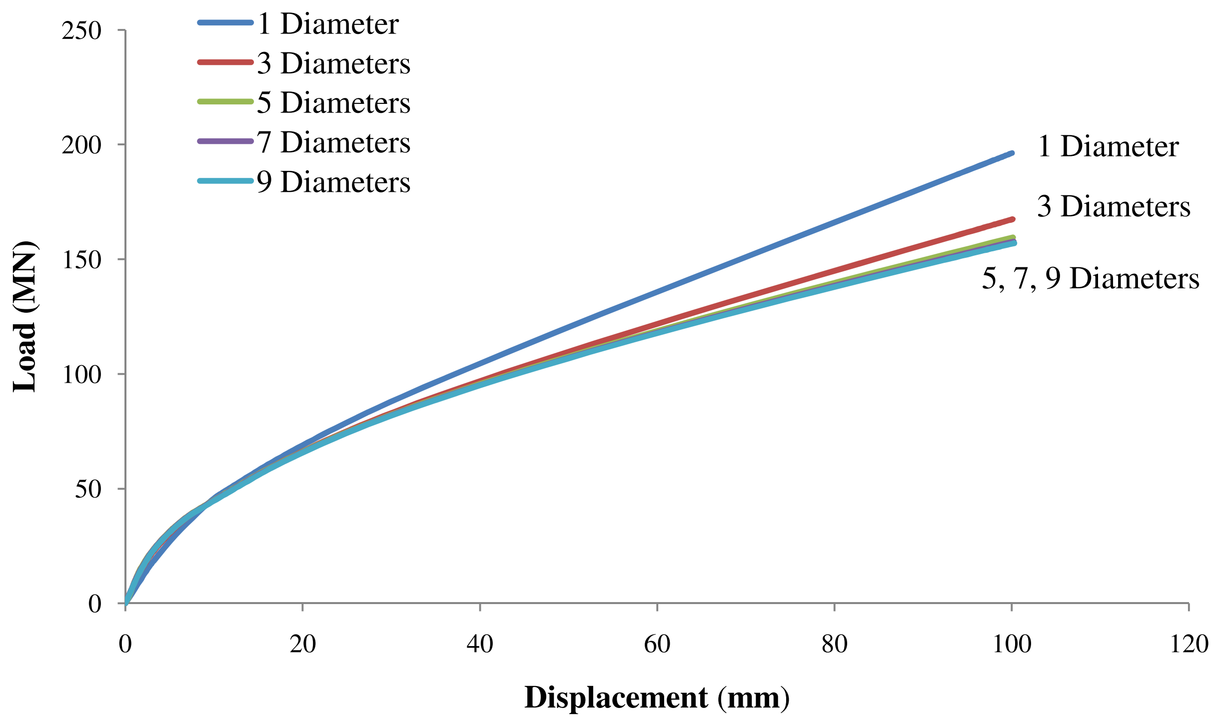

Figure 3.5 Influence of the Amount of Surrounding Rock on 1 meter Diameter Shaft

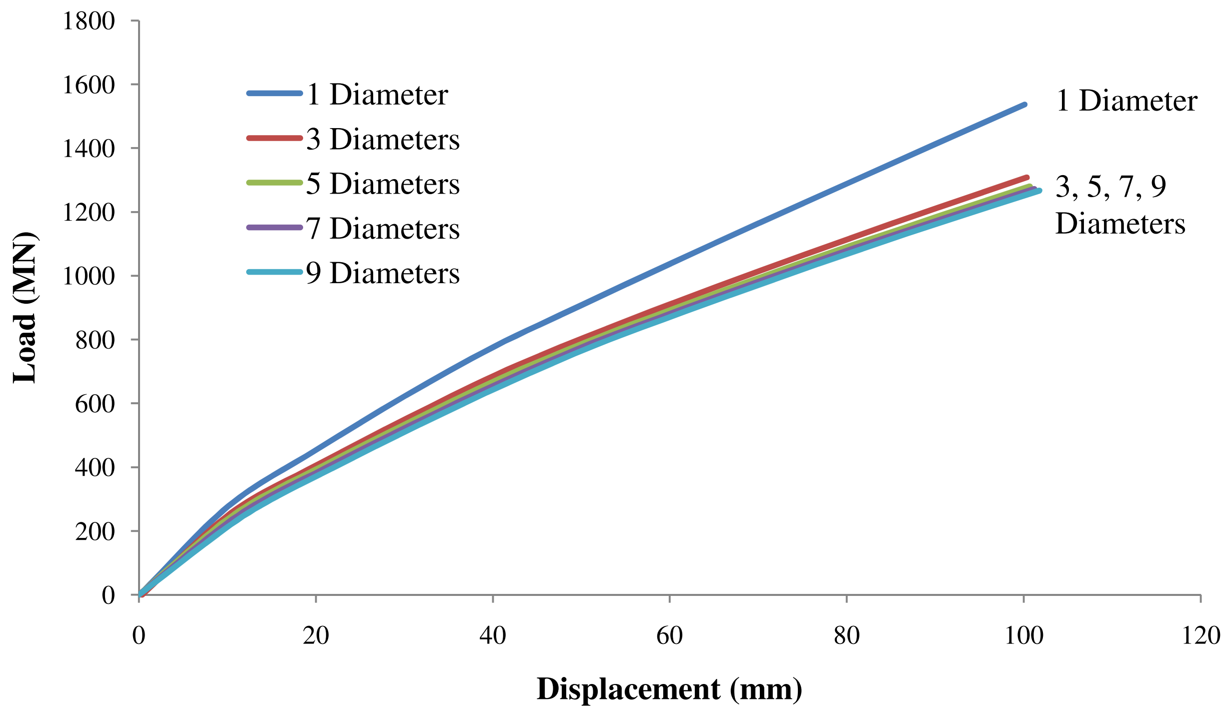

Figure 3.6 Influence of the Amount of Surrounding Rock on 3.5 meter Diameter Shaft

3.5.2 Loading

Loading conditions were applied as done in Osterberg tests and as done for service conditions. All models were subject to a gravity load in the first step of the analysis. A step is nothing more than a set time period within the model. A model can have as many steps as the user would like, but it must have at least one. The time period that a certain step lasts can be as long or as short as the user decides. For the sake of our modeling there was anywhere from two to as many as five steps ranging from 10 to 10,000 time units in total length. In all cases gravity loads were equal to those that are felt at sea level, 9.81 m/sec^2 (32.2 ft/sec^2). In subsequent steps certain parts were subject to applied loads. When modeling O-Cell tests, multiple loads were applied. One load was applied to the base of the shaft in the positive z direction to imitate the upward movement of the Osterberg cell, and one load was applied to the rock at the base of the shaft in the negative z direction to imitate the downward movement of the Osterberg cell. When modeling service loads, the loads were simply applied to the top of the shaft.

To model the loading and unloading cycle of an O-cell test or service load, an amplitude curve was used. Amplitude curves allow the user to use one step for the loading with time. The user specifies time points within the loading step, at which a fraction of the maximum load is designated. Table 3.6 shows an example amplitude curve for a step that lasts 1000 time units. At time 0 the applied load is 0. It increases until it reaches a maximum at time unit 600, at which it begins to unload to 0 at time unit 1000. ABAQUS is a unit-less program, which means it is up to the user to maintain a constant knowledge of the units being used to make sure results are in the desired unit.

Table 3.6 Example Amplitude Curve Used for Loading

Time (unitless)	Amplitude
0	0.0
300	0.5
600	1.0
800	0.5
1000	0.0

A number of the loads applied were done using a velocity vector. Under normal loading conditions a certain amount of force is applied to the top of the shaft or the base of the shaft and the displacements are found. With a velocity vector the surface is displaced in the desired direction, and the reaction forces at the nodes along the surface are found. This method was applied to the model to minimize differential displacements when using uniform distributed loads. At first distributed loads were used, however, they resulted in unrealistic differential displacements when attempting to duplicate O-Cell results. Using velocity vectors also allows the user to set displacement boundaries, which were useful when determining design criteria dependent on maximum allowable displacement of the shafts, which is covered in Chapter Five.

3.6 Obtaining and Reviewing Results

Obtaining results and processing them is one of the most important aspects of the modeling sequence. This section summarizes how results were obtained and processed.

As was previously mentioned, results are gathered at the nodes of the different parts. If the user was interested in the displacement and reaction forces along a surface, the user would have to make calculation at each node along the surface individually. To make this process easier, a node set containing the nodes of interest can be created and a history output request made within ABAQUS CAE. To create a node set, the user indicates that he/she would like to create a node set and then simply highlights the nodes of interest. For a history output, the user can select the node set were calculation will be made and the different variables, such as displacement, force, or energy. In order to obtain cumulative results across a surface or plot results against one another, the finite element results need to be exported to another program, such as a spreadsheet program like Excel, to be further processed and summarized. Figures 3.7 shows results directly from ABAQUS, while Figure 3.8 shows the processed results. Figure 3.7 displays both displacement results and force results plotted against time for a surface consisting of three different nodes. Figure 3.8 shows the summation of the three nodes for both force and displacement plotted against one another.

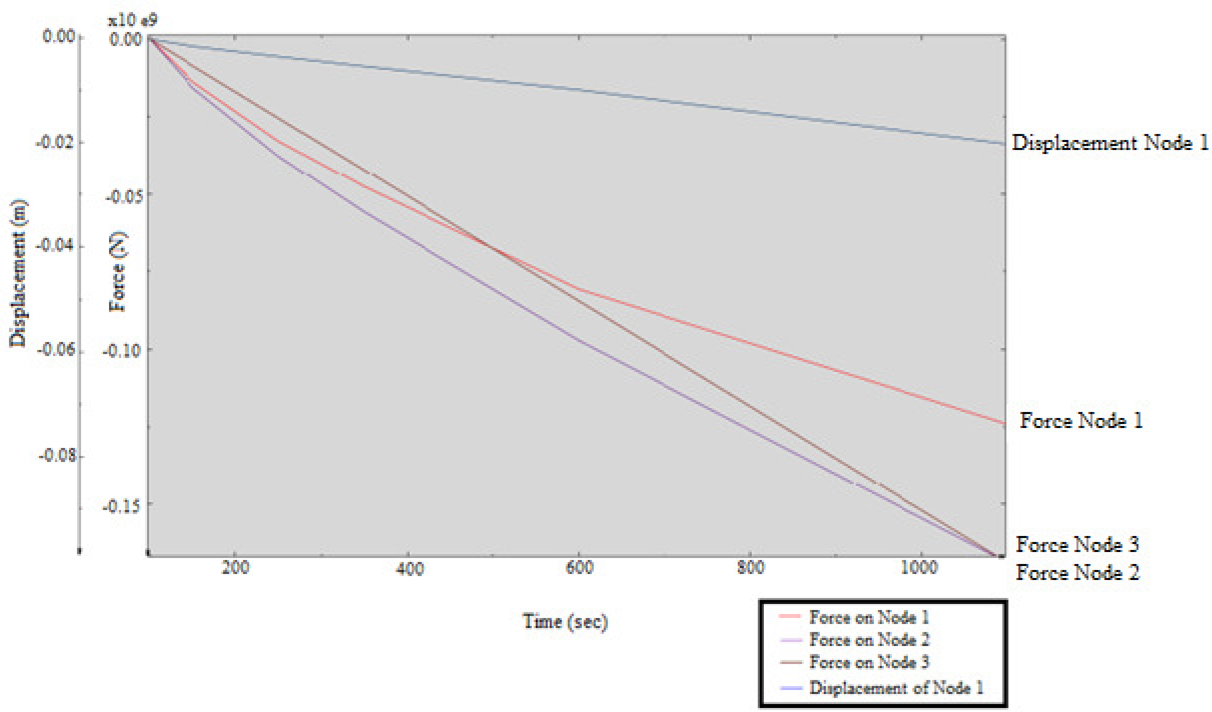

Figure 3.7 ABAQUS Results for Reaction Forces and Displacement

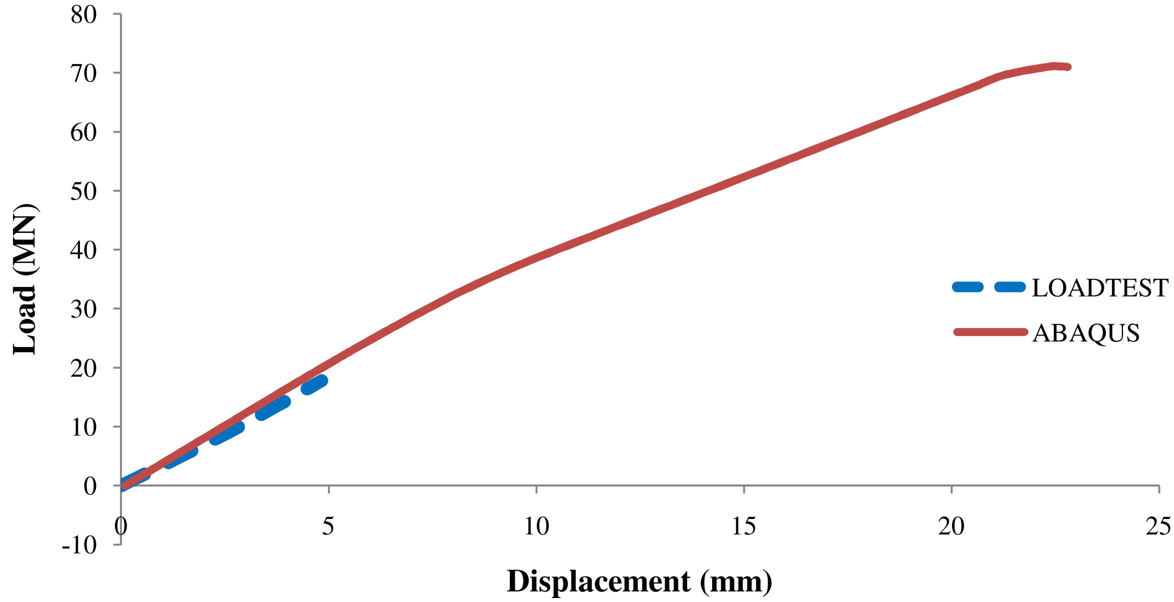

Figure 3.8 Top-Down Load Deflection Curve

Chapter Four

Calibration of Finite Element Model

Chapter Four covers the calibration stage of the finite element model created using ABAQUS software. Additionally, methods for obtaining rock mass properties from laboratory tests and subsurface investigations were calibrated. The model simulated Osterberg Cell tests conducted by LOADTEST Inc., and the results were compared to measured field results. The model was then refined to reduce discrepancies between finite element results and measured field results. The calibration tests of the model were all located in the Northeast and were founded into hard rock. Some of the tests were carried to failure, while others were limited by the capacity of the O-Cells. Soil and rock properties from the field tests were used in the model, and appropriate loads from the tests were applied to the model.

Modeled shafts were compared to field tests in three different ways: 1. Upward movement (O-Cell); 2. Downward movement (O-Cell); 3. Top-down loading (static load test or anticipated top-down load curve). Top-down loading of the model was compared to the equivalent top-down load vs. displacement curve that was provided by LOADTEST Inc.. The top-down loading provided by the by LOADTEST Inc. is a calculated procedure and does not provide test data for calibration. However, comparison of calibrated results with top-down loading serves to evaluate the simple procedure used by LOADTEST Inc.. The remainder of this Chapter outlines information on each shaft used for calibration of the model and provides a comparison of field results against modeled results.

4.1 Sagadahoc Bridge, Bath-Woolwich, Maine

4.1.1 Background of Sagadahoc Bridge

The Sagadahoc Bridge spans the Kennebec River and is a 906 m (2,970 ft) long, balanced cantilever bridge connecting the towns of Bath and Woolwich, Maine. The project was completed in August 2000, making it the second bridge in the state of Maine to utilize rock sockets as its foundation. Two separate shafts were tested on this project, shafts 6C and 7A. Shaft 6C has a diameter of 2.3 m (7.6 ft) and a length of 3.9 m (12.8 ft) in rock. Shaft 7A also has a diameter of 2.3 m (7.6 ft) but has a length of 9 m (30 ft) because rock quality was less desirable at this location than at the location of shaft 6C. Shaft 6C has 3.38 m (11 ft) of concrete to rock side shear side shear, while shaft 7A has 8.2 m (27 ft). Above the intact rock shafts 6C and 7A are both 2.44 m (8 ft) in diameter, which adds additional end bearing resistance (LOADTEST, 1998 a & b; LAW, 1998).

Each shafts had three separate 660 mm (26 inch) diameter Osterberg Cells placed at the base of the shaft, with a total combined capacity of 48 MN (5,400 ton). Because the pattern in which the cells were placed could not be duplicated using an axisymmetric model, an equivalent effective area method was used. This method involved creating one O-Cell footprint that touched the outside edges of all three O-Cells used in the field. This method resulted in a larger overall area; however it provided a more accurate representation of the force distribution created by the three Osterberg Cells. The alternative was to use a footprint that had the same area as the three O-Cells. This method was not used, because it resulted in a relatively small footprint, and thus the loads would be concentrated in a small non-representative area. The equivalent effective area method was only utilized on the two Sagadahoc Bridge shafts since they were the only field tests used in this study that employed more than one Osterberg Cell. Figure 4.1 shows an outline of how the O-Cells were arranged for the Sagadahoc Bridge, and the equivalent effective area used for calibration modeling.

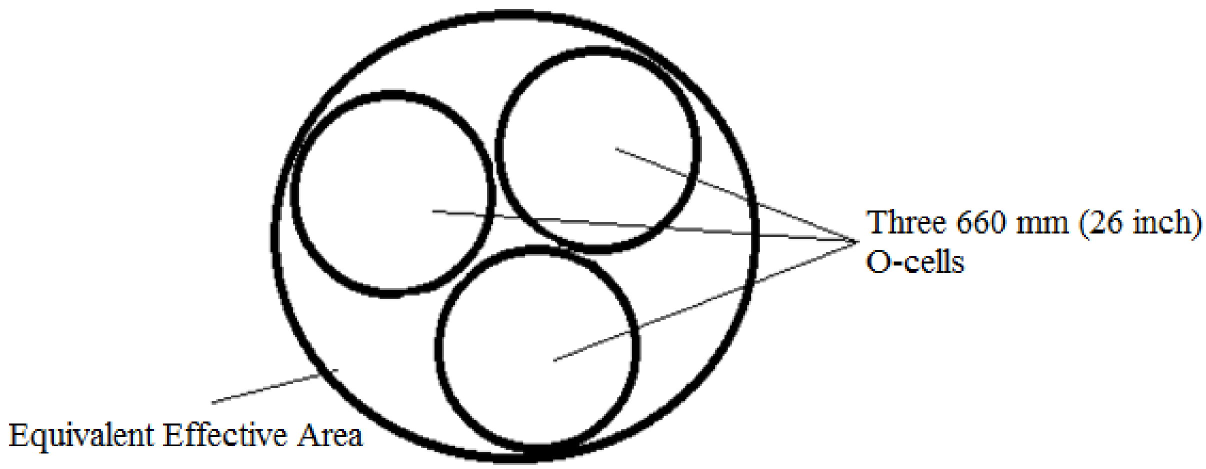

Figure 4.1 Osterberg Cell Arrangement and Equivalent Effective Area Method

The subsurface profile at the Sagadahoc Bridge consisted of glacial sand and gravel overlying sensitive clay, glacial till, and finally bedrock. The bedrock is described as belonging to the Cushing formation and consists of intricately folded biotite schist and gneiss with occasional granofels and granite intrusions. Rock Quality Designation (RQD) values varied between 60% and 90% at shaft 6C, while at the location of 7A values were between 16% and 67%. The RQD values obtained in the vicinity of 7A were the lowest of any location along the Sagadahoc Bridge. Unconfined compressive and elastic modulus tests on intact specimens provided rock strength and elastic modulus values. The rock at shaft 6C had an unconfined compressive strength of 30 MPa (4,350 psi) and an elastic modulus of 8,000 MPa (1,160 ksi). The rock at shaft 7A had an unconfined compressive strength of 13 MPa (1,890 psi), which is lower than the unconfined strength limit for hard rock of 30 MPa (4,350 psi), and an elastic modulus of 5,200 MPa (754 ksi) (LAW, 1998; Haley & Aldrich, 1997). However, the parent rock was a metamorphic rock. The intact values for rock strength and elastic modulus were transformed for rock mass values using methods detailed in Chapter Three. See Tables 4.1 and 4.2 for rock properties at shafts 6C and 7A respectfully.

Table 4.1 Rock Properties of Sagadahoc Shaft 6C

RQD[1] %	85.0
E_i[2] GPa (ksi)	8.0 (1,160)
E_m[3] (see Equation 3.2, and $E_m/2$ adjustment for model) GPa (ksi)	2.40 (348)
q_{ui}[4] MPa (psi)	30.0 (4,350)
c[5] (see Figure 3.3) MPa (psi)	7.0 (1,020)
ϕ[6]	40.0
f side shear[7], MPa (psi)	1.7 (247)

1. Rock Quality Designation 2. Intact Rock Elastic Modulus 3. Mass Rock Elastic Modulus 4. Intact Rock Compressive Strength 5. Mass Cohesion 6. Mass Angle of Internal Friction 7. Cohesion between rock and concrete

Table 4.2 Rock Properties of Sagadahoc Shaft 7A

RQD[1] %	55.0
E_i[2] GPa (ksi)	5.2 (754)
E_m[3] (see Equation 3.1, and $E_m/2$ adjusted for model) GPa (ksi)	0.41 (59.5)
q_{ui}[4] MPa (psi)	13.0 (1,890)
c[5] (see Figure 3.3) MPa (psi)	0.5 (72.5)
ϕ[6]	35.0
f side shear[7], MPa (psi)	1.6 (232)

1. Rock Quality Designation 2. Intact Rock Elastic Modulus 3. Mass Rock Elastic Modulus 4. Intact Rock Compressive Strength 5. Mass Cohesion 6. Mass Angle of Internal Friction 7. Cohesion between rock and concrete

4.1.2 Results for Sagadahoc Bridge

The results for Osterberg Cell tests and top-down loading of the test shafts are outlined in Figures 4.2 – 4.7. Results obtained from field tests conducted by LOADTEST Inc. are presented with a dashed line while results produced by finite element modeling with ABAQUS are displayed as a solid line. Side shear displacement results produced by finite element modeling were close to those of production shafts. End bearing load-displacement results correlated well during loading as shown in Figure 4.2. The loading portion of the end bearing was all that was modeled in the finite element model, since the dead weight loading and maximum live load are applied once to give the maximum displacement. Top-down loading of the model did confirm that the simplified method used by the LOADTEST Inc. predicts the top-down response of the shaft reasonably well.

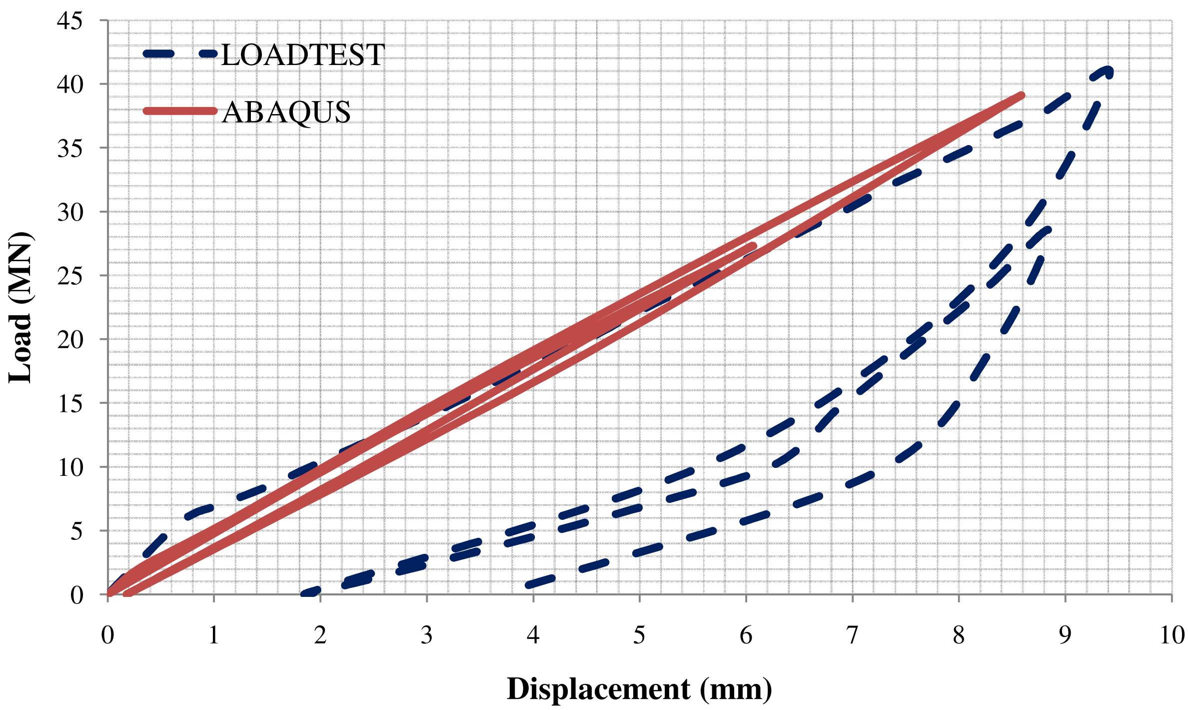

Figure 4.2 Downward O-Cell Results of Sagadahoc Shaft 6C

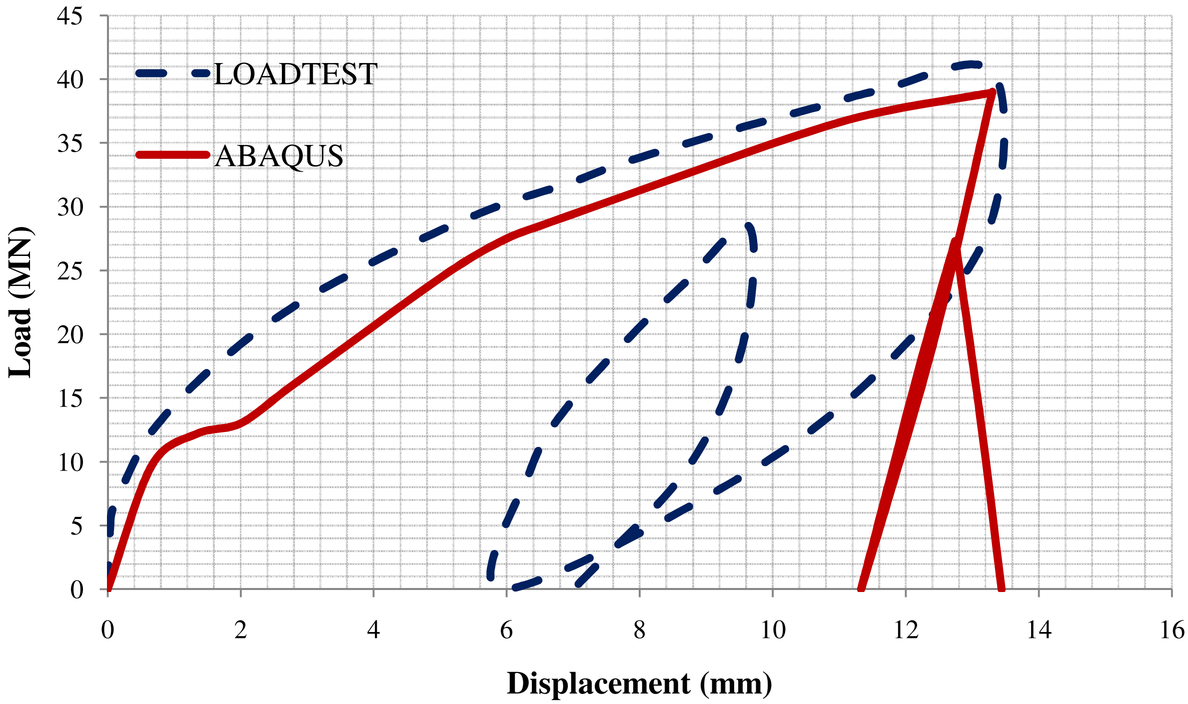

Figure 4.3 Upward O-Cell Results of Sagadahoc Shaft 6C

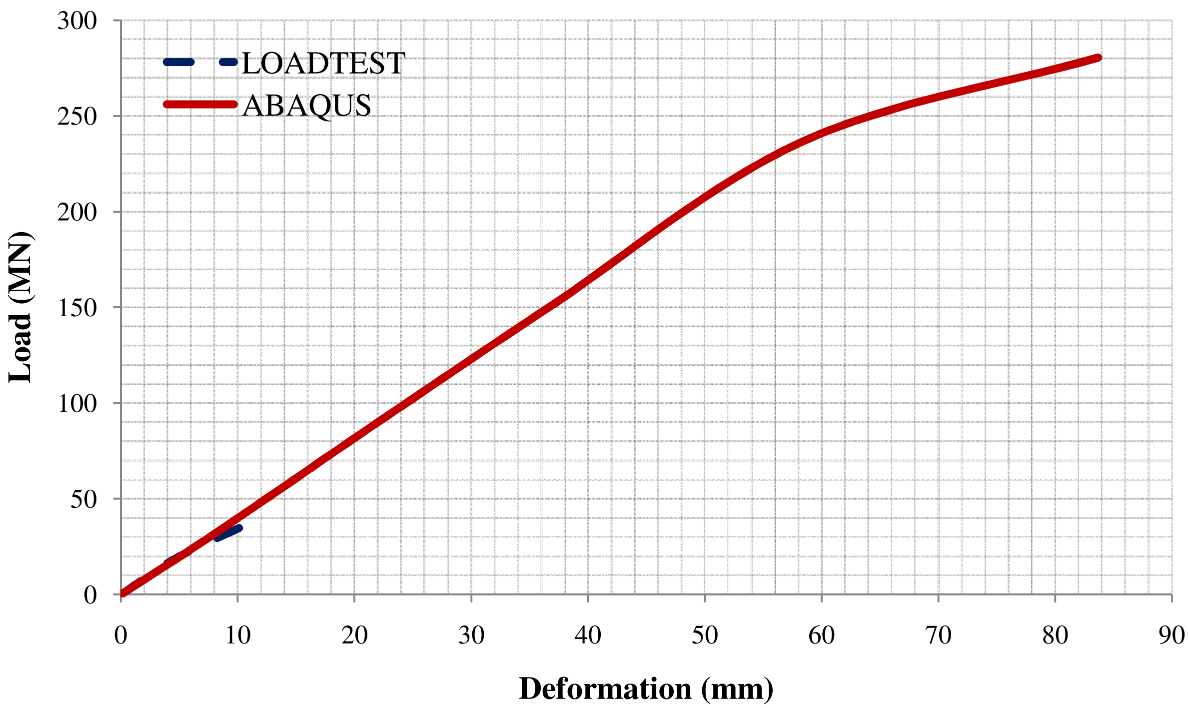

Figure 4.4 Top-Down Load of Sagadahoc Shaft 6C

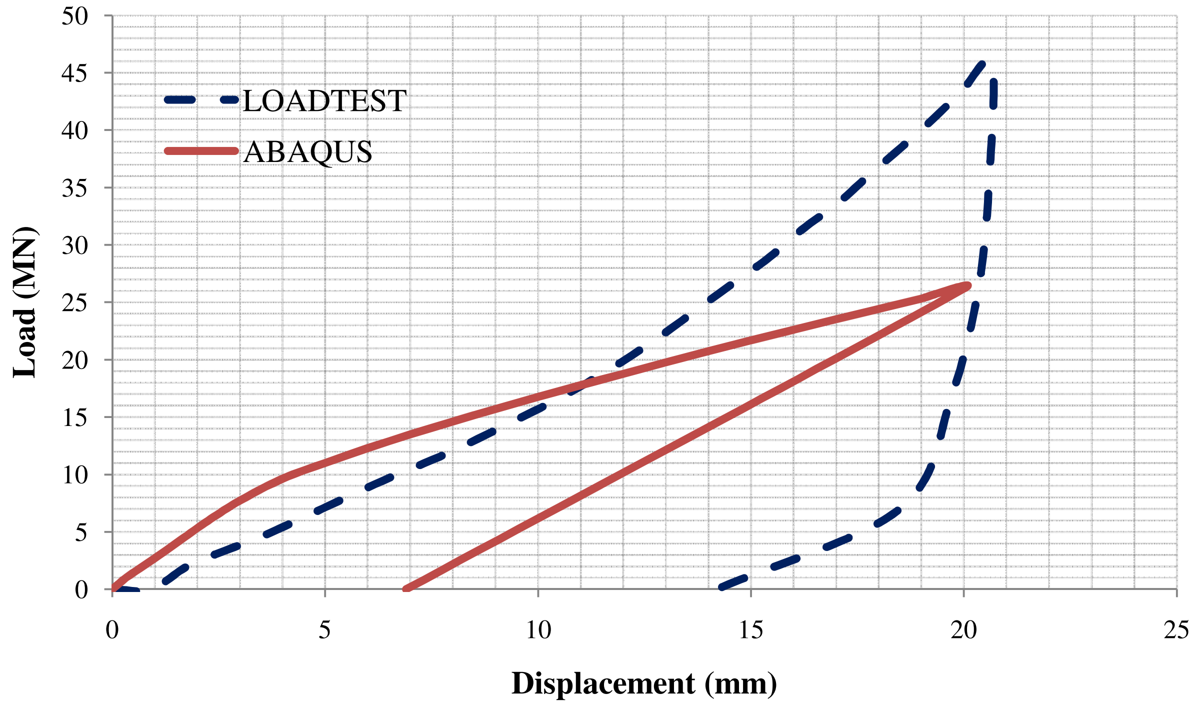

Figure 4.5 Downward O-Cell Results of Sagadahoc Shaft 7A

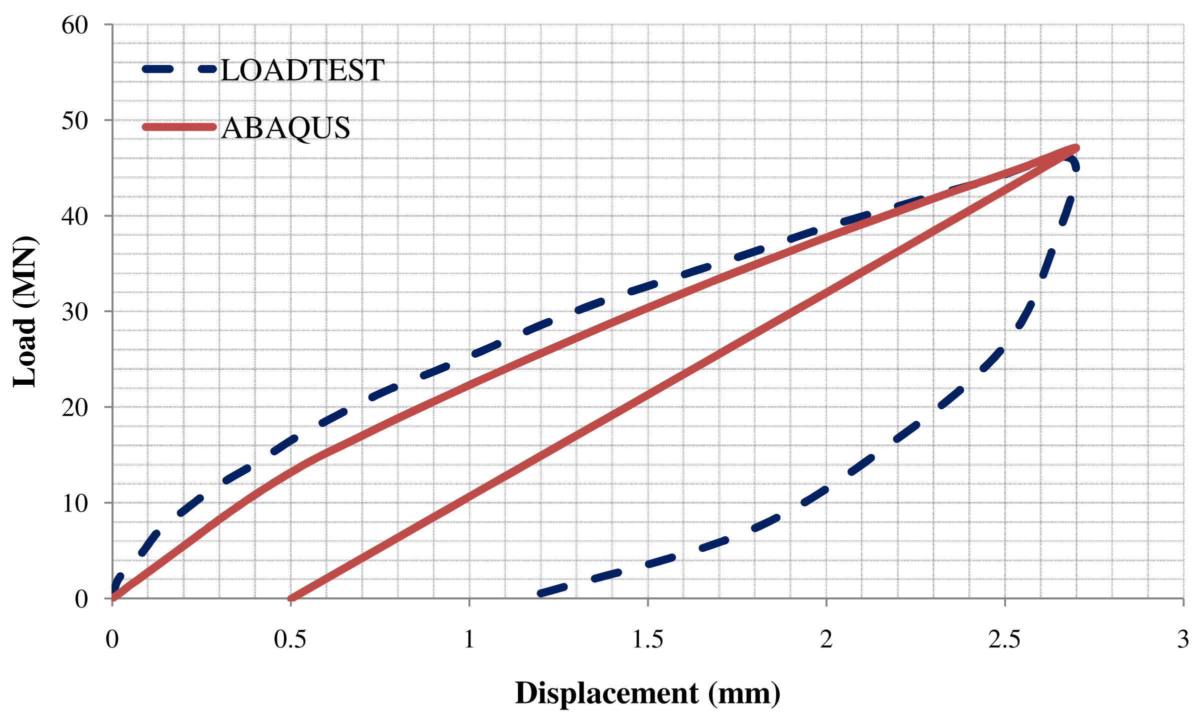

Figure 4.6 Upward O-Cell Results of Sagadahoc Shaft 7A

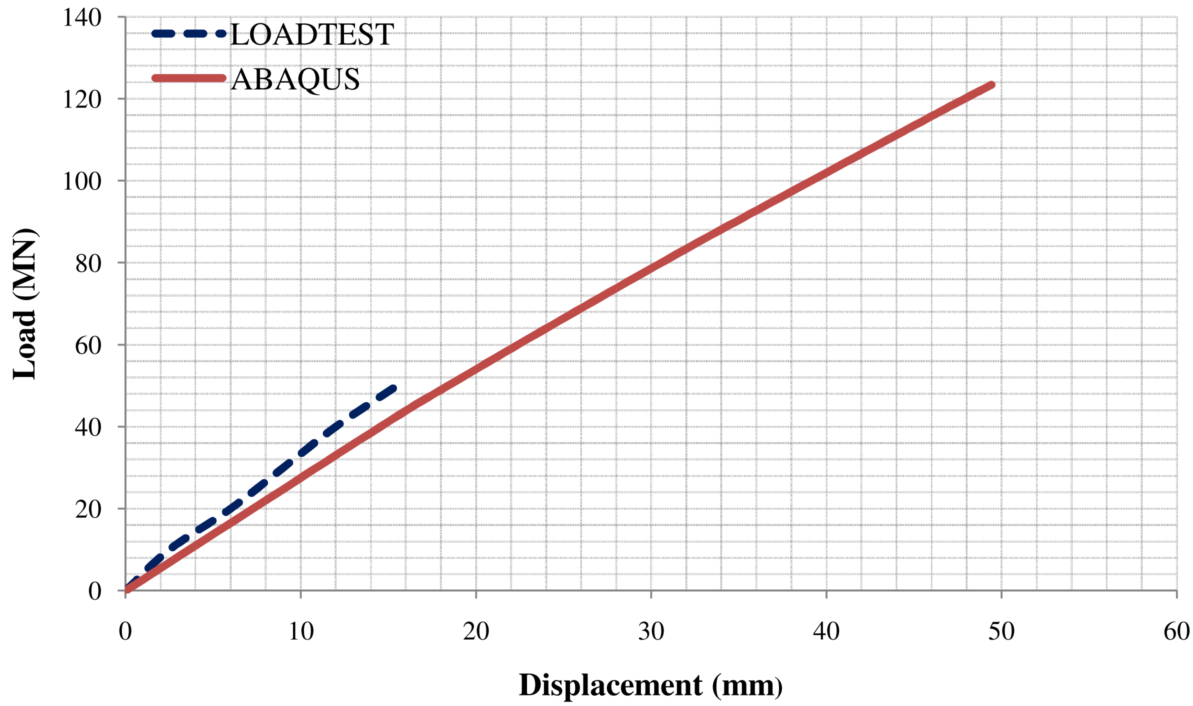

Figure 4.7 Top-Down Load of Sagadahoc Shaft 7A

4.1.3 Discussion of Sagadahoc Results

Figure 4.2 and 4.5 show the end bearing results, which is mobilized by the downward movement of Osterberg Cells, for the Sagadahoc 6C and 7A shafts respectfully. Equation 3.2 was used to determine the mass modulus (E_m) for the 6C shaft, however an additional reduction factor of two was needed to match field results, see 3.3.1.1 for additional information. For the 7A shaft Equation 3.1 was used to determine the mass modulus (E_m) of the rock (RQD < 70), while again a reduction factor of two was used. The Osterberg loading for the 6C shaft in Figure 4.2 shows the stiffer behavior of the rock under cyclic loading. This stiffer loading can be attributed to closing of cracks during the initial loading. ABAQUS has the capability for incorporating such material behavior, but for the purpose of this investigation only the initial loading is important. Therefore only the initial loading was modeled and compared.

Figure 4.3 and 4.6 show correlations between field results and modeled results for side shear, which is produced by the upward movement of the Osterberg cells, on the Sagadahoc 6C and 7A shafts respectfully. Cohesion and corresponding strain values were calculated from field results and assigned to the rock/concrete interface layers. The 6C shaft had significant upward movement; while the 7A shaft had little upward movement despite the fact that 7A had worse RQD and strength values. The difference in response can be attributed to the different depths of shafts. Shaft 7A had three times the depth in rock (9 m (30 ft)) compared to shaft 6c (3 m (10 ft)).

Figures 4.4 and 4.7 do not help to calibrate the finite element model; however they show that LOADTEST Inc.'s simplified method used to predict the top-down load curves correlates well with the model. The loading of the shafts was applied at the surface of the overburden soil. A structural failure of the column occurred in the overburden soil before the nominal resistance of the socket was met. Thus the full capacity of the rock socket was not obtained by loading of the shafts in Figures 4.4 and 4.7. The method used by LOADTEST Inc. is restricted to the movement produced by Osterberg cells, which results in the underestimating the capacity of shaft that do not reach failure during testing. The model has shown that there may be a significant amount of capacity for which LOADTEST Inc.'s method does not account.

4.2 Hancock Sullivan Bridge, Sullivan, Maine

4.2.1 Background of Hancock Sullivan Bridge

The Hancock Sullivan Bridge is a 308 m (1,010 ft) long eight-span bridge that carries US Route 1 over the Taunton River. The bridge is located in rural Down-East Maine connecting the towns of Hancock and Sullivan. Construction of the Hancock Sullivan Bridge was completed in the fall of 1999 in order to replace the aging “singing bridge”. One of the more interesting aspects of the Hancock Sullivan Bridge is the combination of driven H-piles and rock sockets used for foundation purposes.

A single load test was conducted for the Hancock Sullivan Bridge. Testing was conducted on a 1372 mm (54 inch) diameter production shaft. Unlike the Bath shafts there was no increase in diameter above the intact rock. A single Osterberg Cell with a 660 mm (26 inch) diameter was used for the testing procedure of the production shaft. The cell was placed at the base of the shaft approximately 4 m (13 ft) below the top of competent rock, which resulted in 3.9 m (12.8 ft) of concrete on rock side shear. Maximum bidirectional applied loads produced by the Osterberg cell were 18 MN (2,025 ton), which resulted in roughly one millimeter (0.04 inch) in upward deflection and negligible downward deflection (LOADTEST, 1998 c).

Subsurface profiles differ greatly along the Taunton River at the site of the new bridge. Along the western (Hancock) side the profile was characterized by steeply dropping bedrock with overlying soil. Rock sockets were deemed as an unsuitable foundation type along the western shore as a result of the subsurface profile. The eastern (Sullivan) shore has less variable bedrock that runs very close or along the surface. Bedrock in the vicinity is identified as Ellsworth Schist, a fine-grained metamorphic rock characterized by quartz veins and extensive folding. Testing on rock cores revealed average intact unconfined compressive strength and elastic modulus values of 70 MPa (10,200 psi) and 17 GPa (2,470 ksi) respectively. Rock cores also showed that RQD values ranged from 60% near the surface to 80% at depths close to the bottom of the tested shaft (MDOT, 1997). For rock properties of the Hancock Sullivan site see Table 4.3.

Table 4.3 Rock Properties of Hancock Sullivan Bridge

RQD[1] %	80.0
E_i[2] GPa (ksi)	17.0 (2,470)
E_m[3] (see Equation 3.2 and $E_m/2$ adjustment for model) GPa (ksi)	3.95 (573)
q_{ui}[4] MPa (psi)	70.0 (10,200)
c [5] (see Figure 3.3) MPa (psi)	14.0 (2,030)
ϕ[6]	40.0
f side shear[7], MPa (psi)	1.7 (247)

1. Rock Quality Designation 2. Intact Rock Elastic Modulus 3. Mass Rock Elastic Modulus 4. Intact Rock Compressive Strength 5. Mass Cohesion 6. Mass Angle of Internal Friction 7. Cohesion between rock and concrete

4.2.2 Results for Hancock Sullivan Bridge

The results for Osterberg Cell testing and top-down loading of the test shaft are outlined in Figures 4.8 – 4.10. Results obtained from field tests conducted by LOADTEST Inc. are presented with a dashed line while results produced by finite element modeling with ABAQUS are displayed as a solid line.

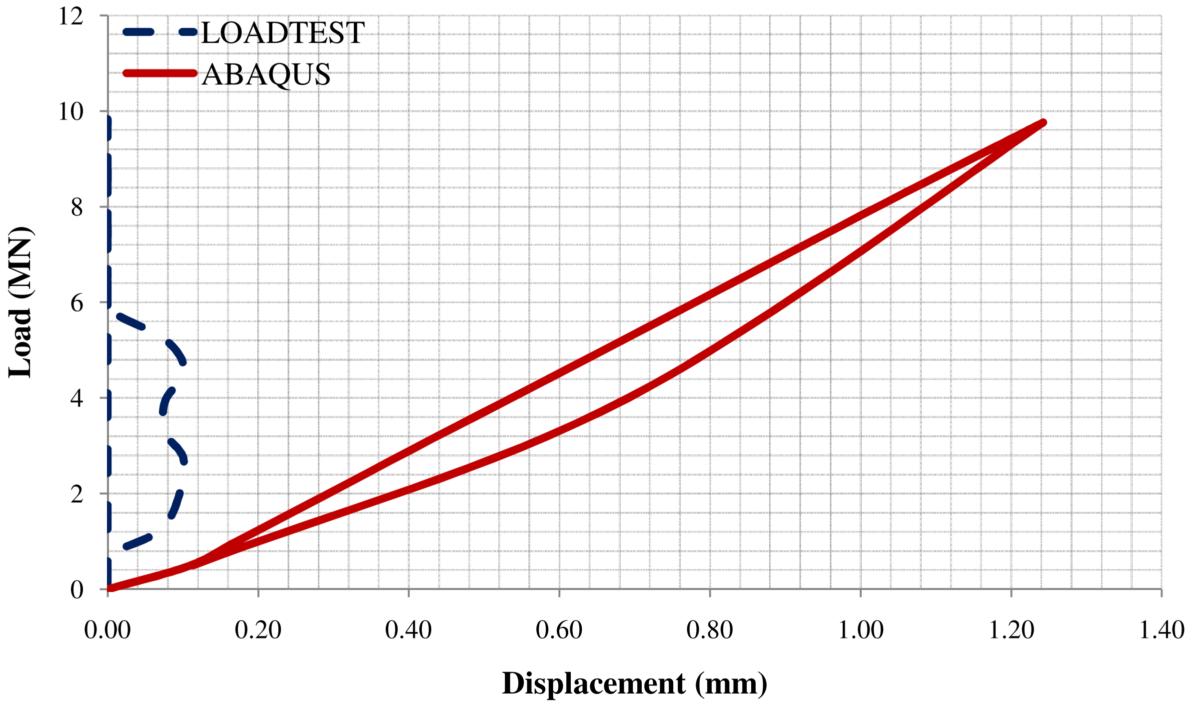

Figure 4.8 Downward O-Cell Results of Hancock Sullivan Bridge

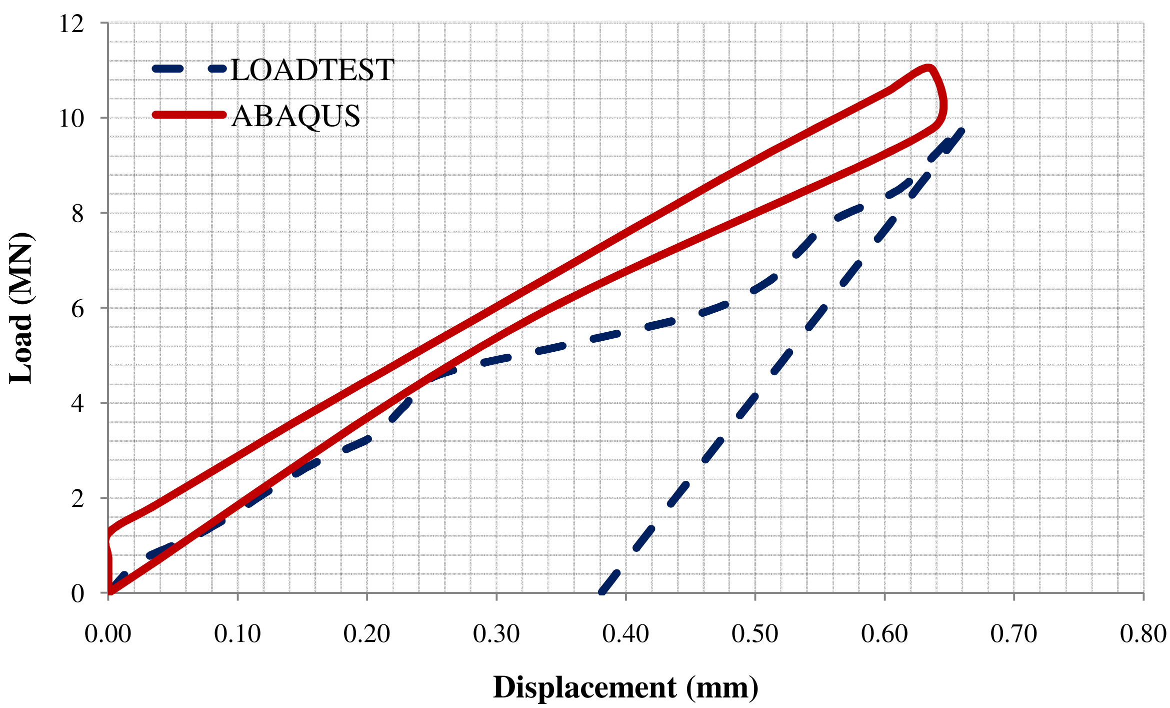

Figure 4.9 Upward O-Cell Results of Hancock Sullivan Bridge

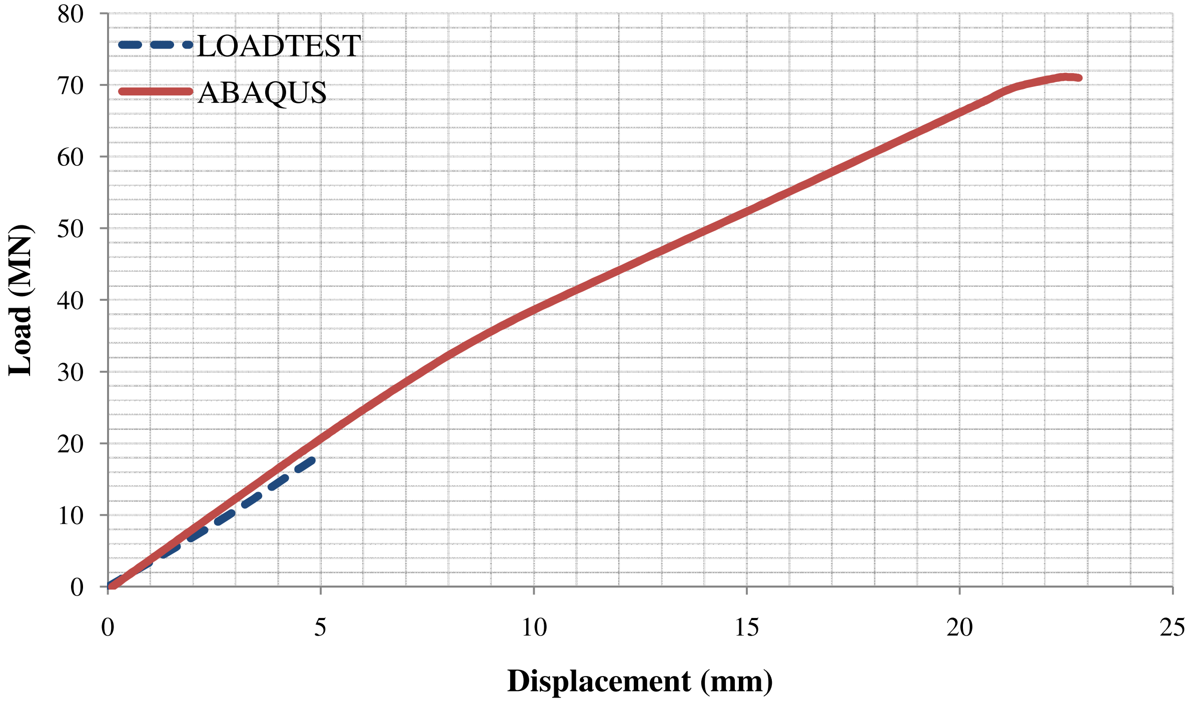

Figure 4.10 Top-Down Load of Hancock Sullivan Bridge

4.2.3 Discussion of Hancock Sullivan Results

Figure 4.8 shows the end bearing results, which are mobilized by the downward movement of Osterberg Cells, for the Hancock Sullivan Bridge. Equation 3.2 was used to determine the mass modulus (E_m) for the rock (RQD > 70). Similar to the Sagadahoc 6C shaft an additional reduction factor of two was needed to match field results. The rock quality at the Hancock Sullivan Bridge was good coupled with the small Osterberg Cell resulted in so little downward movement that field instrumentation measured almost nothing. The model calculated a maximum movement of less than 1.5 mm (0.06 inch), which is almost negligible.

Figure 4.9 shows the correlations between field results and modeled results for side shear of the Hancock Sullivan Shaft. Unlike the Bath shafts, the cohesion is not overcome by the mock Osterberg cell loads. Therefore, there is complete rebound of the interface layer after the loads are released. The field shaft had some rebound, while the lack of complete rebound can be attributed to closing of cracks/joints in the rock.

The top-down load curve shown in Figures 4.10 does not help to calibrate or verify the finite element model. It shows a strong correlation between LOADTEST Inc.'s simplified method and the model. The model has shown that there may be a significant amount of capacity for which LOADTEST Inc.'s method does not account. Similar to the Bath 6C and 7A shafts a structural failure occurred in the column above the rock socket, thus the full potential of the rock socket was not reached.

4.3 Summer St. Bridge, Boston, Massachusetts

4.3.1 Background of Summer St. Bridge

The Summer St. Bridge was constructed as a replacement bridge in the summer of 2003. There are two Summer St. bridge crossings, one over Fort Point channel and one over the reserve channel. This bridge crosses the reserve channel in South Boston.

There were two Osterberg Cell load tests conducted during the construction of the Summer St. Bridge. However, only one of the two tests conducted was carried out to failure of the shaft. Because there were a limited number of shafts carried out to failure, the second shaft was used for calibration. For the testing of the shaft, a single 533 mm (21 inch) diameter Osterberg Cell was used. Rated capacity for the single Osterberg Cell used in the testing of the second Summer St. shaft was 8 MN (900 tons). The shaft was loaded to the rated 8 MN (900 ton) capacity of the Osterberg Cell, which resulted in a complete failure of the upper portion, or side shear portion, of the shaft. The shaft depth into bedrock was rather small compared to the overall height of the shaft. Total height, bedrock to top of soil, was 19 m (62 ft). However the portion imbedded into bedrock was only 3 m (10 ft), and only 1.96 m (6.4 ft) contributed side shear. The test shaft diameter was also small at 0.762 m (2.5 ft) compared to other shafts involved in this study. Above intact rock the shaft had a diameter of 0.915 m (3.0 ft).

The subsurface profile of the Summer St. Bridge consisted of silty clay and organic silt overlying gravel and bedrock. Silt and clay deposits in the vicinity of the second shaft were roughly 16 m (52 ft) deep. Bedrock is described as highly jointed gray argillite. Six borings were performed for the subsurface investigation for this project, including thirteen bedrock core runs of 1.5 meters (4.4 ft) each. RQD of the cores ranged from 13 – 92% with an average value of 58%. The results of uniaxial compressive strength tests performed on six intact portions of rock cores, one from each boring, indicated that strength ranged from 61.7 - 119.6 MPa (8,950 – 17,350 psi) with an average value of 101.0 MPa (14,650 psi) (MHD, 1999). For a summary of the rock properties at the tested Summer St. rock socket see Table 4.4.

4.3.2 Results for Summer St. Bridge

The results for Osterberg Cell testing and top-down loading of the second Summer St. test shaft are outlined in Figures 4.11 – 4.13. Results obtained from field tests conducted by LOADTEST Inc. are presented with a dashed line while results produced by finite element modeling with ABAQUS are displayed as a solid line.

Table 4.4 Rock Properties of Summer St Bridge

RQD[1] %	58.0
E_i[2] GPa (ksi)	6.0 (870)
E_m[3] (see Equation 3.1 and $E_m/2$ adjusted for model) GPa (ksi)	0.5 (72.5)
q_{ui}[4] MPa (psi)	80.0 (11,600)
c[5] (see Figure 3.3) MPa (psi)	3.2 (464)
ϕ[6]	35.0
f side shear[7], MPa (psi)	1.73 (251)

1. Rock Quality Designation 2. Intact Rock Elastic Modulus 3. Mass Rock Elastic Modulus 4. Intact Rock Compressive Strength 5. Mass Cohesion 6. Mass Angle of Internal Friction 7. Cohesion between rock and concrete

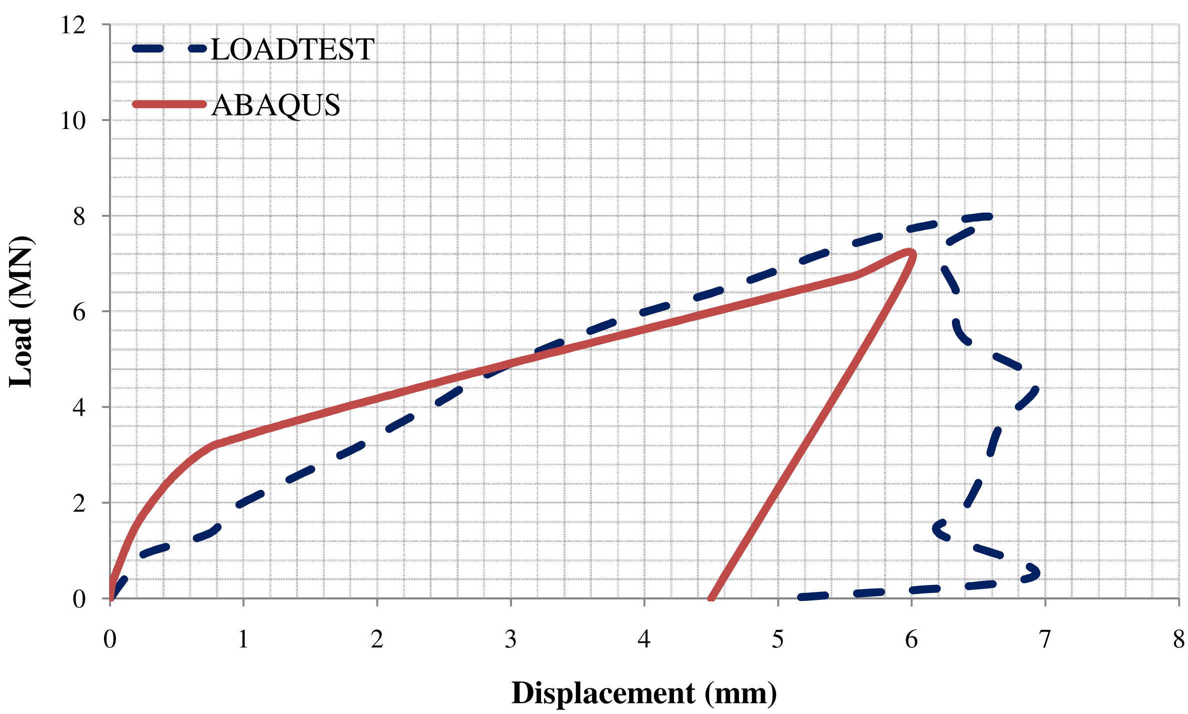

Figure 4.11 Downward O-Cell Results of Summer St. Bridge

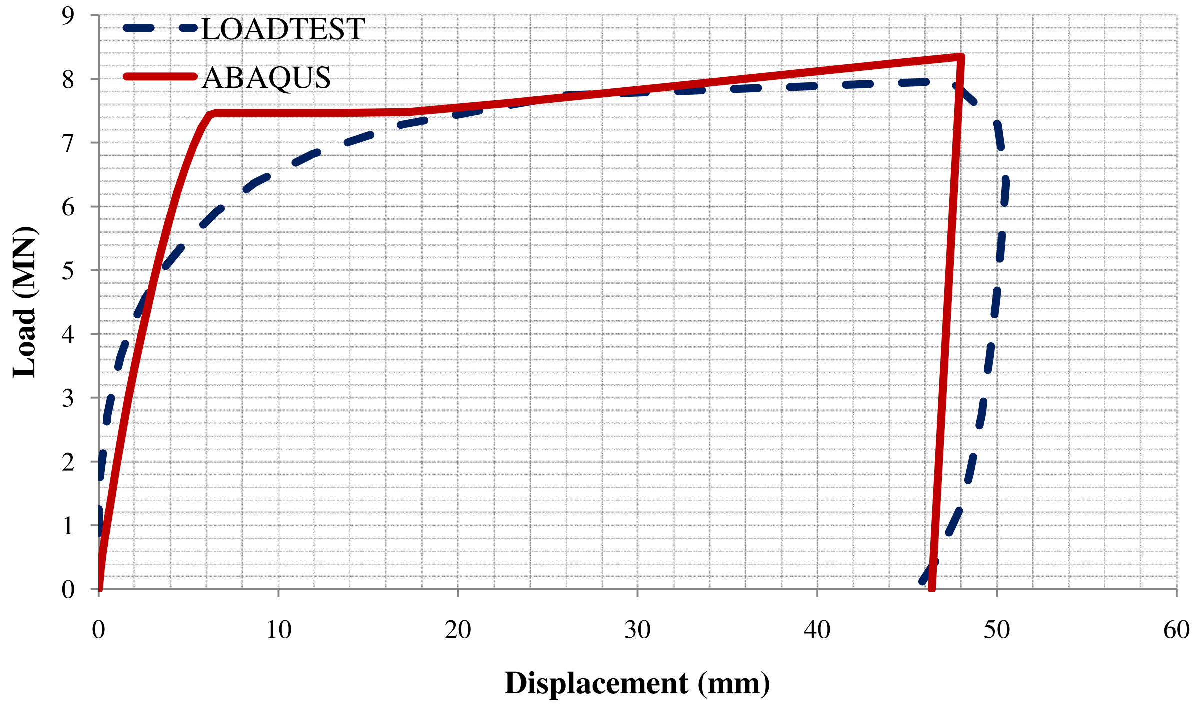

Figure 4.12 Upward O-Cell Results of Summer St. Bridge

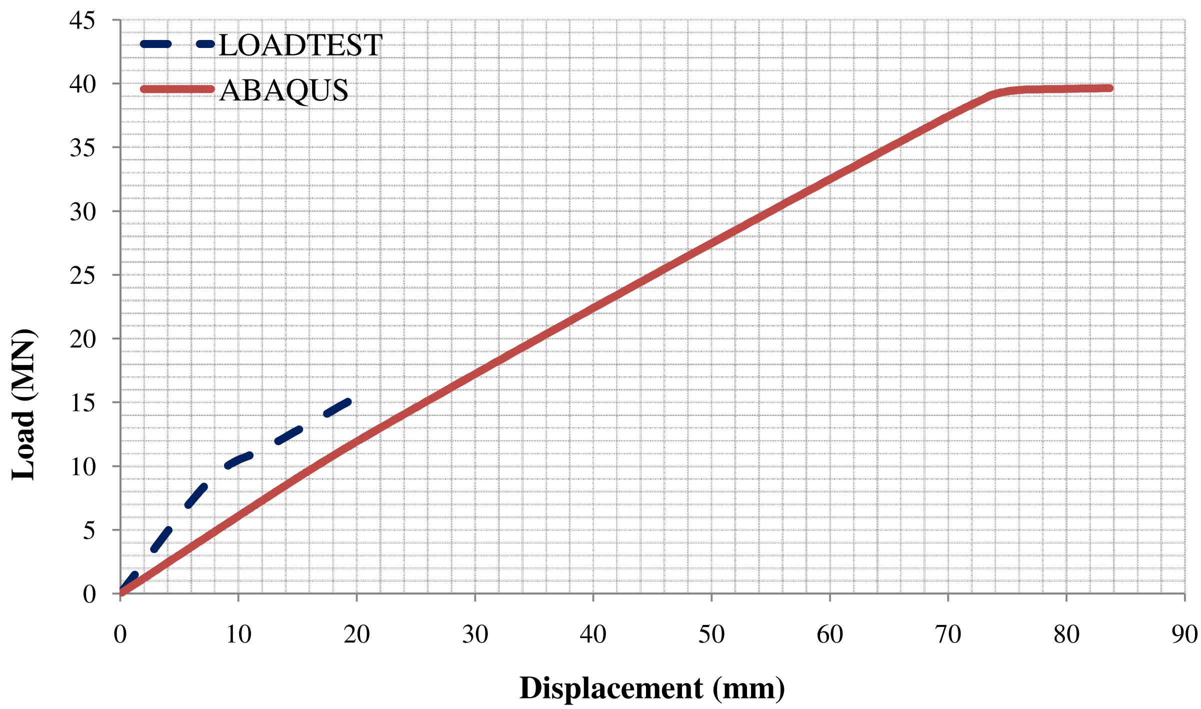

Figure 4.13 Top-Down Load of Summer St. Bridge

4.3.3 Discussion of Summer St. Results

Figure 4.11 shows the end bearing results for the Summer St. Bridge shaft. Equation 3.1 was used to determine the mass modulus (E_m) for the rock (RQD < 70). Similar to the Sagadahoc shafts and Hancock shaft, a reduction factor of two was needed to match field results. Poor rock conditions may explain the lack of elastic recovery in the field test. Similar to other shafts the cracks and joints in the rock become compressed under loading. Compressed joints have little or no capability to expand once loads are removed, unless outside forces, such as frost, are introduced.

Figure 4.12 shows the correlations between field results and modeled results for side shear of the Summer St. shaft. At the point of failure the modeled results come to a sharp point, while field results have a nice rounded curve. This is because only one cohesion/strain pair was used to define the load displacement curve. Had more points been used a more representative curve could have been created. One cohesion/strain pair was used in the calibration stage because one pair was used in the parametric study. Only one pair was used in the parametric study because of some uncertainty; however, an ultimate cohesion/strain pair could be confidently estimated after the calibration of the model.

The top-down load curve presented in Figures 4.13 does not help to calibrate the finite element model. They show a strong correlation between LOADTEST Inc.'s simplified method the model. The model has shown that there may be a significant amount of capacity that LOADTEST Inc.'s method does not account for. Similar to previous shafts, a structural failure occurred in the column above the rock socket, thus the full potential of the rock socket was not reached.

4.4 Moses Wheeler Bridge, Milford/Stratford, Connecticut

4.4.1 Background of Moses Wheeler Bridge

At the time of this study the Moses Wheeler Bridge is still under construction, however initial testing for drilled shafts has been conducted at this time. The Moses Wheeler Bridge connects the towns of Milford and Stratford, Connecticut. It carries Interstate 95 over the Housatonic River. Estimates indicate 135,000 vehicles use the Moses Wheeler Bridge on a daily basis. When replacement of the Moses Wheeler Bridge is completed, it will utilize 35 three m (10 ft) diameter drilled shafts as support for the 400 m (1,300 ft) long 41 m (136 ft) wide anticipated superstructure (CDOT, 2010).

Two test shafts were initially tested. The first of which was tested with an Osterberg Cell and the second tested with statnamic load testing equipment. The shaft tested with Osterberg Cell equipment was 1220 mm (48 inch) in diameter and extended two m (7 ft) into competent bedrock. There was 1.43 m (4.7 ft) of concrete to rock side shear. The lower 0.97 m (3.2 ft) had a diameter of 1.22 m (4 ft), while the upper 0.46 m (1.5 ft) had a diameter of 1.37 m (4.5 ft). The concrete only extended 2.13 m (7 ft) above the top of rock, which left 6.4 m (21 ft) of the shaft empty. A large portion of the shaft was left unfilled because engineers were interested in the capacity of the rock only. One 870 mm (34 inch) diameter cell was used at the base of the shaft. A maximum bi-directional load of 9 MN (1,000 tons) was reached during testing before the maximum side shear value was reached. For testing using statnamic techniques a single 762 mm (30 inch) diameter shaft that extended only 305 mm (12 inch) into bedrock was tested. There was no bonding or any interaction between the sides of the shaft and the rock walls because a casing was inserted prior to the placement of concrete. This was done because engineers wanted to examine the bearing capacity of the rock below the top weathered layer (LOADTEST, 2003; Applied Foundation Testing inc., 2004).

The subsurface profile of the Moses Wheeler Bridge consisted of fill with varying composition and compactness, organic silts and sands, sand/gravel, glacial till, and schist bedrock. Fill layers were often thin, usually less than two meters (7 feet). While silt, sand and gravel layers ranged from 3 to 11 meters (10 to 36 feet). Bedrock was reported as mica schist with RQD values ranging from 58% to 79%. Uniaxial compressive strength tests showed that intact specimens had a failure strength of 33.5 MPa (4,860 psi). A rock mass strength of 12.5 MPa (1,810 psi) was also provided within test data, which correlated well with our estimate for this project of 12 MPa (1,740 psi) (LOADTEST 2003; GeoDesign, 2002). For a summary of rock properties at the Moses Wheeler test shafts see Tables 4.5 and 4.6.

Table 4.5 Rock Properties of Moses Wheeler Osterberg Test

RQD[1] %	80.0
E_i[2] GPa (ksi)	41.0 (5,950)
E_m[3] (see Equation 3.1 and $E_m/2$ adjustment for model) GPa (ksi)	9.5 (1,380)
q_{ui}[4] MPa (psi)	30.0 (4,350)
c[5] (see Figure 3.3) MPa (psi)	6.0 (870)
ϕ[6]	40.0
f side shear[7], MPa (psi)	1.4 (203)

1. Rock Quality Designation 2. Intact Rock Elastic Modulus 3. Mass Rock Elastic Modulus 4. Intact Rock Compressive Strength 5. Mass Cohesion 6. Mass Angle of Internal Friction 7. Cohesion between rock and concrete

Table 4.6 Rock Properties of Moses Wheeler Statnamic Load Test

RQD[1] %	30.0
E_i[2] GPa (ksi)	9.5 (1,380)
E_m[3] (see Equation 3.1 and $E_m/2$ adjustment for model) GPa (ksi)	0.82 (119)
q_{ui}[4] MPa (psi)	33.0 (4,790)
c[5] (see Figure 3.3) MPa (psi)	0.2 (29)
ϕ[6]	35.0
f side shear[7], MPa (psi)	N/A

1. Rock Quality Designation 2. Intact Rock Elastic Modulus 3. Mass Rock Elastic Modulus 4. Intact Rock Compressive Strength 5. Mass Cohesion 6. Mass Angle of Internal Friction 7. Cohesion between rock and concrete

4.4.2 Results for Moses Wheeler Bridge

The results for Osterberg Cell testing, statnamic testing, and top-down loading of the Moses Wheeler Bridge are outlined in Figures 4.14 – 4.17. Results obtained from field tests conducted by LOADTEST Inc. or Applied Foundation Testing Inc. are presented with a dashed line while results produced by finite element modeling with ABAQUS are displayed as a solid line.

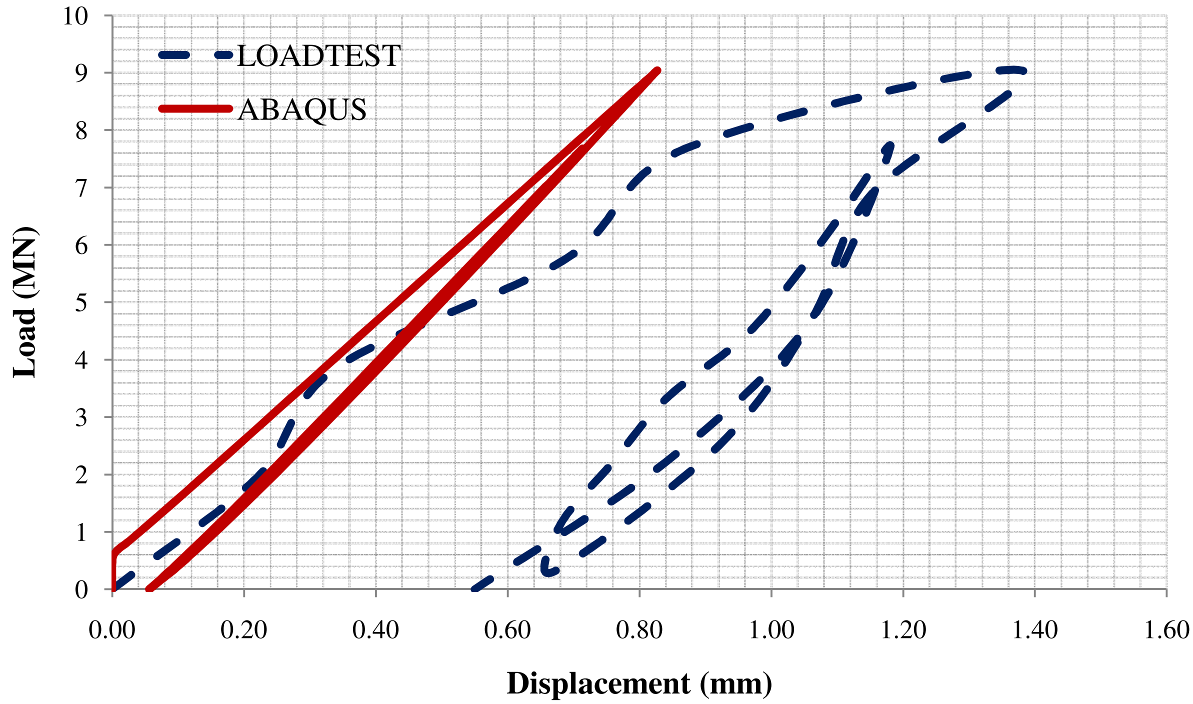

Figure 4.14 Downward O-Cell Results of Moses Wheeler Bridge

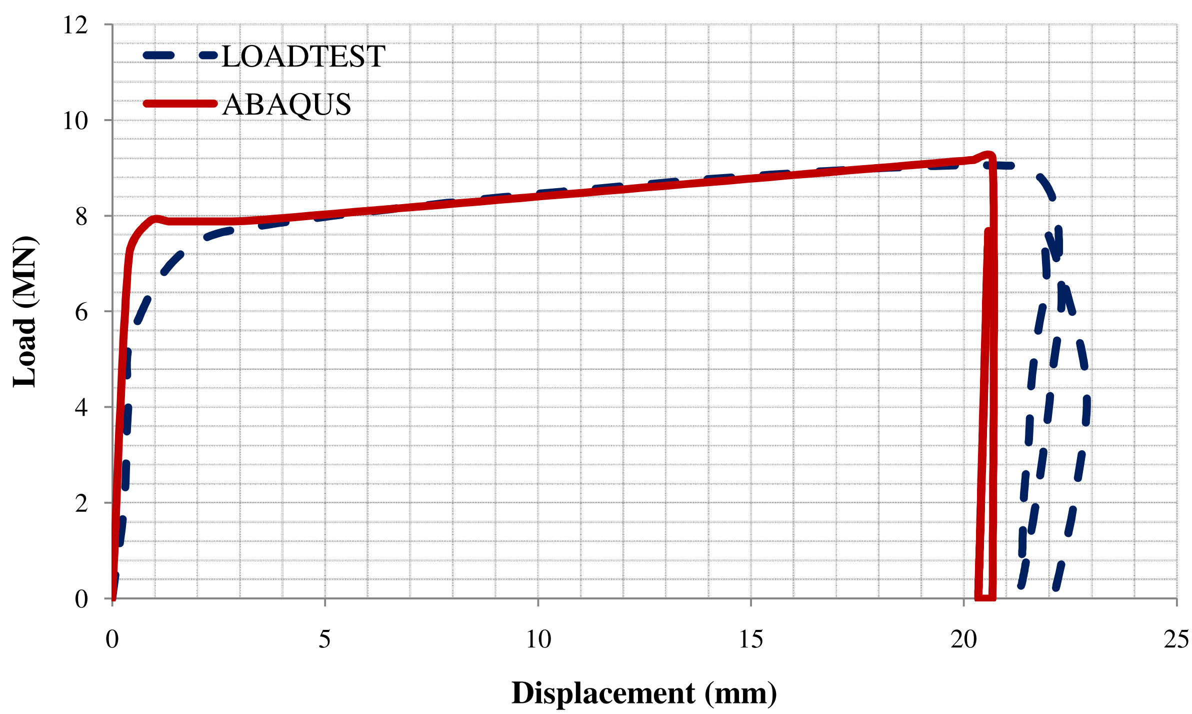

Figure 4.15 Upward O-Cell Results of Moses Wheeler Bridge

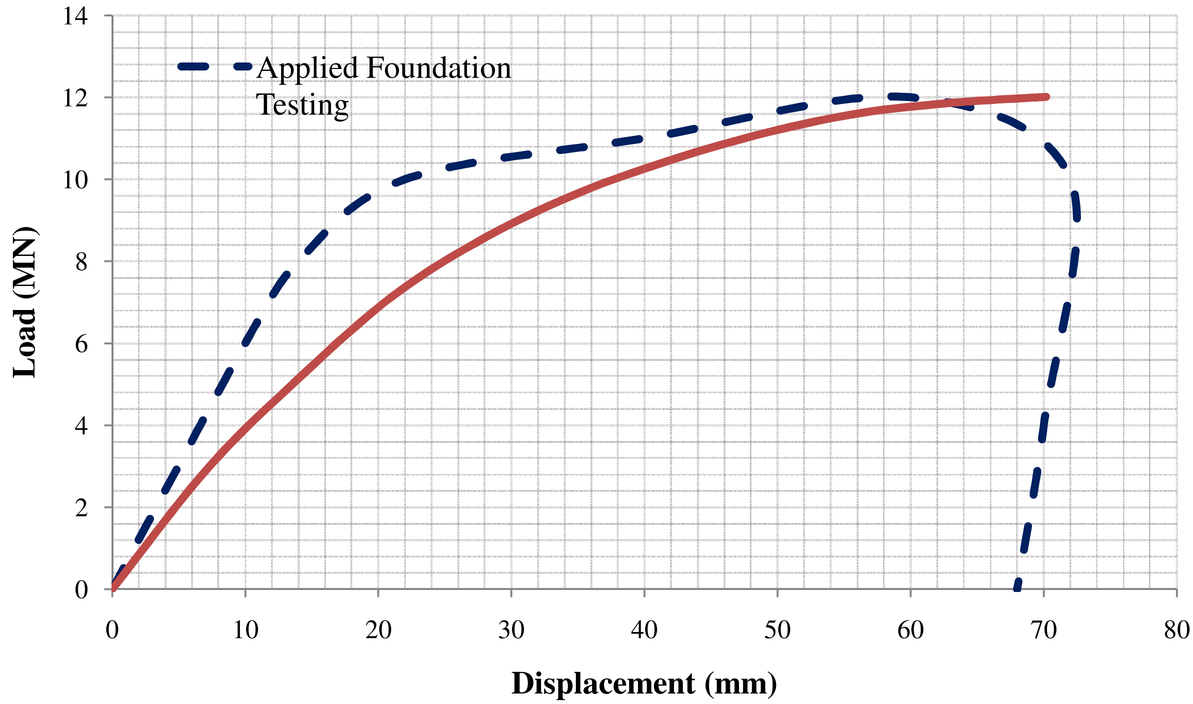

Figure 4.16 Static Load Results of Moses Wheeler Bridge

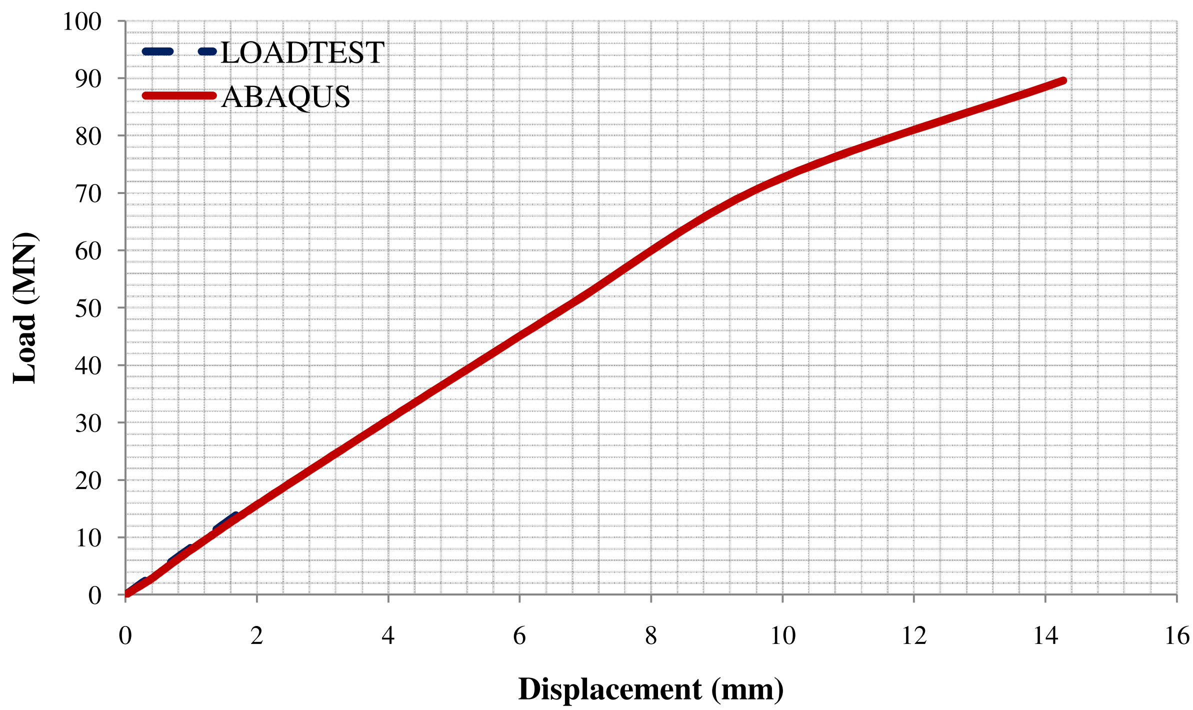

Figure 4.17 Top-Down Load of Moses Wheeler Bridge

4.4.3 Discussion of Moses Wheeler Bridge Results

Figure 4.14 shows the end bearing results, which is mobilized by the downward movement of Osterberg Cells, for the Moses Wheeler Bridge. Equation 3.2 was used to determine the mass modulus (E_m) for the rock (RQD > 70). Similar to the Sagadahoc 6C and Hancock shafts an additional reduction factor of two was needed to match field results. Displacements were so small that it is hard to assess how closely related the field and modeled shaft results are. However, for the first millimeter of displacement the two seem to follow the same general path. The field shaft showed permanent displacement when the load was removed and a stiffer reload curve. This unloading and reloading aspect was not modeled since the initial loading was important for this investigation.

Figure 4.15 shows correlations between field results and modeled results for side shear of the Moses Wheeler Bridge shaft. Like the Summer St. shaft at the point of failure the modeled results come to a sharp point, while field results have a nice rounded curve. This is because only one cohesion/strain pair was used to define the load displacement curve. Had more points been used a more representative curve could have been created.

A top-down loading of a second shaft was conducted at the Moses Wheeler site. This test was conducted to analyze the end bearing only of the shaft. Results of the field test and modeled shaft are present in Figure 4.16. The strong correlation helps to show that that the equation used to determine mass modulus of the rock (E_m) and mass strength (q_m) work well in the model after an additional factor of 2 was applied to the rock modulus ($E_m/2$). Although the rock quality at the Osterberg Cell shaft site was good, the quality was poor at the statnamic loading shaft site (RQD < 70).

The top-down load curve shown in Figures 4.17 does not help to calibrate or verify the finite element model. In this case the two curves are almost identical up to the max value obtained by the LOADTEST inc.'s simplified method. The model has again shown that there may be a significant amount of capacity that LOADTEST inc.'s method does not account for.

4.5 Route 18 over George St. New Brunswick, New Jersey

4.5.1 Background of Route 18 over George St.

The Route 18 Bridge over George St. is a newly constructed bridge that carries Route 18 over George St. in the town of New Brunswick, NJ. Reconstruction of the previous Route 18 Bridge began in 2004 as a multi-stage part of the 200 million dollar rehabilitation of Route 18 project. The bridge is supported by 60 drilled shafts that extend into the underlying shale bedrock of the New Brunswick area.

A single initial Osterberg Load Cell test was performed for the construction of the Route 18 Bridge. The test shaft was 1.8 m (5.9 feet) in diameter and extended 9 m (26 ft) into bedrock. 8.67 m (28.4 ft) of the depth contributed to the concrete on rock side shear. Above the intact rock the diameter of the shaft increased to 1.85 m (6.1 ft), which increases the end bearing area. A single 870 mm (34 inch) Osterberg Cell was used in the test and reached a maximum bi-directional load of 27.5 MN (3,000 tons). The test resulted in large downward movement and much less upward movement of the shaft (LOADTEST, 2006). These results were different from others collected in the study, and illustrated why the metamorphic and igneous rocks of the Northeast are different from sedimentary rocks.

The project site is located within the Piedmont Geographic Province, which lies at the foot of the Appalachian Highlands and just above the coastal plain. In general, the subsurface stratigraphy encountered on the site consists of 1 – 5 m (3 – 16 ft) of fill overlying 2 – 4 m (6 - 13 ft) of sandy and clayey silts intermixed with gravel overlying brownish red shale of the Brunswick Formation. Unconfined compressive strength of intact shale was between 40.7 – 128.9 MPa (6,050 – 18,700 psi) with an average value of 71.4 MPa (10,350 psi). RQD and core recovery values both ranged from 0 – 100% with average values of 69% and 93%, respectively. RQD and core recovery values represent samples from both upper weathered portion of the rock and underlying intact rock mass, which explain the high degree of variability (Gannet Fleming, 1999; Site-Blauvelt, 2002). A summary of the rock properties at the Route 18 rock socket test site are provided in Table 4.7.

Table 4.7 Rock Properties of Route 18 over George St.

RQD[1] %	90.0
E_i[2] GPa (ksi)	14.0 (2,030)
E_m[3] (see Equation 3.1 and $E_m/2$ normal adjustment, also $E_m/30$ to match field results) GPa (ksi)	5.25 (761) & 0.35 (50.8)
q_{ui}[4] MPa (psi)	65.0 (9,430)
c[5] (see Figure 3.3) MPa (psi)	13.0 (1,890)
ϕ[6]	40.0
f side shear[7], MPa (psi)	1.60 (232)

1. Rock Quality Designation 2. Intact Rock Elastic Modulus 3. Mass Rock Elastic Modulus 4. Intact Rock Compressive Strength 5. Mass Cohesion 6. Mass Angle of Internal Friction 7. Cohesion between rock and concrete

4.5.2 Results for Route 18 over George St.

The results for Osterberg Cell testing of the Route 18 Bridge are shown in Figures 4.18 – 4.20. Results obtained from field tests conducted by LOADTEST Inc. are presented with a dashed line, while ABAQUS results are presented in a solid line.

Bearing capacity was over-predicted by a factor of ten using the rock property correlations used for metamorphic/igneous rocks and finite element modeling. Despite good RQD and intact strength values of the rock, the bearing capacity of the production shaft was poor. One possible explanation is that sedimentary rocks undergo more disturbance than do igneous or metamorphic rocks during the drilling process. Sedimentary rocks may be more susceptible to physical weathering with exposure to water and air during drilling, resulting in less bearing capacity of the production shaft.

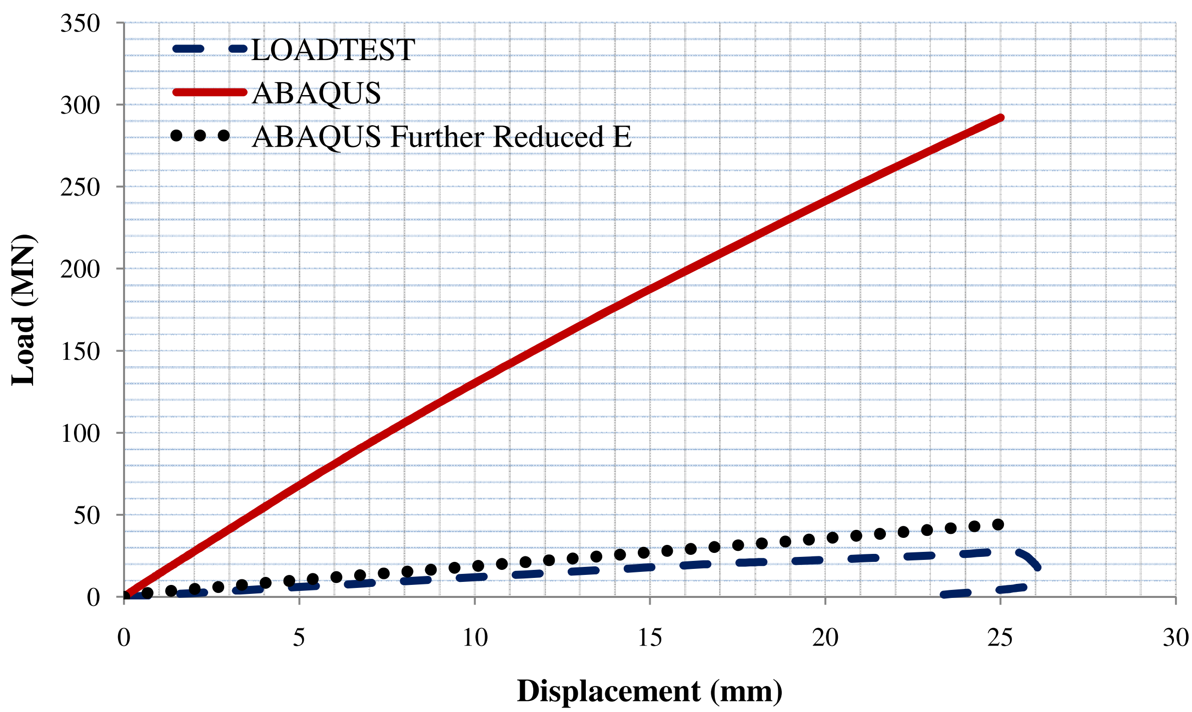

Figure 4.18 Downward O-Cell Results of Route 18 Bridge

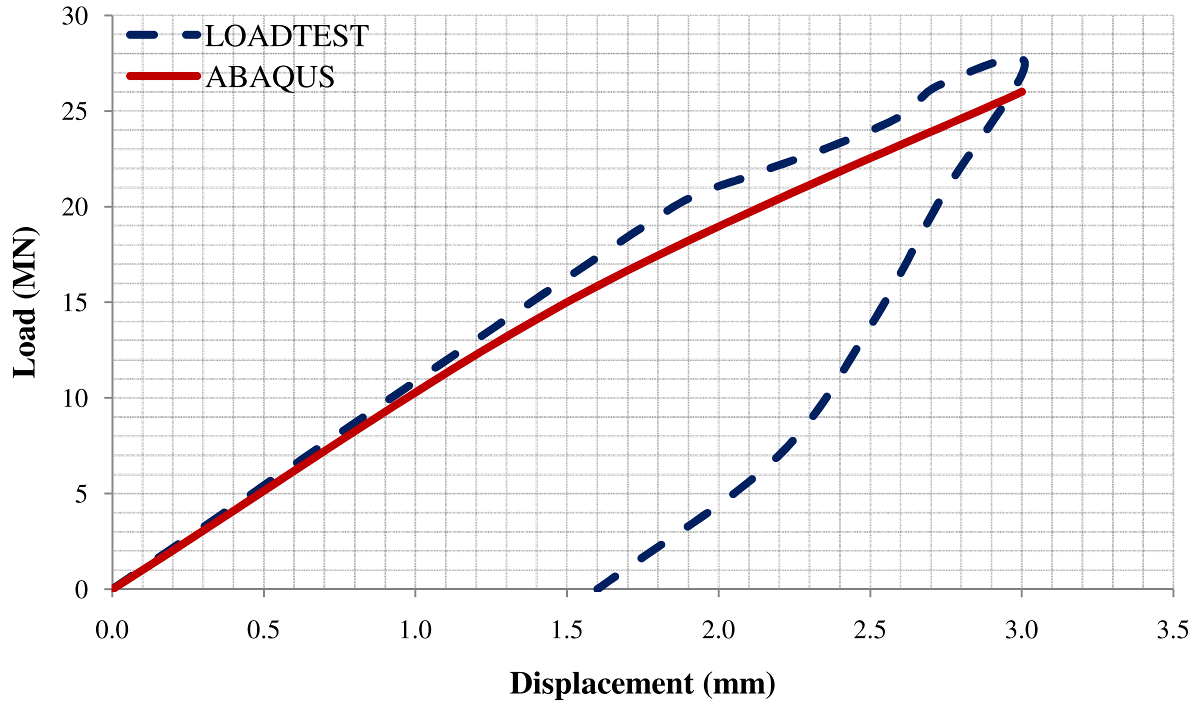

Figure 4.19 Upward O-Cell Results of Route 18 Bridge

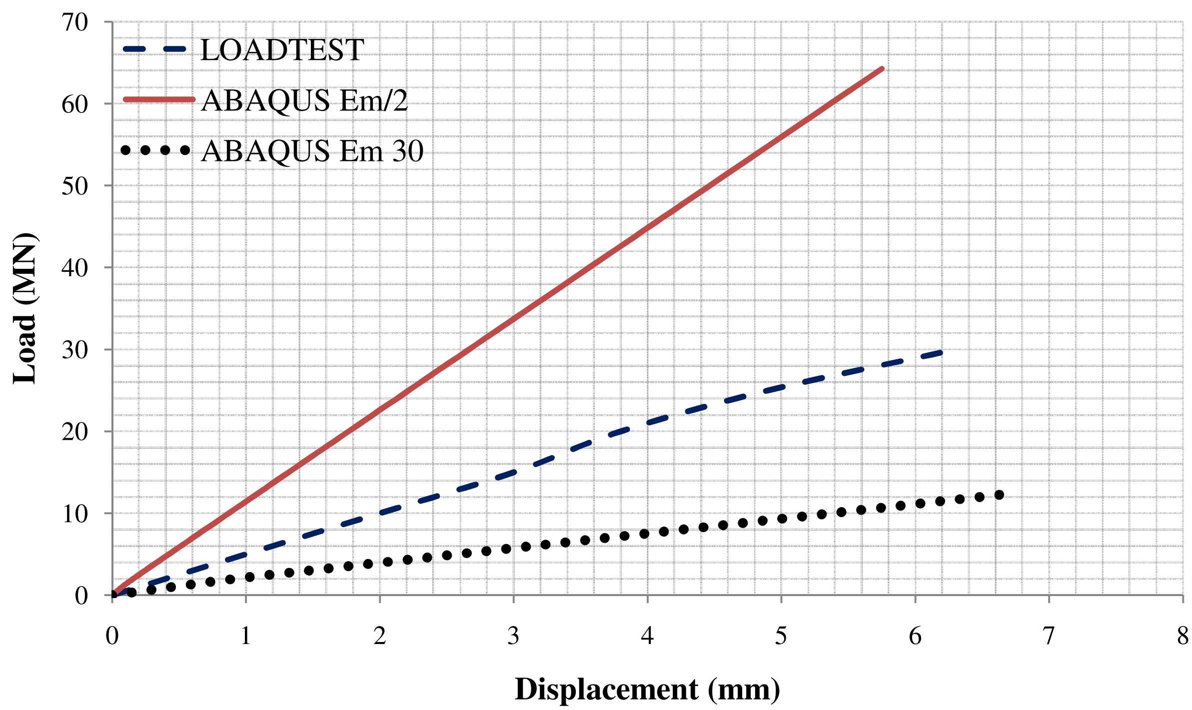

Figure 4.20 Top-Down Load of Route 18 Bridge

The side shear below the limiting value shown in Figure 4.19 behaves similar to that of metamorphic/igneous rock. However, the shear limit was not obtained since there was only 3 mm (0.12 inch) of upward movement.

4.5.3 Discussion of Route 18 over George St. Results

Figure 4.18 shows the end bearing results for the Route 18 Bridge shaft. Equation 3.2 was used to determine the mass modulus (E_m) for the rock (RQD > 70). Similar to the Sagadahoc shafts, Summer St. shaft, and Moses Wheeler shaft, additional reduction of the mass modulus was made (E_m / 2). However, results were still off by a factor of 10. In order to match field results for end bearing an additional reduction factor of 15 needed to be applied to the elastic modulus mass (E_m) on top of the normal reduction factor of 2. Figure 4.18 shows end bearing results for field testing, ABAQUS testing with normal elastic modulus reduction factors (2), and ABAQUS testing with reduction factors necessary to match field tests (30). The field results showed a large amount of non recoverable displacement, despite high intact strengths and good RQD values. Likely sedimentary rock is highly damaged during drilling, which is not accounted for in the model. The need for the extra reduction factor is believed to be the cause of disturbance in the sedimentary rock during drilling.

Figure 4.19 shows the correlation between field results and modeled results for side shear of the Route 18 Bridge shaft. The side shear value of 1.60 MPa (232 psi) is typical of metamorphic/igneous rock. The side shear correlated well with field results at low displacements; however, it is unsure how well these values would compare to field results at larger displacements.

Figure 4.20 displays results of top-down loading for anticipated results based on field tests (dashed line), ABAQUS modeling using $E_m/2$ (solid line), and ABAQUS modeling using $E_m/30$. The ABAQUS model using $E_m/2$ over-predicted the capacity compared to LOADTEST Inc., although not to the extent that bearing capacity alone was over-predicted. When the elastic modulus was reduced by 30 the model under-predicted the capacity compared to LOADTEST Inc.. In both cases the ABAQUS model ultimately had a structural column failure in the overburden soil, thus the capacity of the rock socket was not reached. Overall there was a poor correlation between ABAQUS models and field results for the Route 18 Bridge over George St.

4.6 Results for Model Calibration

To match the models to the field tests in hard rock required that rock properties in the model be adjusted for both side shear and end bearing. This adjusting revealed much about the nature of the rock socket and the relationships between side shear and end bearing to that of laboratory test values. It also allowed end bearing modulus values to be found from Osterberg tests.

4.6.1 Side Shear

For side shear the major result was that the shear stress at failure was in a narrow band of strengths from 1.4 MPa (203 psi) to 1.7 MPa (247 psi), with an average of 1.6 MPa (232 psi) for those rocks with an unconfined strength greater than 30 MPa (4,350 psi). There were clear side shear failures with significant displacements at the Summer St. and Moses Wheeler shafts. These values of side shear are well below the shear strength of intact concrete or intact rock, which could be expected to be at least 15 MPa (2,180 psi). This indicates a preferential shear plane along the contact that appears to be controlled by the smoothness of the shaft side, or possibly drilling debris at the contact as well as possible damage to the rock along the contact surface.

It is of interest to compare the values of side shear obtained for the shafts tested in the Northeast and examined in this study to those in the literature. Kulhawy and Phoon (1993) give a relation of unconfined strength to side shear resistance for a number of drilled shafts both in rocks and clays. The rocks covered are primarily weak rocks with an unconfined strength of less than 20 MPa (2,900 psi), although there are a few medium strength rocks similar to some of the rocks in this study. Kulhaway and Phoon's relationship between unconfined strength and side shear is shown in Figure 4.21.

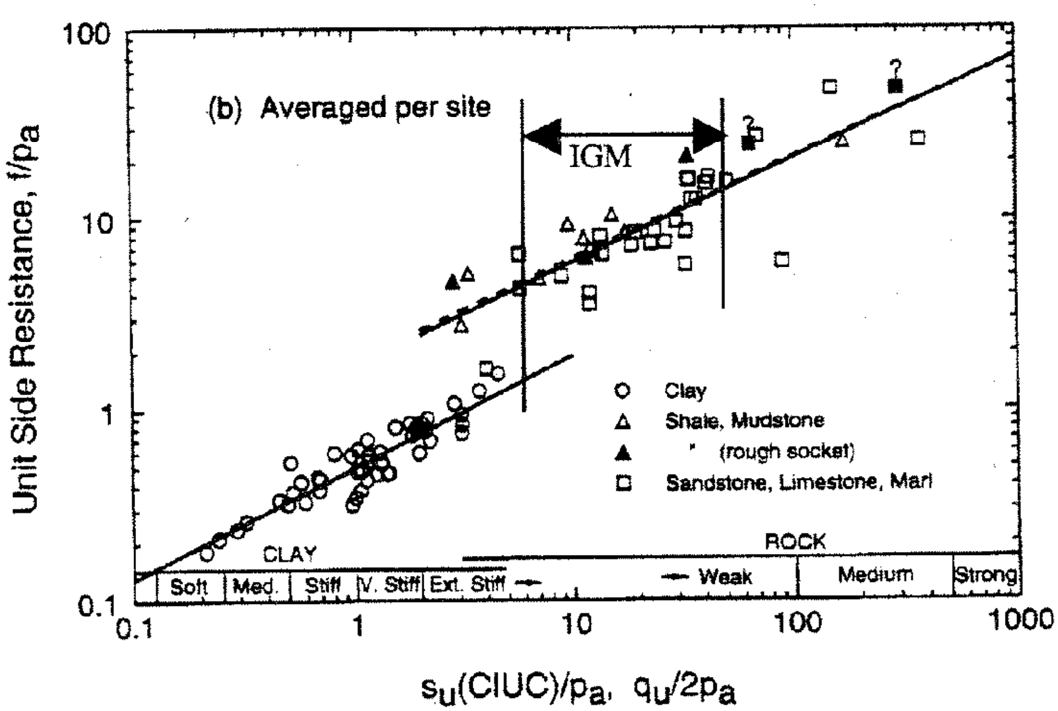

Figure 4.21 Side Resistance Versus Geomaterial Strength (Turner, 2006)

The normalized (by a nominal atmospheric pressure of 0.1 MPa (14.5 psi)) unconfined strengths and side shear strengths for the tests in this study are given in the same format in Figure

4.22. A comparison shows that the side shear strengths in this study are roughly ½ of the strengths found by Kulhaway and Phoon (1993). This indicates that smoothness of the walls, damage to the side walls or excess drilling debris on the sides have lowered the values below what is expected on other drilling projects.

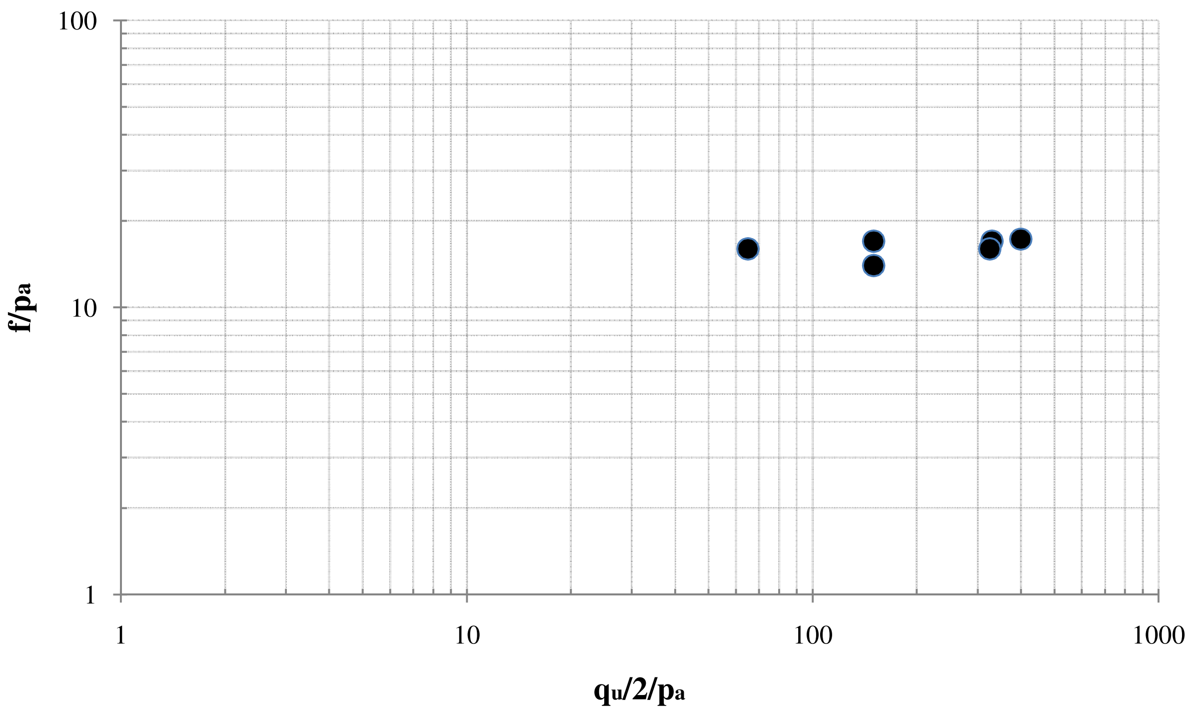

Figure 4.22 Side Resistance Versus Rock Strength

The causes of the low shear along the side walls can be caused by the nature of the rock or by the drilling process. Perhaps the foliations of the metamorphic rock along the shaft in this study open up more than other rocks. This may result in a damaged zone close to the surface of the rock. This would indicate that some non-vertical grooving that penetrates below the damaged zone along the side would raise side shear considerably. Most drilling occurs in softer rock, and so many drillers may have equipment more suitable for softer rock. Perhaps with drills more suitable to hard rock the thickness of damaged zone on the side wall can be reduced. Also possible deposition of drilling cuttings on the side walls may have reduced the shear strength.

Another possibility is that shafts in hard rock are not artificially roughened to the extent that softer rocks are. This would mean that there is less dilation as concrete and rock asperities move over one another in hard rock. Essentially there is a smooth surface with post drilling debris, thus there is little dilation of the rock and concrete and minimal bonding of the two.

The shear stress at failure from the Osterberg tests can also be compared to the AASHTO expressions for determining the side shear resistance, q_s (see Equation 2.7). The results in Table 4.8 show that the limit shear resistance from AASHTO is lower than measured or inferred values from the Osterberg tests. The Osterberg mean values are about twice the mean values of the unit shear resistance related to rock strength.

Table 4.8 Comparison of Modeled Side Shear to AASHTO Unit Shear Resistance

Site	q_s[1], MPa (psi)	f[2], MPa (psi)
Bath 6C	0.8 (116)	1.7 (247)
Bath 7A	0.4 (58)	1.6 (232)
Hancock Sullivan	1.1 (160)	1.7 (247)
Summer St.	1.0 (145)	1.7 (247)
Moses Wheeler	0.7 (102)	1.4 (203)
Rt. 18 over George St.	1.2 (174)	1.6 (232)

1. Unit side shear resistance related to rock (Equation 2.7) 2. Modeled unit side shear

The value of side shear of 1.6 MPa (232 psi) that was found in this calibration for hard rock was used in developing the responses for various diameters and depths of shafts. The only test with an unconfined strength greater than 30 MPa (4,350 psi) and an RQD close to 50% (the rest had RQD greater than 80%) was Summer St.. It had a side shear strength of 1.7 MPa (247 psi), so the effect of the drilling process or the nature of the rock were more important than the RQD for determining the side shear.

4.6.2 End Bearing

The major result for the end bearing was that there was a large difference of the response of the metamorphic/igneous rocks as compared to the one shale rock (sedimentary). The resultant modulus of the shale was about 1/10 of that of the metamorphic/igneous rocks as a result of the shale disintegration during drilling. Although there could be some structural damage to the metamorphic/igneous rocks during drilling, there was no indication of disintegration from water and air exposure as with the shale. Another significant result was that the mass elastic modulus of the hard rock was lower than expected from published relationships given by Equation 3.1 and 3.2 as developed by Bieniawski (1978) that considered RQD and the modulus of the intact rock.

The lack of disintegration during drilling in the hard rock is perhaps a distinguishing characteristic of hard rock compared to weaker rocks. This property allows the end to be cleaned of debris with washing without reducing the strength. Lack of disintegration allows the end bearing to be more reliably counted on in hard metamorphic/igneous rock to develop significant design capacity.

In comparing the values needed in the model to match test values, the values of mass modulus in this study were approximately ½ of those obtained by the Bieniawski relations as shown in Figure 4.23. The reasons for the lower values as compared to values in other rock could be related to the particular nature of the metamorphic/igneous rock. It also may reflect the limitations of using Rock Quality Designation (RQD) to find mass modulus rather than using a more sophisticated rock quality system like Rock Mass Rating (RMR). It also could be related to possible damage during the drilling process. If the drilling process is causing a reduction in the mass modulus, then the drilling process likely has room for improvement.

For larger diameter shafts in hard rock, the modulus values are important in determining the service limit state resistance of rock sockets. For smaller diameter shafts, the strength limit state resistance for rock bearing capacity becomes an important limiting factor. The mass bearing capacity based on the quality of the rock as given in Figure 3.3 compared to the bearing capacity of intact rock (RQD = 100%) was used to provide a ratio that was applied to intact cohesion (obtained by dividing the unconfined strength by two) to obtain a value of cohesion for rock mass. There was no indication from the matching that this had to be changed.

As a result, the parametric study uses mass modulus values based on the Bieniawski equations divided by two. The mass cohesion of the rock was found from Figure 3.3 based on RQD and the unconfined strength of intact rock without further adjustment.

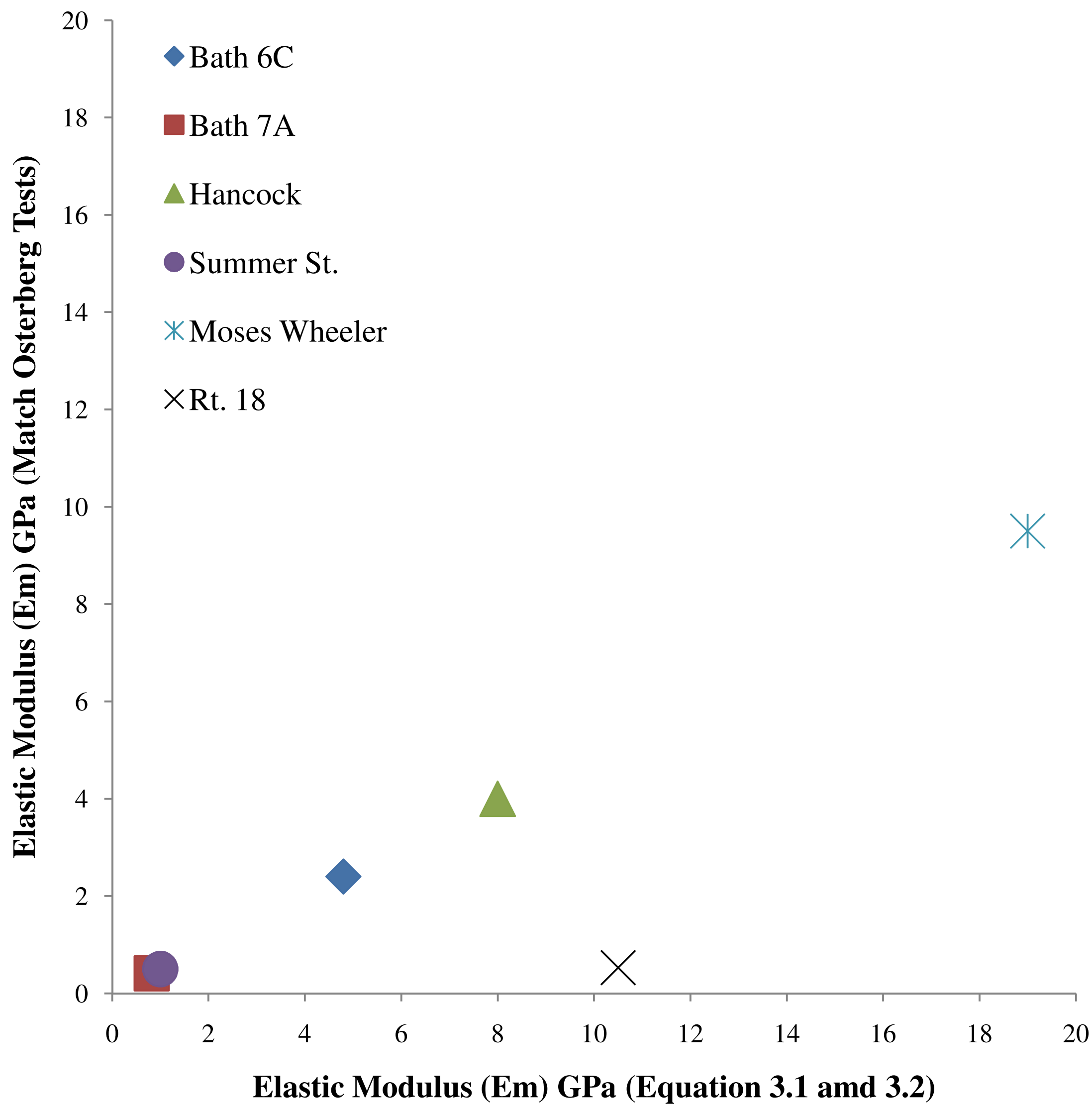

Figure 4.23 Relationship of Elastic Modulus for Equations and Tested Values

Chapter Five

Design Method Incorporating Side Shear and End Bearing

Once the finite element model for shafts in rock was calibrated using test results from field tests, the model was used to find the response for sockets with varying depths, diameters, and rock quality. The top-down loading and resulting displacements of the shaft at the top of rock formed the basis for an axial capacity design method that incorporates both side shear and bearing resistance.

5.1 Parametric Study Models

The finite element model discussed in Chapter Three and calibrated in Chapter Four was utilized to provide more information on the behavior of Rock Socketed Drilled Shafts. For the purpose of this study different socket diameters, depths, and rock properties were analyzed to determine the contributions of side shear and end bearing resistance to the displacements of shafts subjected to top-down loading.

5.1.1 Shaft Dimensions

The majority of common/economical shaft dimensions and rock properties that may be used or encountered in the field were covered within the study. Shaft dimensions include only the part that was founded within hard rock. Shaft lengths and diameters in overburden soil layers above the top of rock are completely separate and independent from those included in this study. Five separate socket depths ranging from 0-11 m (0-36 ft) were included. For every depth four separate diameters were used and for every depth/diameter combination two different Rock Quality Designation (RQD) values were used for the surrounding rock. This resulted in 40 separate sockets of varying depth, diameter, and rock quality. For each socket, the resistance for eleven different displacements (1, 2, 3, 4, 5, 6, 8, 10, 15, 20, and 25) was analyzed. A summary of socket depths, diameters, and RQD values are presented in Figure 5.1.

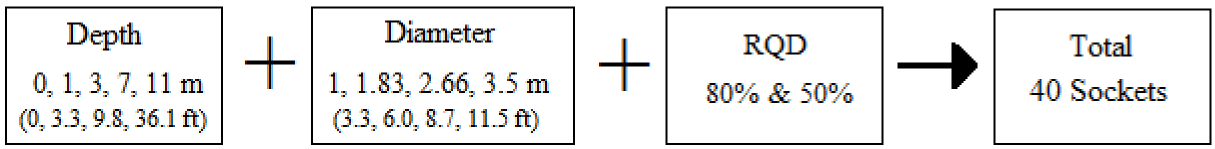

Figure 5.1 Shaft Dimensions for Parametric Study

5.1.2 Bedrock Material Properties

Bedrock material properties were based on results from projects used in the calibration stage. The five shafts that were used for calibrating the finite element model were analyzed to determine mean values for rock mass modulus (E_m) and shear of the interface layer, which were dependent on the RQD values. It was the original intention to have three or more RQD values for every socket dimension; however, there was limited data available for other RQDs in rock that met the "hard rock" criteria. The five sockets used were split into good quality and poor quality rock based on RQD values, which ranged from 75-85% and 50-58% respectively. Good quality samples were obtained from the Bath-Woolwich 6C, Moses Wheeler, and Hancock shafts. Poor quality samples were gathered from the Bath 7C and Summer St. shafts.

Rock material values that were influential on the base resistance or the side resistance for the parametric study were then determined by averaging values. To capture the proper end bearing resistance, the mass elastic modulus (E_m) of the rock was most influential, but other contributing factors were the friction angle (ϕ) and mass cohesion (c_r) of the rock. Side shear is mostly influenced by the shear (f) of the interface; however, the interface layer is between the concrete shaft and surrounding rock. Thus it can be affected by the elastic modulus, friction angle, and cohesion of the rock or concrete. Under the conditions used in the study the model calibration indicated that the material properties of the concrete and rock played a small role in the interface layer and the side shear capacity. Our model captures the interface layer by using shear strength data from field tests. A summary of mean rock properties for both RQD ranges are presented in Table 5.1. Concrete material values are based on 28 MPa (4000 psi) concrete, identical to those used in creating and calibrating the finite element model.

Table 5.1 Summary of Parametric Study Material Values

Material Property	RQD = 50%	RDQ = 80%
Elastic Modulus E (rock) GPa (ksi)	0.46 (66.7)	5.40 (783)
Friction Angle ϕ (rock)	35^o	40^o
Cohesion c (rock) MPa (psi)	1.85 (268)	9.00 (1,310)
Cohesion f (interface layer) MPa (psi)	1.65 (239)	1.70 (247)

5.1.3 Loading Techniques

Loading in the parametric study was top-down, as would be applied during typical bridge construction and service. Top-down load testing was used to determine the response when both end bearing and side shear are resisting. As was done in the calibration stage, displacement criteria was placed on the loading surface via a velocity vector, while calculations on the resulting reaction forces at the nodes that make up the surface were made to determine the magnitude of the applied load on the surface.

5.2 Limitations of Drilled Shafts Due to Column Resistance

Concrete column loads are limited by nominal shear resistance of the concrete. The soil within the overburden provides some confinement. However this confinement is minor compared to the confinement provided by steel reinforcement within the shaft. Confinement within the column itself comes from either ties or spiral reinforcing that holds the longitudinal bars together. In seismic regions or for shafts built for high axial strength limit state resistance, spiral reinforcing is generally used, while ties are sufficient for most other applications (Wight et al.,2009).

Equation 5.1 from AASHTO LRFD Bridge Specification 2007 provides the axial nominal resistance of a column without bending moments. Under normal circumstances the nominal resistance values would be further reduced by a resistance factor (ϕ), which usually is equal to 0.75. As a result axial strength limit state resistance (P_r) would equal 75% of the nominal axial resistance (P_n).

$$P_n = 0.85 * (0.85 * f'_c*(A_g - A_{st}) + f_y * A_{st}) \qquad \text{(Equation 5.1)}$$

P_n = nominal axial resistance
f'_c = specific strength of concrete at 28 days (MPa)
A_g = gross area of section (m^2)
A_{st} = total area of longitudinal reinforcement (m^2)
f_y = specific yield strength of reinforcement (MPa)

In order to reflect the nominal resistance of the four different shaft diameters used for the parametric study, column calculations were performed for each diameter. Table 5.2 summarizes the column calculation. Refer to Appendix A for complete calculations of column capacity for four sizes. These values will be used to help select the diameter of shaft for design.

Table 5.2 Column Capacity

Shaft Diameter (m)	P_n MN (ton)	P_r MN (ton)
1.00 (3.3 ft)	21 (2,360)	16 (1,800)
2.00 (6.6 ft)	84 (9,450)	63 (7,100)
3.00 (9.8 ft)	190 (21,350)	142 (15,950)
3.50 (11.5)	258 (29,000)	194 (21,750)

Shaft Diameters are often larger above the rock socket. Rock sockets are smaller in diameter than the shaft to make the drilling process and the installation of the rock socket easier on the contractor. The change in diameter creates a lip at the top of the rock socket that can add to the bearing capacity. When the shaft diameter above the rock socket is increased then an increased axial shaft capacity can be used corresponding to the increased diameter. Consideration of the bearing capacity of this lip are addressed in section 5.6.

After reviewing upwards of 25 drilled shaft plans provided by LOADTEST Inc., including those used for calibration of the finite element model, shaft diameters are generally increased by 0.15 m (0.5 ft) above bedrock. For instance five of the six shafts used in the calibration stage had an increased diameter of 0.15 m (0.5 ft) above hard rock. The only exception was the Hancock Sullivan Bridge, which had bedrock within 0.2 m (0.7 ft) of the ground surface.

5.3 Parametric Study Findings

The figures following indicate the relationship of socket service limit state resistance to displacement at the top of the rock socket, for various socket diameters, socket depths, and for two different rock qualities. Column strength limit state resistances without bending moments are also indicated on the figures. Figures 5.2 – 5.7 provide an example of design charts at 5, 15 and 25 mm (0.20, 0.59, 0.98 inch) displacements. For design charts see Appendix C.

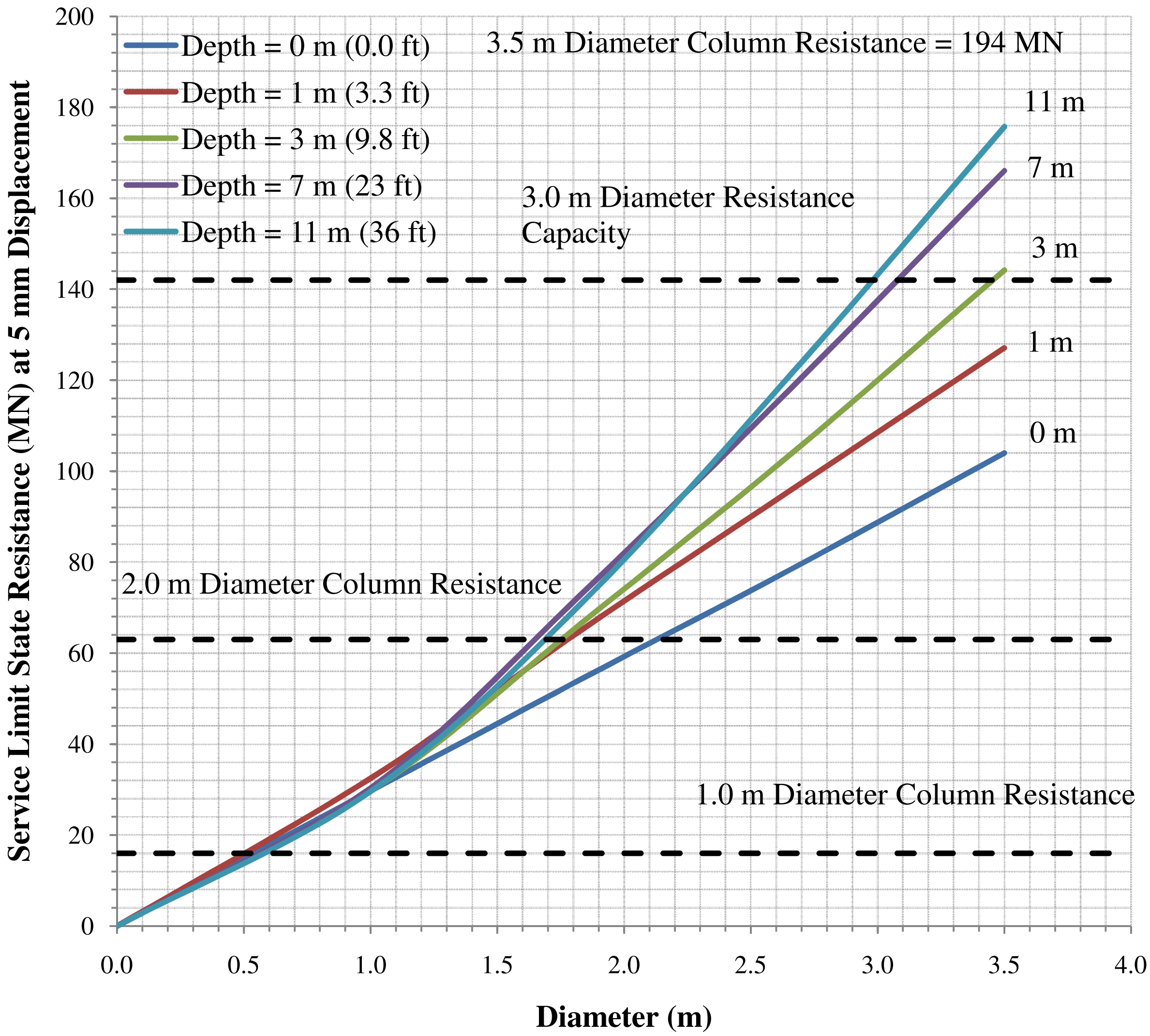

Figure 5.2 Service Limit State Resistance at 5 mm (0.20 inch) Displacement for RQD = 80%

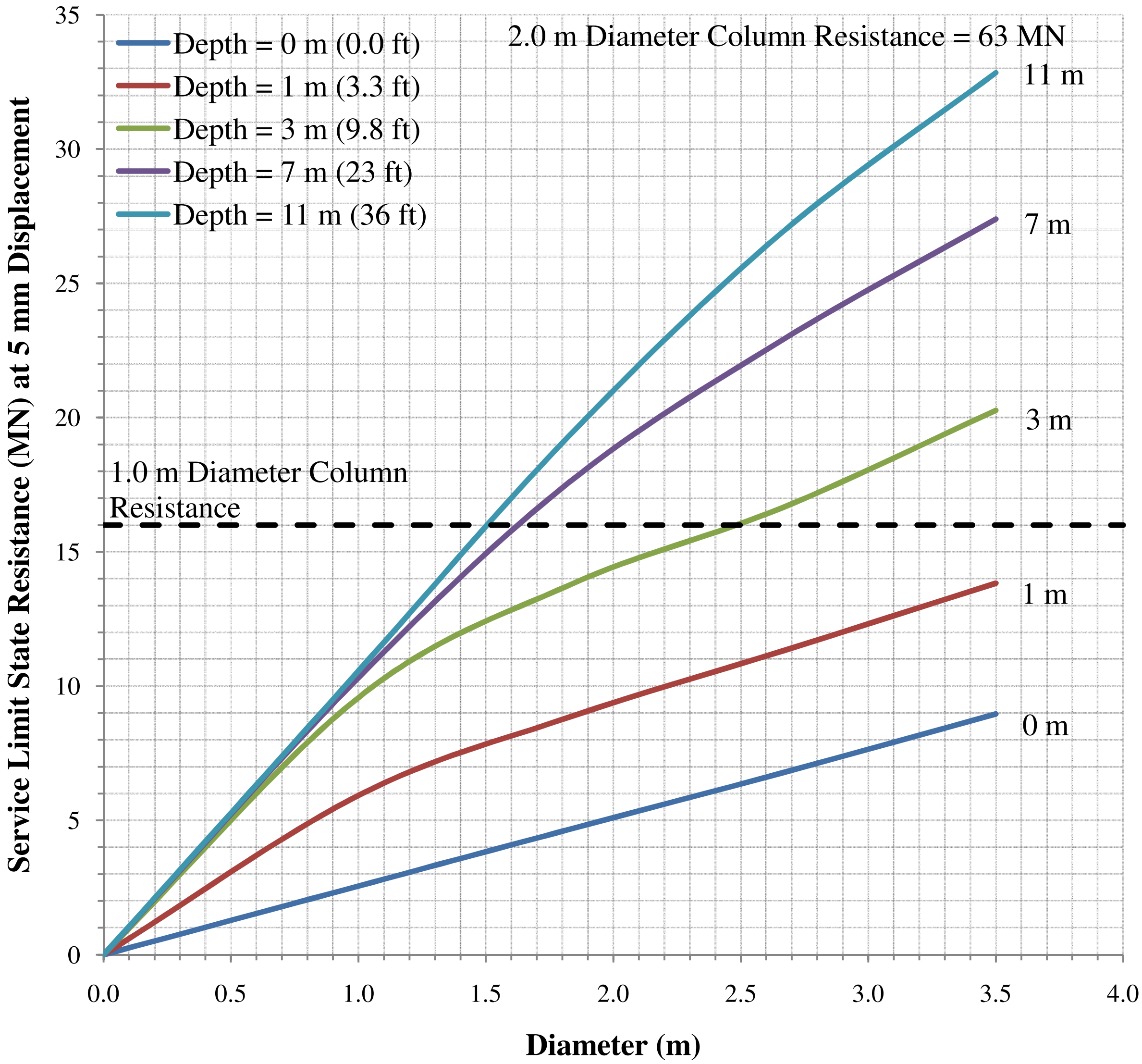

Figure 5.3 Service Limit State Resistance at 5 mm (0.20 inch) Displacement for RQD = 50%

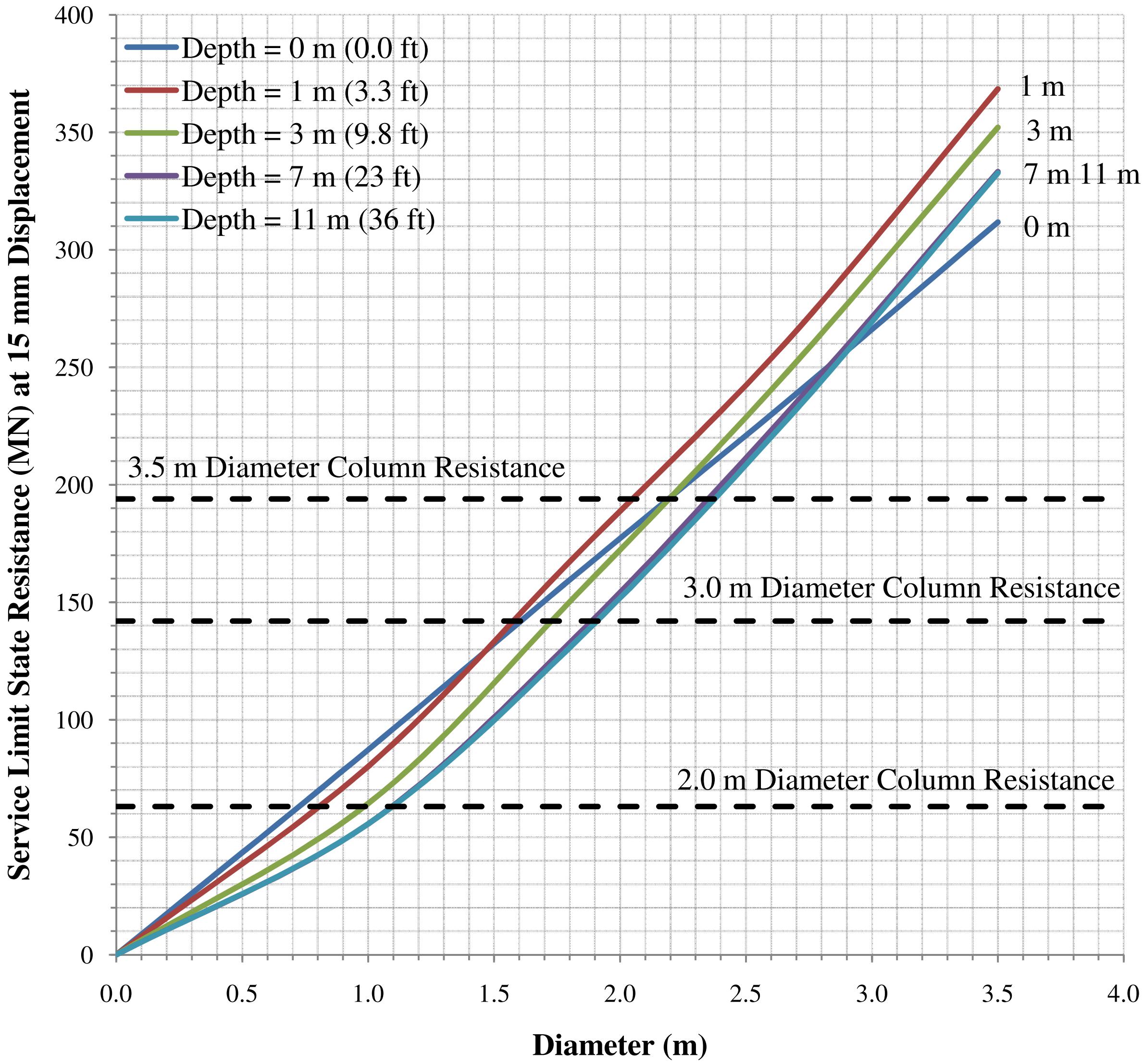

Figure 5.4 Service Limit State Resistance at 15 mm (0.59 inch) Displacement for RQD = 80%

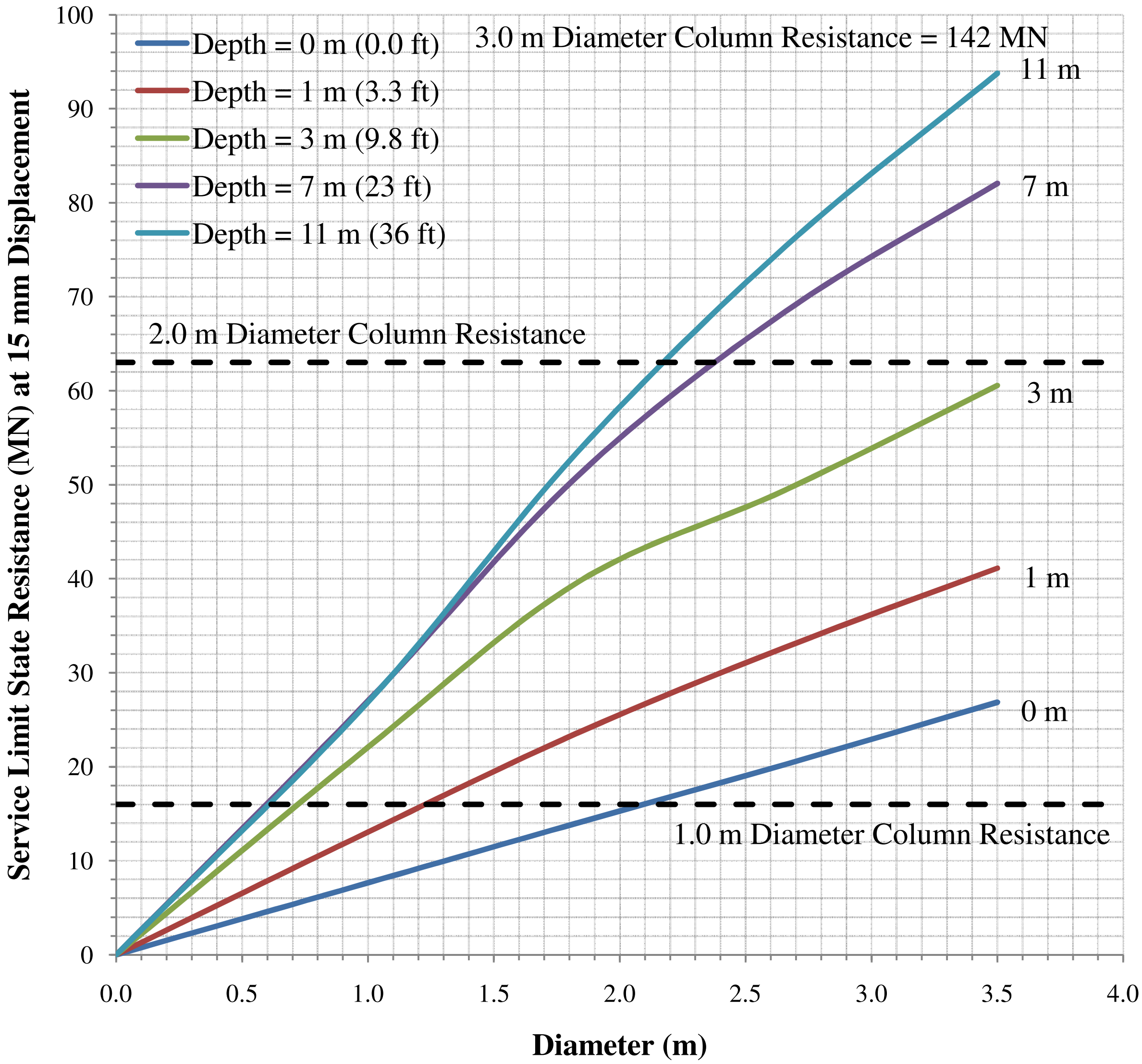

Figure 5.5 Service Limit State Resistance at 15 mm (0.59 inch) Displacement for RQD = 50%

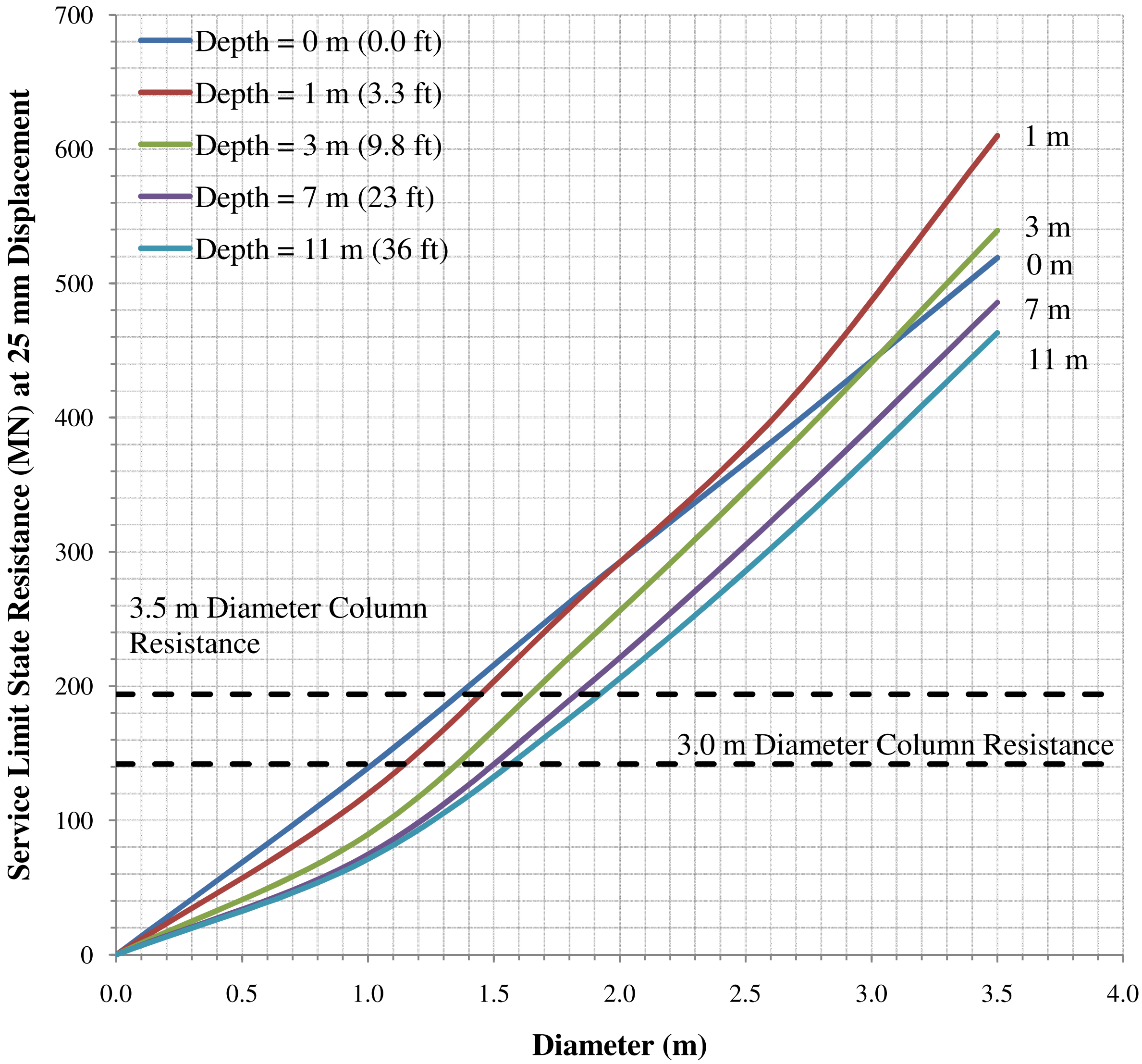

Figure 5.6 Service Limit State Resistance at 25 mm (0.98 inch) Displacement for RQD = 80%

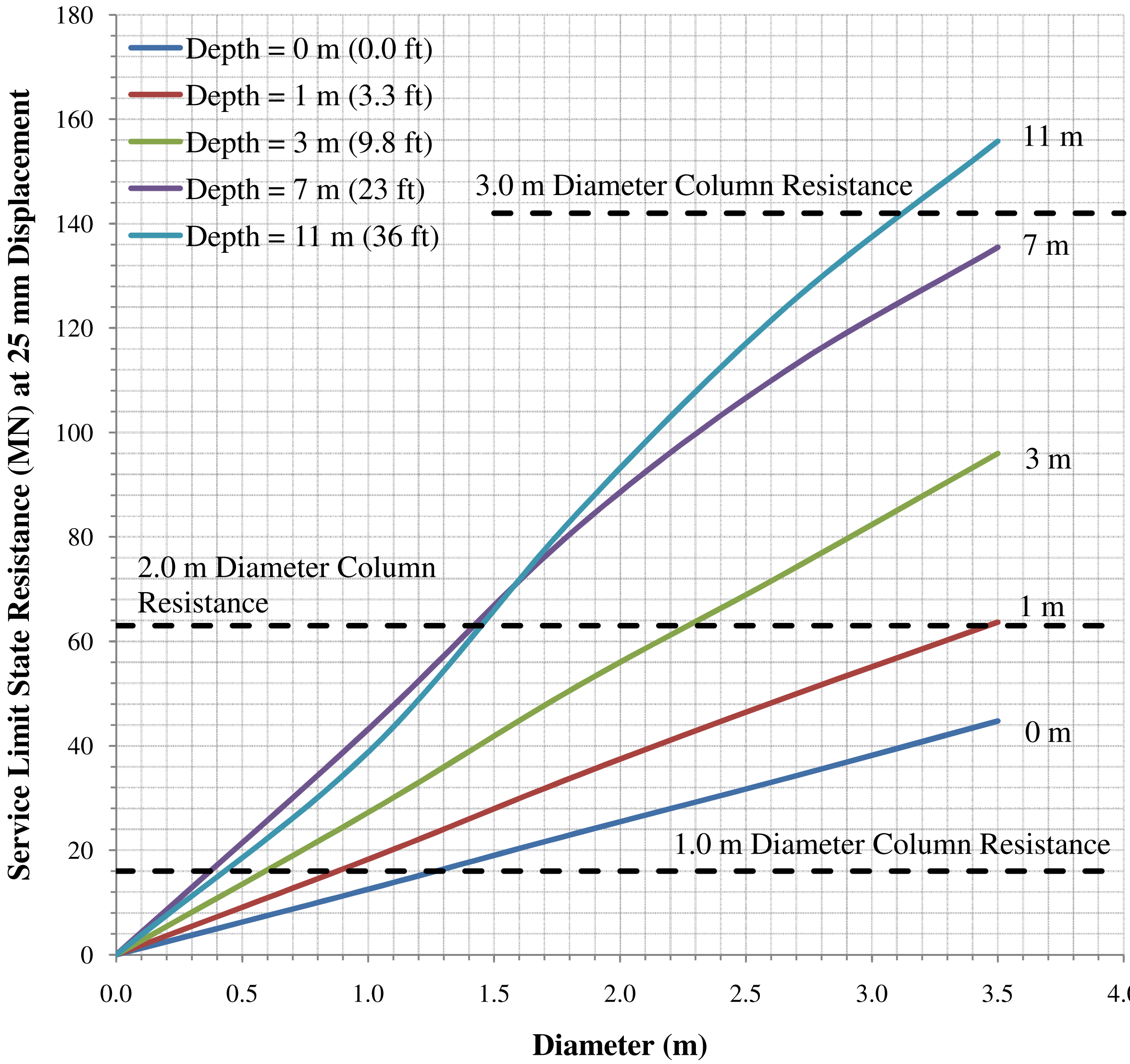

Figure 5.7 Service Limit State Resistance at 25 mm (0.98 inch) Displacement for RQD = 50%

5.4 Explanation of Results

The quality of the rock has a substantial effect on the results. For a given displacement of the top of the shaft (at top of rock level), a good quality rock (RQD = 80%) has 2.5 - 13 times the resistance of a poor quality rock (RQD = 50%). This can be seen by comparing results of Figure

5.2 to 5.3, Figure 5.4 to 5.5, and Figure 5.6 to 5.7. The lower resistance in poor quality rock reflects the lower mass elastic modulus of the rock below the tip of the shaft.

Some of the results displayed in Figures 5.2 -5.7 may seem counter intuitive, especially those founded in better quality rock. For instance Figure 5.6 shows that a shaft founded on top of good quality rock (Depth = 0) can support more load at a displacement of 25 mm (0.98 inch) than a shaft founded 11 meters deep into good quality rock. Concrete shaft compression is the cause of this anomaly. The 11 meter (36 ft) concrete shaft is compressing in addition to the displacement of the underlying rock. An ABAQUS test was conducted with two shafts of identical diameter (1 m (3.3 ft)) and surrounding rock quality (RQD = 80%), but different depths, to verify this assumption. The first test was conducted on a 1 m (3 ft) diameter shaft with a socket depth of 1 m (3 ft). When subjected to a 25 mm (0.98 inch) top-down displacement as in Figure 5.6 there was 16 mm (0.63 inch) of displacement at the base of the shaft. The second shaft had a diameter of 1 m (3 ft) and a socket depth of 11 m (36 ft). When subject to the same top displacement as the first shaft, 25 mm (0.98 inch), the base only deflected 5 mm (0.20 inch). Therefore there was 11 mm (0.43 inch) more compression in the concrete of the 11 m (36 ft) deep shaft than in the 1 m (3.3 ft) deep shaft. Thus the 11 m (36 ft) deep shaft mobilized less end bearing resistance than the 1 m (3.3 ft) deep shaft.

Shafts founded in poorer quality rock do not show this anomalous behavior. Figure 5.7 illustrates that longer shafts have higher resistances for a specified top displacement of 25 mm (0.98 inch). Additional figures have been included (Figure 5.8 – 5.10) to show stress distribution with depth as well as bearing resistance independent of top displacement.

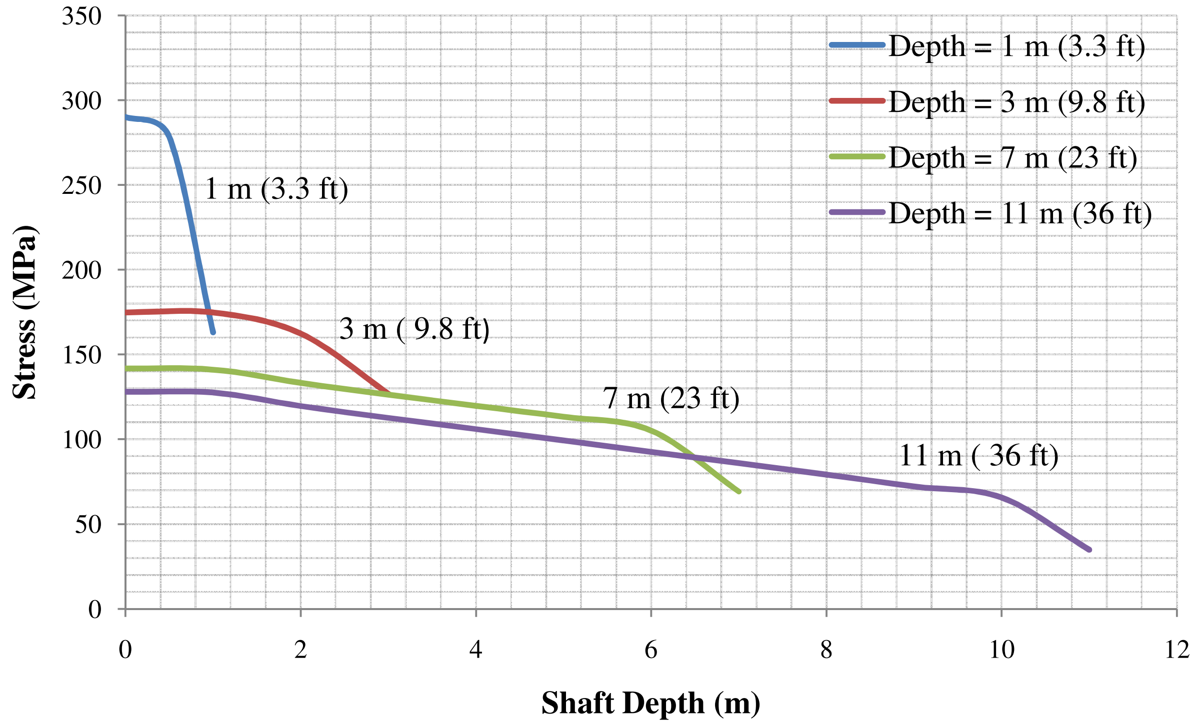

Figure 5.8 Shaft Stress with Depth for 50 mm (1.97 inch) Top Displacement (Rock RQD = 80%)

Figure 5.8 displays four different shafts of various lengths that have been subjected to 50 mm top displacement. The surrounding rock was of good quality (RQD = 80%). The horizontal axis represents the depth below the top of rock, while the vertical axis represents the stress within the center of the concrete shaft. The depth to which stress can be recorded is limited by the length of the shaft. Figure 5.8 shows that the stress is lower at the base of a deeper shaft than it is at a shorter shaft when subjected to the same top displacement. The lower stress state at the base of a deeper shaft means that less end bearing resistance is activated compared to shorter shafts. Vertical stresses in the concrete exceeding the unconfined strength in Figure 5.8 can occur since the concrete is confined by the rock.

Figures 5.9 and 5.10 present load-displacement curves at the top of the shaft and are independent of top displacement. These figures disregard the effects of shaft compression, which is responsible for the anomalous behavior in Figures 5.4 and 5.6. Instead of calculating forces and displacements at the top of the shaft, forces and displacement were calculated at the base of the shaft. Loads were applied in the same manner as they were when loads and displacements were calculated at the top.

Load-displacement data was independent of depth and identical for shafts of the same diameter when calculated at the base. Models were again run for four different diameters (1.00, 1.83, 2.66, and 3.5 m (3.3, 6.0, 8.7, and 11.5 ft)), each diameter was run at five different depths (0, 1, 3, 7,and 11 m (0, 3.3, 9.8, 23, and 36 ft)). For example a 1 m (3.3 ft) diameter shaft with a socket depth of 0 m (0 ft) had the same load-displacement curve as a 1 m (3.3 ft) diameter shaft with a socket depth of 11 meters (36 ft). Because load-displacement data was identical of alike shaft diameters the length of shafts was excluded from Figures 5.9 and 5.10. Besides showing the effect of shaft concrete compression, Figures 5.9 and 5.10 also show that depths have little effect on bearing resistance for the dimensions and loads of shafts in hard rock.

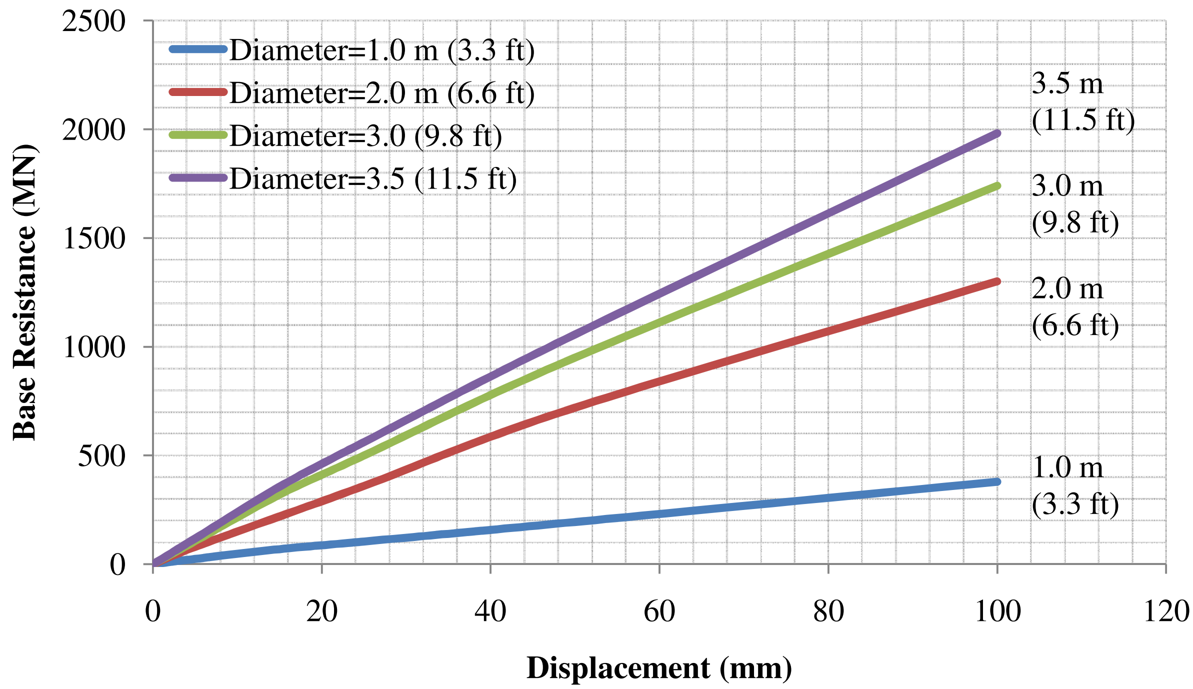

Figure 5.9 Bearing Resistance for RQD = 80%

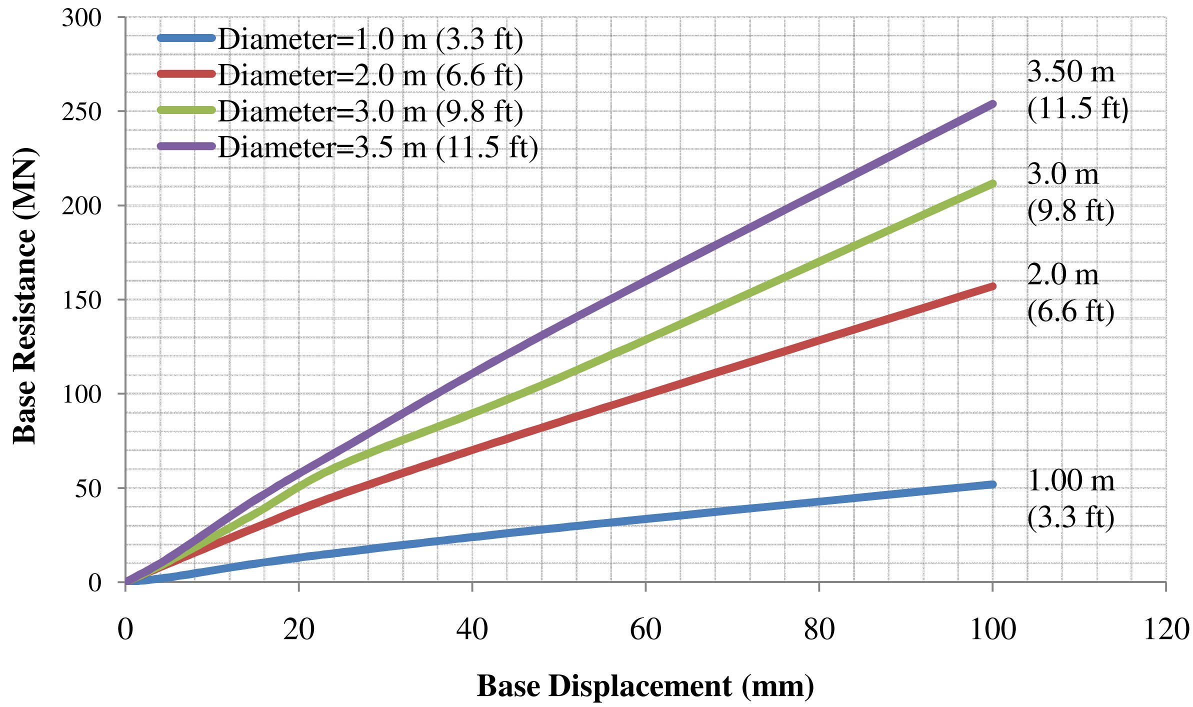

Figure 5.10 Bearing Resistance for RQD = 50%

5.5 Service Limit State Criteria

Figures 5.2 – 5.7, along with charts from Appendix C, allow design engineers to calculate shaft service limit state resistance capacities based on tolerable shaft movements. However the strength limit state resistance for side shear and end bearing must still be met. But now a tolerable displacement at the top of the shaft must be additionally known to complete the design.

The displacement at the top of the shaft is a key element in the design of the shaft. In the current practice the displacement does not explicitly enter the strength limit state resistance capacity evaluation. Instead with a conservative current practice that only includes side shear, it is implicit in this approach that the resulting top of the shaft displacement is tolerable upon application of the load equal to the strength limit state resistance. With the proposed use of both side shear and end bearing resistance in this report, use of strength limit state resistance may result in top of shaft displacements that are not tolerable. Thus the tolerable displacement must be explicitly considered in the design of the shaft when both side shear and end bearing resistance are included.

The tolerable displacement at the top of the shaft is a function of the structure. However, the implicit displacements tolerated in current practice now are likely in excess of those accepted to be permissible by calculation on a completed structure. Much of the top of shaft displacement occurs during construction before the structure is complete. Thus it becomes important to examine top of shaft displacements tolerated in current practice to provide guidance on a base level of displacements that can be tolerated. If displacements are monitored during construction in the future, it may be possible to demonstrate tolerable displacements above this base level of current practice.

To find displacements that have occurred in current practice, measured displacements in Osterberg testing are used together with strength limit state resistance values obtained from Osterberg testing. To obtain the top of shaft displacement from the measured displacements at the location of the Osterberg cell, the top-down loading curves given by LOADTEST, Inc. are utilized. These have been found in this study to match the top-down results from the finite element model. The calibrated finite element model represents the best estimate of full scale behavior during loading.

By examining top-down movements at the strength limit state resistance of previous projects, that were tested using Osterberg equipment, appropriate service limit state criteria can be established. Table 5.3 summarizes displacements of shafts, including the six shafts used for calibration and seven supplemental shafts from various locations throughout the United States.

A number of these shafts, including both Bath, Maine shafts, did not reach failure during testing, and were used as production shafts for their respective projects.

Table 5.3 Top-Down Movement at Strength Limit State Resistance

Project	Max Osterberg Cell Load[1], MN (tons)	Max Side Shear Displacement[2], mm (inch)	Factored Axial Resistance[3], MN (tons)	Top Displacement Corresponding to Factored Axial Resistance[4], mm (inch)
Bath 6C	38.0 (4,270)	14.0 (0.55)	26.6 (3,000)	8.0 (0.32)
Bath 7A	45.0 (5,050)	3.0 (0.12)	31.5 (3,540)	9.0 (0.36)
Hancock/Sullivan	10.0 (1,129)	0.6 (0.02)	7.0 (790)	2.0 (0.08)
Moses Wheeler	9.0 (1,010)	20.0 (0.79)	6.3 (710)	1.2 (0.05)
Summer St.	8.0 (900)	45.0 (1.77)	5.6 (630)	6.3 (0.25)
Route 18 over George St.	27.0 (3,030)	3.0 (0.12)	18.9 (2,120)	3.5 (0.14)
Biscayne Miami, FL	11.0 (1,240)	5.0 (0.20)	7.7 (870)	15.0 (0.60)
Brightman St. Bridge 14 w Somerset, MA	49.0 (5,510)	1.3 (0.05)	34.3 (3,850)	8.0 (0.32)
Market St. Guideway Philadelphia, PA	3.0 (340)	4.0 (0.16)	2.1 (240)	8.2 (0.33)
New Benicia Martinez Bridge San Francisco, CA	68.0 (7,640)	7.0 (0.28)	47.6 (5,350)	10.5 (0.42)
Route 35 Victory Bridge Perth Amboy, NJ	67.0 (7,530)	2.5 (0.10)	46.9 (5,270)	16.5 (0.66)
Sikorsky Bridge Stratford, CT	53.0 (5,960)	3.0 (0.12)	37.1 (4,170)	8.1 (0.32)
Sunland Park Drive Sunland Park, NM	7.0 (790)	15.0 (0.59)	4.9 (550)	13.0 (0.52)

1. Max load (MN) obtained by Osterberg Cell 2. Max upward movement produced by Osterberg Cell 3. Max side shear load LRFD (ASD FS=2) 4. Top down movement corresponding to factored axial capacity (Loadtest anticipated top down load curve)

The maximum side shear obtained from Osterberg testing, shown in Table 5.3, was the nominal resistance used in the design. A LRFD resistance factor of 0.70 was used to determine the strength limit state resistance, based on side shear only. LOADTEST Inc.'s anticipated top-down load-displacement curve was used to determine the movement of the top of the shaft under the strength limit state resistance.

A mean displacement of 8.4 mm (0.33 inch) was obtained corresponding to the strength limit state resistance from the thirteen shafts outlined in Table 5.3. However, Table 5.3 contains a number of shafts that have withstood greater top of the shaft displacements at the strength limit state resistance. Displacements up to 15 mm (0.59 inch) at the strength limit state resistance are not uncommon.

5.6 Service Limit State Method for Drilled Shaft Axial Capacity in Hard Rock

5.6.1 Introduction

Shafts founded in hard rock are over-designed in current practice, which is evident in Figure 2.1 that shows shafts designed in hard rock usually have more than five times the capacity than is anticipated by engineers. Current practice use either side shear or end bearing resistance, but rarely a combination of both. The difficulty in using both side shear and end bearing resistance to determine axial socket capacity is the prediction of the service limit state of the end bearing under tolerable top of the shaft displacements. The end bearing service limit state is a function of the quality of the rock and the diameter of the shaft. The displacements for the end bearing strength limit state resistance can result in displacements in excess of tolerable top of shaft displacements. With the risk of excess displacement corresponding to the end bearing limit state resistance, then drilled shafts are primarily designed using side shear strength limit state resistance only.

To be able to use bearing resistance together with side shear resistance in axial capacity design, one must meet the service limit state criteria at the top of the shaft, be able to estimate the magnitude of shaft displacement that will occur at the base end of the shaft, and then be able to estimate the resulting end bearing resistance generated by the shaft base. Service limit state criteria are discussed in Section 5.5. The magnitude of displacement of the shaft base depends upon the interaction of side shear and end bearing resistances and the corresponding displacements, which will vary with socket dimensions, rock quality, and resistance magnitudes. This complex interaction was modeled through finite elements as described in Chapter Three and calibrated to Osterberg tests results in Chapter Four. The results are given in Figures 5.2 to 5.7 for the service limit state resistance and in Figures 5.11 to 5.16 for side to end distribution. For a full range of service limit state criteria see Appendix C.

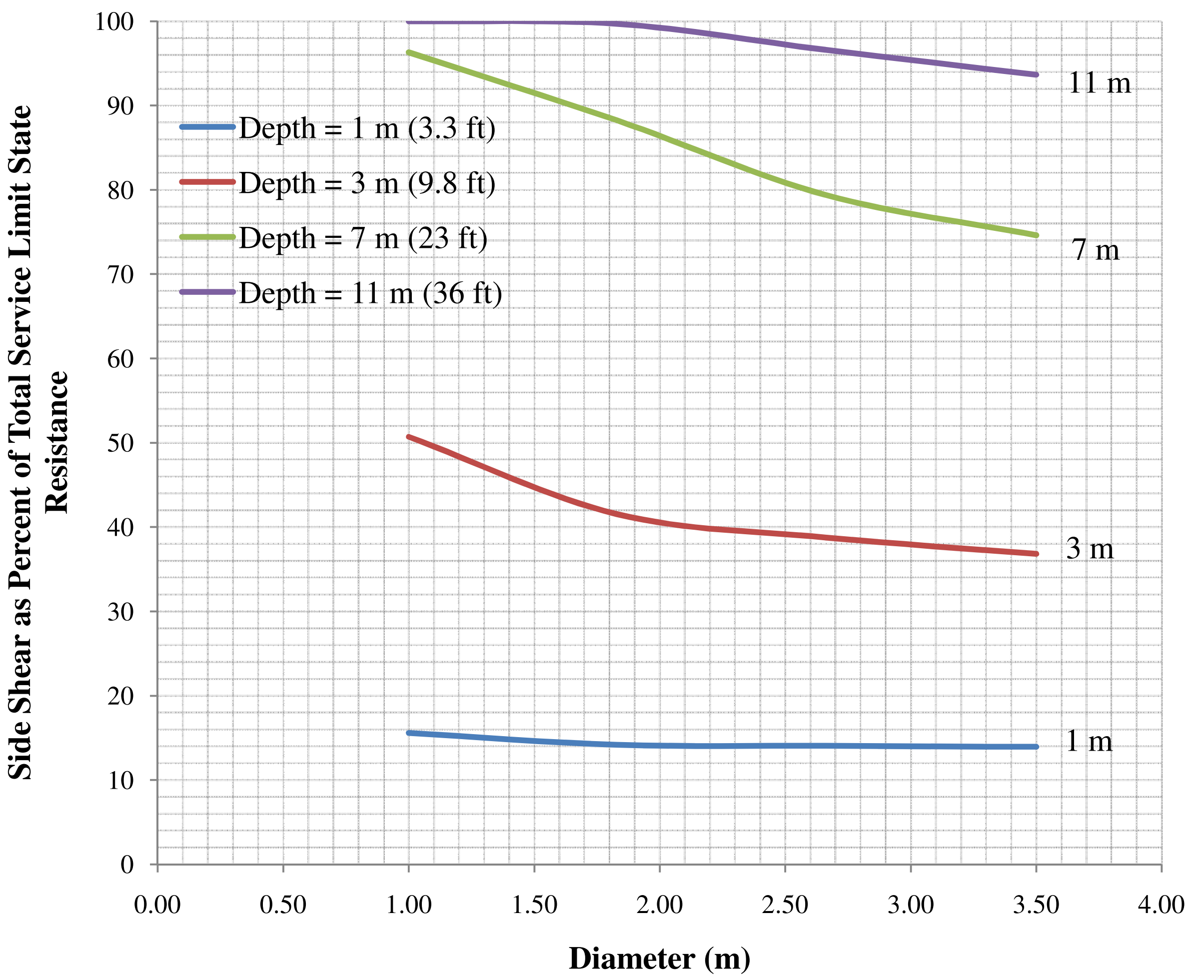

Figure 5.11 Percent Side Shear at 5 mm (0.20 inch) Top of Shaft Displacement RQD = 80%

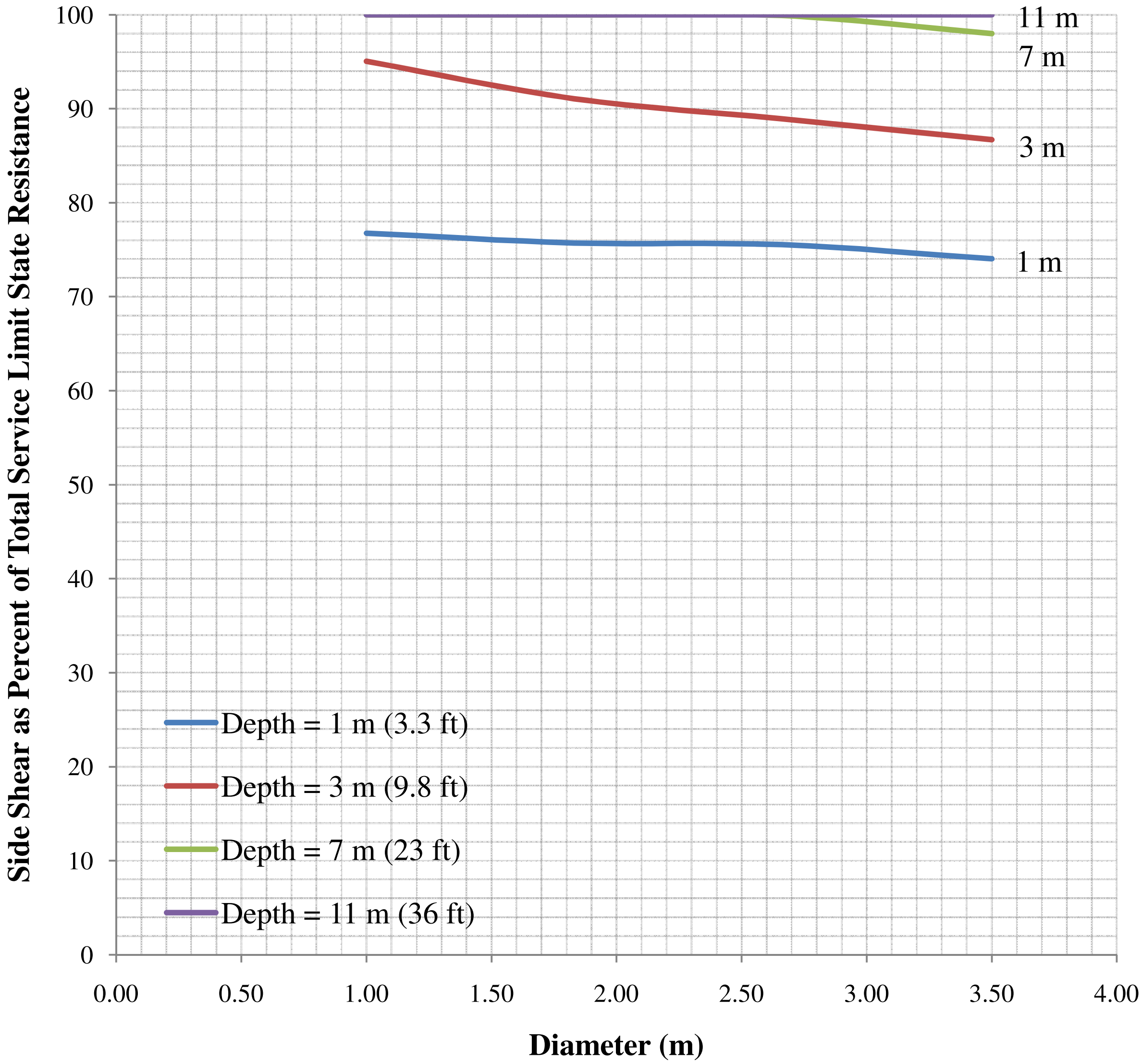

Figure 5.12 Percent Side Shear at 5 mm (0.20 inch) Top of Shaft Displacement RQD = 50%

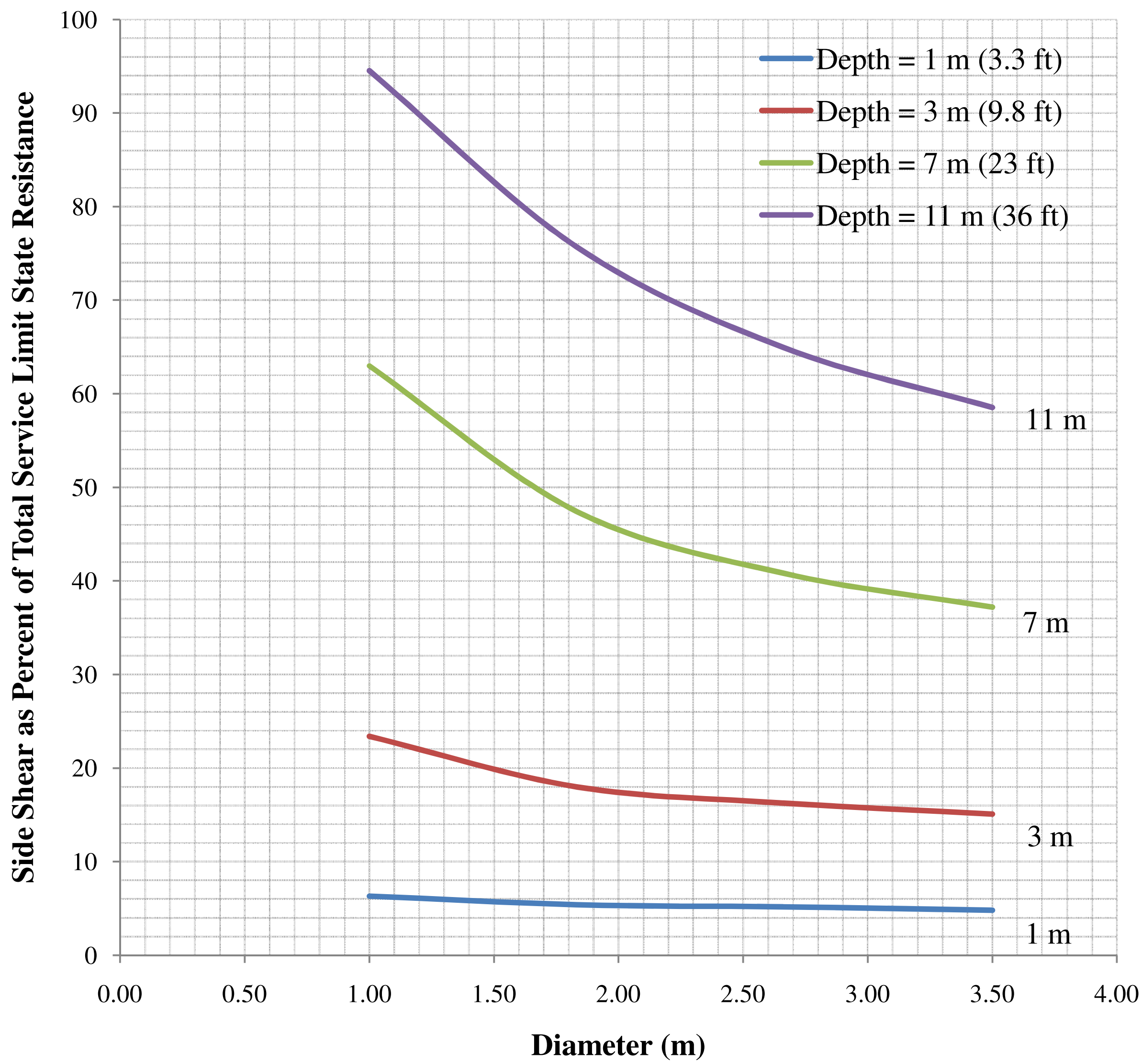

Figure 5.13 Percent Side Shear at 15 mm (0.59 inch) Top of Shaft Displacement RQD = 80%

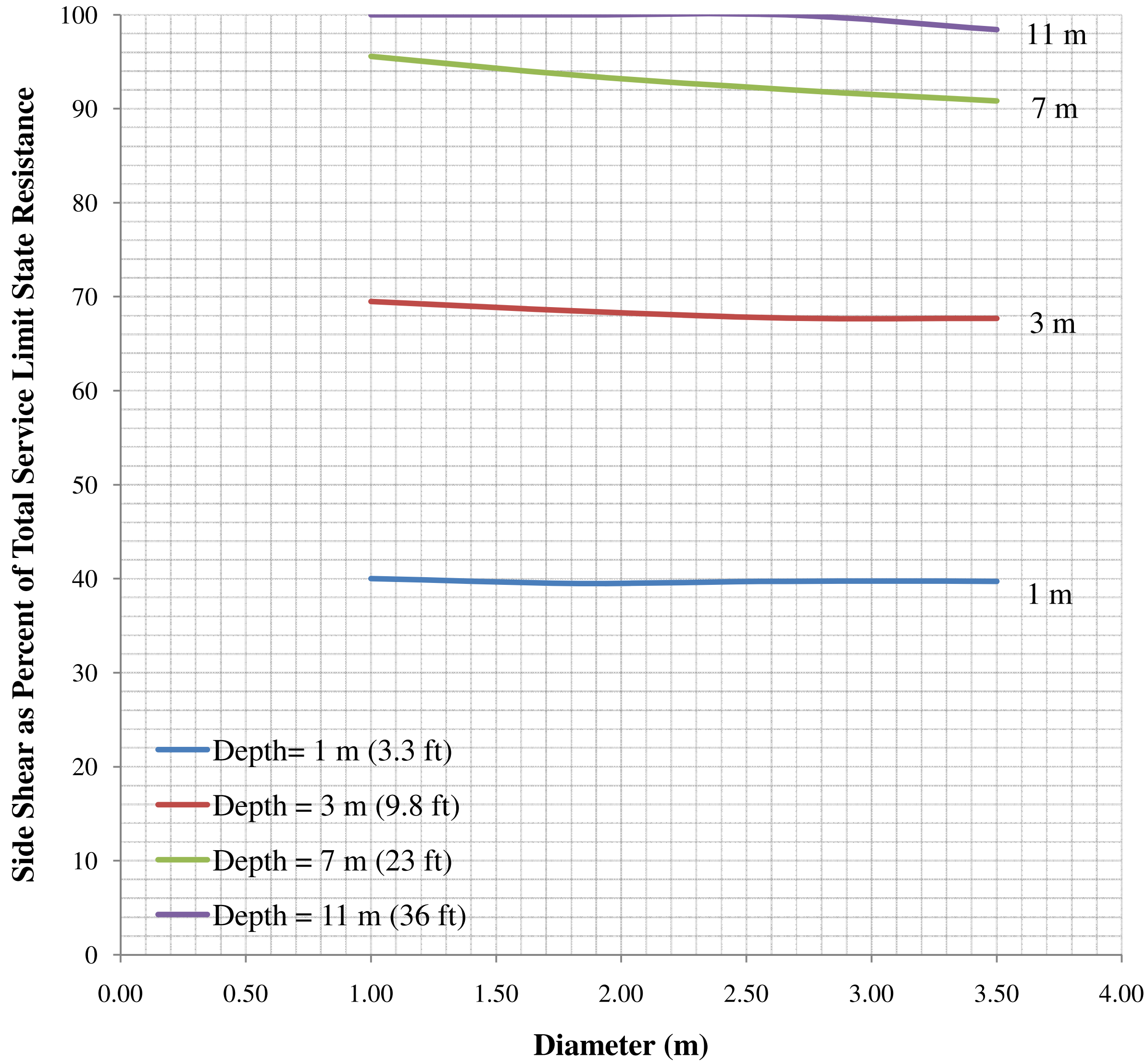

Figure 5.14 Percent Side Shear at 15 mm (0.59 inch) Top of Shaft Displacement RQD = 50%

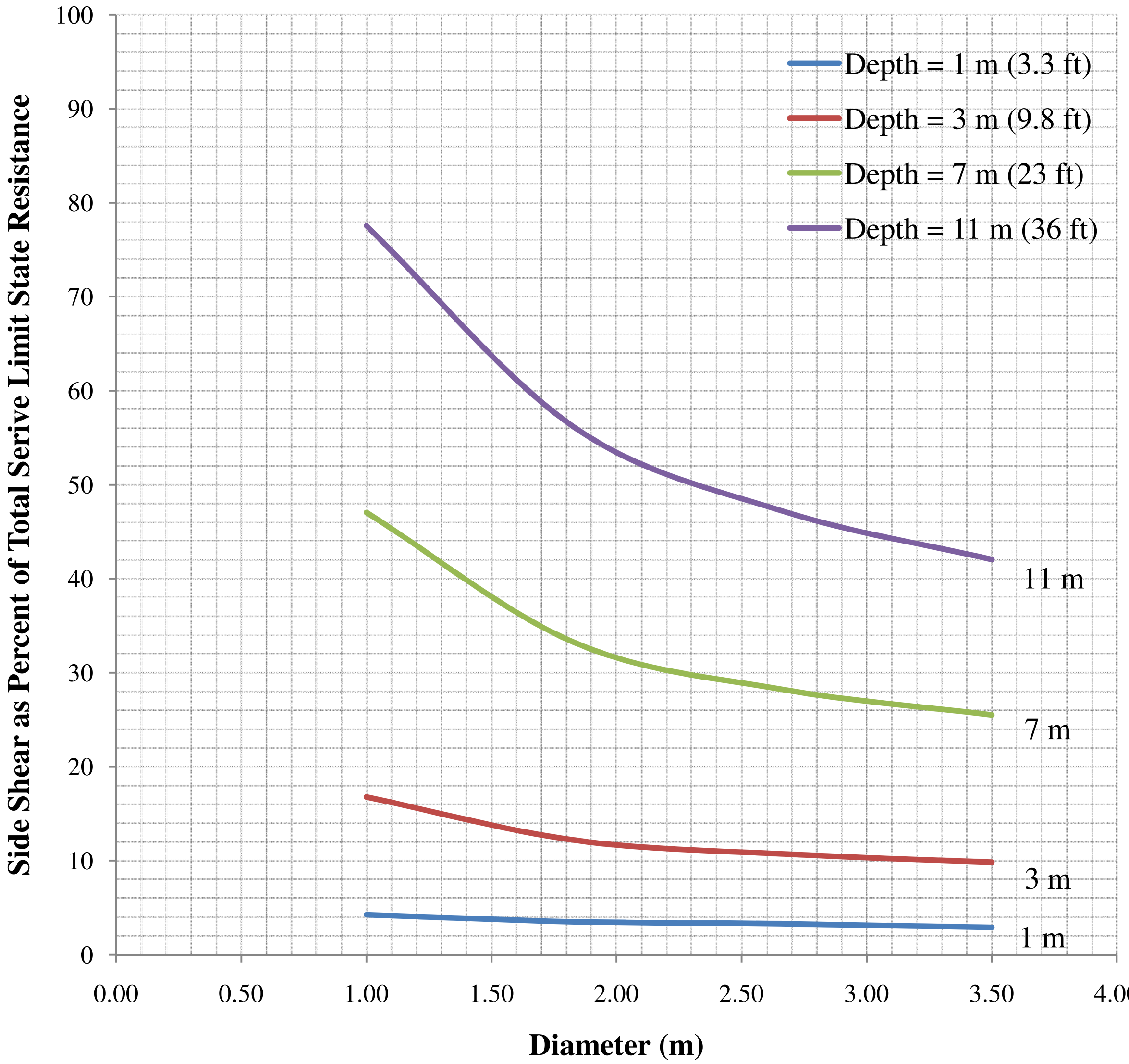

Figure 5.15 Percent Side Shear at 25 mm (0.98 inch) Top of Shaft Displacement RQD = 80%

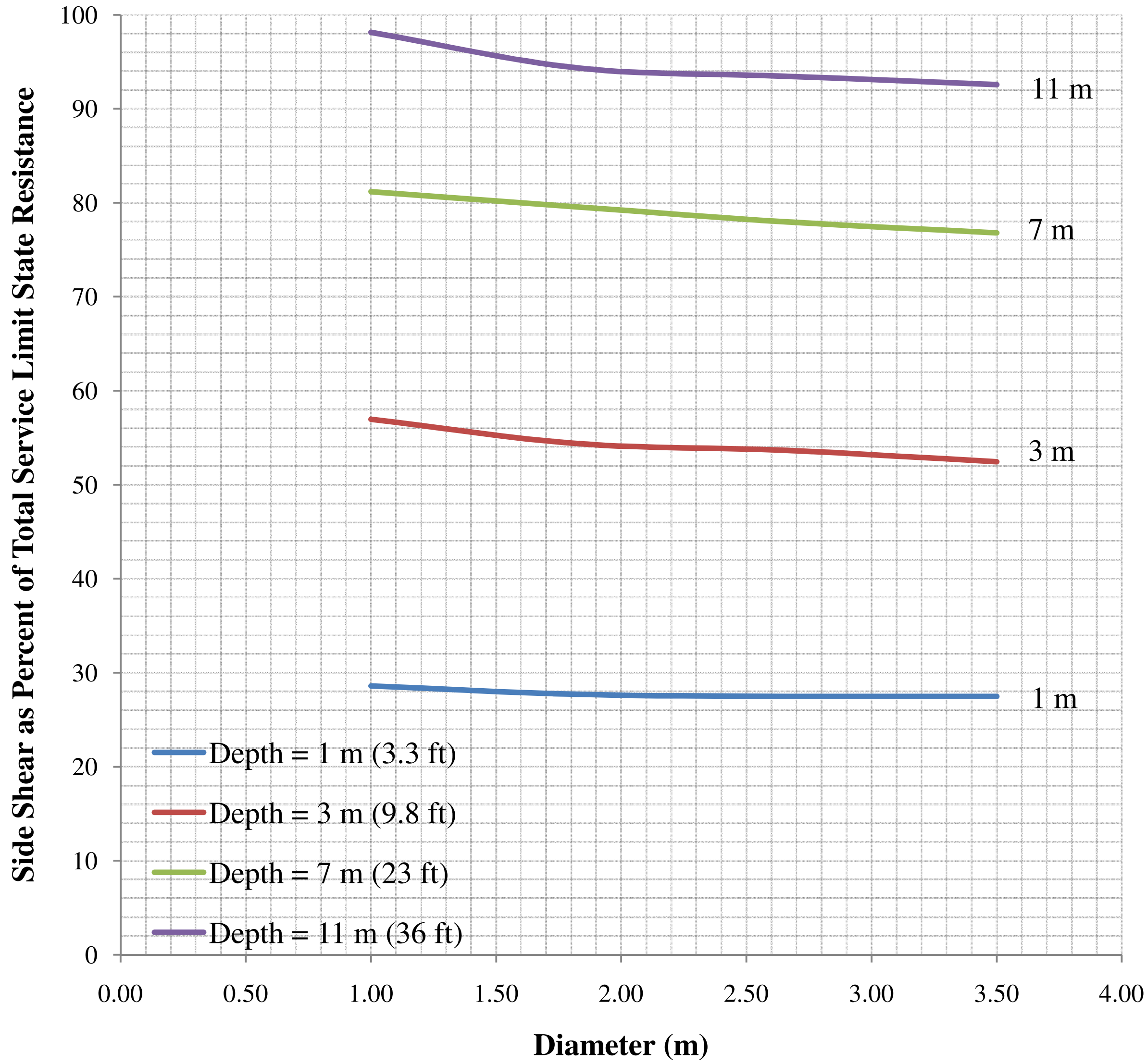

Figure 5.16 Percent Side Shear at 25 mm (0.98 inch) Top of Shaft Displacement RQD = 50%

5.6.2 Proposed Hard Rock Axial Capacity Design Method Incorporating Side Shear and End Bearing

A service limit state resistance of a drilled shaft in hard rock that has contributions of end bearing in addition to side shear can be estimated from the calibrated results given in Chapter Five and Appendix C. The proposed design method for axial resistance capacity by analytical methods consists of the minimum of three failure criteria: 1. Concrete column strength limit state resistance; 2. Service limit state resistance; and 3. Strength limit state resistance from calculated nominal resistance or from Osterberg tests.

5.6.2.1 Concrete Column Design Capacity

Concrete column axial strength limit state resistance becomes important, because the unconfined strength of the concrete is equal to or less than the unconfined strength of hard rock. Failure may occur in the shaft within the overburden soils before failure in the rock socket. For details on this criteria see Section 5.2 or the AASHTO LRFD Bridge Design Manual. Strength limit resistance capacity for a number of shaft diameters have been included on the design charts in Figures 5.2 to 5.7 and in Appendix C. AASHTO recommends using a resistance factor of 0.75 on the nominal resistance to obtain the strength limit state resistance. An example is given in Appendix B.

5.6.2.2 Service Limit State Resistance

Applying service limit state criteria can limit the bearing resistance capacity that is available. For this method, find the combination of diameter and depth of shaft for a quality of rock corresponding to the site that will meet a service limit state criteria and loading. Implied service limit state criteria for past practice are given in Section 5.5. Figures 5.2 to 5.7 and expanded design charts in Appendix C allow service limit state resistance diameters and depths to be selected for given service limit state criteria and rock quality. For the design conditions selected, find the relative distribution of the service limit state resistance side shear and end bearing resistances from Figures 5.11 to 5.16. The results for other service limit state criteria are given in Appendix C. An example is given in Appendix B.

5.6.2.3 Strength Limit State Resistance

The axial strength limit state resistance should be equal to or exceed the service limit state obtained in the above step 5.6.2.2. Additionally the end bearing strength limit state resistance should be equal to or exceed the service limit state bearing resistance. The resistance factors for side shear do not have meaning since side shear resistance may reach nominal values as end bearing is mobilized. Uncontrolled displacement does not occur for side shear resistance at the nominal value since the shaft is restrained by the end bearing resistance.

The end bearing nominal resistance can be found from Equation 2.5 or Equation 2.6 and the side shear nominal resistance value can be found from Equation 2.7. Consult AASHTO (2007) or CGS (1985) for more detail. Resistance factor $\phi = 0.50$ for LRFD for the sum of the side shear nominal resistance and nominal end bearing resistance is used to obtain the strength limit state resistance. For the case where only the end bearing strength limit state is compared the end bearing service limit state, the resistance factors are the same. An example is given in Appendix B.

5.6.2.4 Shaft Axial Design with Osterberg Tests and Tolerable Displacement

Osterberg tests are often used to obtain the axial strength limit state resistance. In order to find the strength limit state resistance a higher resistance factor $\phi = 0.70$ for LRFD reflecting less uncertainty is used with the nominal resistance found by testing than the resistance factor used with the nominal resistance calculated by analytical methods. Utilizing service limit state criteria at the top of shaft, both side shear and end bearing from the Osterberg test can be used for axial service limit state resistance capacity.

To provide a top-down load displacement curve from the Osterberg test, the Osterberg side shear resistance and end bearing resistance at the same displacement are summed (the top-down load is equal to the sum of side shear and end bearing resistance). Then the top of the shaft displacement is found by adding in the elastic compression of the concrete shaft under the loading conditions. These curves are often given by LOADTEST, Inc. as part of the Osterberg test results. It has been found in Chapter Four that the top-down loading curves produced by LOADTEST, Inc. correspond well with the model used in this study. However, caution must be used with the LOADTEST, Inc. top-down curves, since LOADTEST, Inc. often extrapolates resistance beyond the tested amount.

Once the top-down load displacement curve has been constructed then the strength limit state resistance can be found. The highest resistance tested can be taken as the nominal resistance. If the displacement in the top-down load curve corresponding to the strength limit state resistance exceeds the tolerable displacement, than the tolerable displacement can be used with the top-down load curve to select a corresponding service limit state resistance. An example is given in Appendix B.

Chapter Six

Summary/Conclusions and Recommendations

Chapter Six provides a summary of the work performed in order to produce a resistance method incorporating both side shear and end bearing for Rock Socketed Drilled Shafts in the hard rock found throughout New England. For the purpose of this study hard rock is considered to have an intact unconfined strength greater than 30 MPa (4,350 psi). Also included are recommendations for future investigations to refine the proposed method that includes both side shear and end bearing resistance.

6.1 Summary of Work Performed

The following sections summarize the work performed including the development of the finite element model, the parametric study, and the development of the capacity method including both side shear and end bearing resistance. For more detail on certain items please refer to the appropriate chapter.

6.1.1 Finite Element Modeling

A finite element model capable of duplicating field results was developed using ABAQUS version 6.8. The model was calibrated to match the performance of five separate field tested Rock Socketed Drilled Shafts in hard rock. This model was then used to produce results for configurations of sockets with different dimensions and rock qualities that have not been tested in the field.

To incorporate the cylindrical shape of the shaft an axisymmetric modeling technique was used. In this approach stresses and displacements were taken to be the same in the radial direction. The majority of model parts were created using bilinear axisymmetric stress elements (CAX4R) with the exception being the interface layer used to model the rock/concrete interface. The interface layer used cohesive axisymmetric elements (COHAX4) which allowed it to stretch infinitely. Mesh densities of the different parts depended on the proximity of the part to areas of sharp stress changes or interest, such as rock/concrete contact, loading surfaces, or calculation points. Typical material values were used for structural materials, such as Osterberg cell steel loading plates. Geotechnical material properties, such as rock quality and modulus values, were determined from test reports when possible; however, all material properties were not always tested, and thus missing properties were estimated based on available data.

To create the model, the parts were properly arranged within an assembly. Within the assembly contact definition was allocated, such as frictional parameters or tied surfaces. Other factors assigned within the assembly were loading criteria and boundary conditions. For detailed information on the development of the finite element model used for this research refer to Chapter Three.

6.1.2 Calibration of Finite Element Model

The finite element model was calibrated by duplicating, within limits, the performance of five separate Osterberg field tests. Four of the five field tests were founded within hard metamorphic rock (unconfined strength > 30 MPa (4,350 psi)). The location of the Rock Socketed Drilled Shafts were in New England, with three being in Maine, one in Massachusetts, and one in Connecticut. During the calibration stage an attempt was made to duplicate a sixth shaft in New Jersey shale, which had an unconfined strength of 65 MPa (9,430 psi). However, for the shale rock at the site, the bearing capacity did not correspond well with the bearing capacity of hard New England metamorphic rock. The performance of the end bearing and the excessive leveling course (1.0 m (3.3 ft)) at the base of the socket indicated disturbance or insufficient cleaning of the socket. For this reason conclusions taken from this study are limited to rock formations with high intact compressive strength that can be cleaned well. Most New England metamorphic and igneous rocks are hard and can be cleaned similar to the five calibration sockets. For more information on the calibration of the finite element model used for this research see Chapter Four.

6.1.3 Parametric Study and Hard Rock Method

After the model was calibrated to the Osterberg field tests, the model was used to obtain axial load-displacement data for a number of different shafts subjected to simulated structural and service loads. A range of socket dimensions, representing the range of designs, and two different rock conditions, representing poor and good rock, were used for the study. Rock material properties used for this study were based on unconfined tests and Rock Quality Designation (RQD) values from the calibration projects founded in the two rock conditions. The results of the parametric study were part of the hard rock design method incorporating both side shear and end bearing for Rock Socketed Drilled Shaft capacity in hard rock. For findings on the hard rock method along with explanations of results refer to Chapter Five.

6.2 Conclusions

The following conclusions regarding the behavior and design of Rock Socketed Drilled Shafts were made after completing the work described above.

1. Side shear and end bearing resistance can be incorporated into axial design capacity of a drilled shaft in hard rock that is cleaned well by considering service limit state criteria at

the top of the shaft. Although hard metamorphic/igneous rock (unconfined strength > 30 MPa (4,350 psi)) that can be well cleaned occurs widely throughout New England, this method must be used with more caution in hard sedimentary rock, since cleaning of the socket in sedimentary rock may be often an issue. In any case, the timing of the cleaning and subsequent inspection of the rock socket relative to the placement of the reinforcement and concrete must be considered, as some soil may settle or infiltrate into the socket bottom after inspection.

2. The method used in the Osterberg tests to obtain a top-down load displacement curve matched results from the calibrated finite element model. The top-down load displacement curves for the Osterberg tests were then used to estimate service limit state criteria for current strength limit state resistances. Based on Osterberg tests and current practice using side shear strength limit state resistances only, it was found that Osterberg top-down load displacement curves give a typical top of shaft displacement of 8 mm (0.31 inch) with some displacements up to 15 mm (0.59 inch). Charts have been presented for service limit state resistances corresponding to displacements from 1 mm (0.04 inch) to 25 mm (0.98 inch). The tolerable displacement will be a function of the type of structure and also of the amount of displacement occurring during construction of the structure.
3. The quality of the hard rock, i.e. the frequency of discontinuities and to a secondary degree the uniaxial strength, has a major effect on the drilled socket nominal resistance. The quality of the rock, as expressed by the Rock Quality Designation (RQD), affects primarily the service limit state resistance of the end bearing. Based on the availability of

relevant Osterberg tests, the effect of RQD was classified into poor rock (RQD = 50%) and good rock (RQD = 80%).

4. The side shear stress at failure in hard rock was found from Osterberg tests to be in a narrow range of 1.4 to 1.7 MPa. This shear stress is below that expected in softer rocks and thus appears to be the result of smooth wall drilling techniques in hard rock, damage to the rock, or drilling debris. The side shear stress at failure from the Osterberg tests exceeded the nominal resistance calculated by AASHTO. If future drilling methods increase the side shear stress (say by having a rougher surface) then the herein proposed hard rock method will be conservative, but the Osterberg load test with service limit state criteria of the hard rock method will incorporate the changes.
5. The dimensions of the drilled shaft, diameter and depth, as well as the smooth wall construction method to construct the shaft have a major effect on the percentage of overall service limit state resistance that is side shear or end bearing resistance. The end bearing increases with the square of the diameter, while the side shear increases proportional to the depth and diameter. The compression of the concrete shaft can become significant for deeper shafts because it contributes to displacements at the top of the shaft.
6. The concrete shaft strength limit state resistance in the overburden soil above the top of rock can become less than the strength limit state resistance of the socket. This column criteria becomes important for the shaft that passes through overburden to hard rock.
7. When Osterberg Testing is not done, strength limit resistances are is still needed. The hard rock method herein allows side shear to exceed the strength limit state resistance and even equal to the nominal resistance. This is the consequence of having a displacement

at the end of the shaft large enough to mobilize end bearing resistance. However, the consequences of reaching the nominal resistance value in side shear is not uncontrolled movement since the displacement of side shear at the nominal resistance is limited by end bearing resistance during top-down axial loading. Therefore the end bearing resistance factor should be applied to the sum of side shear and end bearing nominal resistance to determine strength limit state resistance. Separately the service limit state resistance for end bearing should be less than or equal to the end bearing strength limit state resistance, since attaining the nominal resistance in bearing capacity will cause uncontrolled displacement.

8. The design resistance of a drilled socket in hard rock without load testing is governed by the minimum of: 1. The strength limit state resistance of the shaft column in the soil above the rock; 2. The service limit state resistance; 3. The strength limit state resistance based on the calculated nominal resistance; 4. If the quality of construction or inspection is not high quality, than the service limit state resistance (hard rock method) should not be used and end bearing strength limit state resistance should not be used. However, the hard rock method with an Osterberg test can be used.
9. The top-down load-displacement curve, found for the Osterberg test by summing side shear and end bearing resistances at a given displacement and incorporating concrete shaft compression under load, matches results from the calibrated model. This concept allows service limit state criteria to be applied to Osterberg Tests to incorporate both side shear and end bearing in resistance. However, resistance factors for Osterberg test results should be applied only to tested resistance and not to extrapolated results.

6.3 Recommendations

The following are recommendations on the hard rock design method in hard rock.

1. The available data only allowed for two categories of rock quality in the hard rock design method. If more categories of rock quality are desired, then monitoring of additional tests should be conducted in order to refine the design method.
2. AASHTO equations for nominal resistance in end bearing of rock use Rock Mass Rating (RMR). The use of Rock Quality Designation (RQD) to describe fracturing in rock requires correlations and assumptions to convert RQD to RMR. A more reliable RMR for nominal resistance analysis of end bearing can be obtained if rock quality was described in field explorations using RMR. RMR takes into account the RQD, as well as strength, ground water, and conditions of joints.
3. Instrument drilled shafts to monitor displacement for drilled shafts designed to service limit state criteria. Monitoring of displacement during construction can indicate the displacement that occurs before the structure has achieved fixity, e.g. while concrete in decks is still wet. Construction loading displacements may have little or no effect on the final structure stress. Monitoring results may allow much greater development of bearing resistance, which in turn has a greater displacement that occurs during construction loading.
4. The cleanliness of the bottom of the socket is the key to incorporating bearing resistance into the total socket resistance. Minimum cleanliness procedures or equipment should be specified to the contractor. The bottom cleanliness should be thoroughly inspected shortly before the placement of the socket concrete.
5. Study the impacts of socket roughness and its relation to side shear.

References

AASHTO (2007), AASHTO LRFD Bridge Design Specifications, Fourth Edition, 2007 Full Text, American Association of State Highway and Transportation Officials, Washington, D.C.

Applied Foundation Testing inc. (2004) Final Report of Statnamic Load Testing I-95 Moses Wheeler Bridge, Jacksonville, FL.

Bowles, J. E. (1977), “Foundation Analysis and Design” second edition, McGraw-Hill Book company, New York, NY

CDOT (2010) Moses Wheeler Bridge, Connecticut Department of Transportation, Newington, Ct.

Delano, J. G. (2004), “Behavior of Pile-Supported Integral Abutments at Bridge Sites with Shallow Bedrock,” MS Thesis University of Maine 196 pp.

Drumm. E. C. et al., (2004), “Numerical Analysis of Drilled Shaft O-Cell Testing in Mica Schist” American Society of Civil Engineers

Gannet Fleming (1999) Unpublished Laboratory Test Results, NJDOT RT 18, Gannet Fleming Engineers and Planners Inc., Harrisburg, PA.

GeoDesign, Inc. (2002) Table No. 1 Summary of Rock Parameters Design Phase Drilled Shaft Testing Program Reconstruction of the Moses Wheeler Bridge. Portland, OR.

Haley & Aldrich (1997) Subsurface Report: Bath-Woolwich Bridge Project, Haley & Aldrich Inc. South Portland, ME.

Hassan. K. M, et al. (1997), “Side Load-Transfer Mechanisms in Drilled Shafts in Soft Argillaceous Rock”, Journal of Geotechnical and Geoenvironmental Engineering, ASCE, February 1997, Vol. 123, No. 2, pp 145-152

HKS, Inc. (2001). ABAQUS/Standars Version 6.2 User’s Manual. Pawtucket, RI. Hibbitt, Karlsson & Sorensen, Inc.

Law (1998) Final Geotechnical Design Submittal Kennebec River Piers, Bath-Woolwich Bridge Project, Sagadahoc County, Maine Law Engineering and Environmental Services, Inc., Sterling, VA.

Liu, C., & Evett, J. B., (2000), “Soil Properties Testing, Measurement, and Evaluation”, fourth edition Prentice Hall printing company 403 pp.

LOADTEST (1998a) “Test Shaft No. 1, Bath/Woolwich Bridge, Pier 6C, Bath, ME (LT 84271)” Report on Drilled Shaft Load Testing (Osterberg Method), LOADTEST Inc., Gainesville, FL.

LOADTEST (1998b) “Test Shaft No. 2, Bath/Woolwich Bridge, Pier 7A, Bath, ME (LT 84272)” Report on Drilled Shaft Load Testing (Osterberg Method), LOADTEST Inc., Gainesville, FL.

LOADTEST (1998c) “Pier 6 – Downstream, Hancock/Sullivan Bridge, Hancock, Maine (LT8443)” Report on Drilled Shaft Load Testing (Osterberg Method), LOADTEST Inc., Gainesville, FL.

LOADTEST (2003) “Test Shaft #1 – Moses Wheeler Bridge, Milford/Stratford, CT (LT8914)” Report on Drilled Shaft Load Testing (Osterberg Method), LOADTEST Inc., Gainesville, FL.

LOADTEST (2006) “Test Shaft #1 - Rt 18 Sec. 2F, 7E & 11H New Brunswick, NJ (LT-90951)” Report on Drilled Shaft Load Testing (Osterberg Method), LOADTEST Inc., Gainesville, FL.

McVay. M. C., et al., (1992), “Design of Socketed Drilled Shafts in Limestone”, Journal of Geotechnical Engineering, ASCE, Vol. 118, No. 10, pp 1626-1637

MHD (1999) Unpublished Design Calculations, Summer Street over Reserve Channel in Boston, Massachusetts Highway Department, Geotechnical Section, Boston, MA.

MDOT (1997) Design Report, Hancock-Sullivan Bridge Project, Maine Department of Transportation, Augusta, ME.

NAVFAC (1986), “Design Manuel DM 7.2 – Foundations and Earth Structures”, United States Naval Facilities Engineering Command publication

O’Neill, M. W., (2005) “Construction Practices and Defects in Drilled Shafts,” Advances in Designing and Testing Deep Foundations, ASCE Geotechnical Special Publication No. 129, pp. 39-47

O'Neill, M. W. and K. H. Hassan (1994) "Drilled Shafts: Effects of Construction on Performance and Design Criteria," in Proceedings, International Conference on Design and Construction of Deep Foundations, U.S. Federal Highway Administration, Vol. 1 pp. 137-187

O’Neill, M. W., & Reese, L. C. (1999), Drilled Shafts: Construction Procedures and Design Methods, Report FHWA-IF-99-025, FHWA, Washington, D.C., 758 pp.

Osterberg, J, O., (1998) “The Osterberg Load Test Method for Bored and Driven Piles: The First Ten Years,” Presented at the 7th International Conference & Exhibition on Piling and Deep Foundations, Deep Foundations Institute, Vienna, Austria, June 1998.

Osterberg, J. O., (1999) “What Has Been Learned About Drilled Shafts From the Osterberg Load Test,” presented at the Deep Foundations Institute Annual Meeting, October 1999.

Reese, L.C. & O'Neil, M.W. (1987), "New Design Method for Drilled Shafts from Common Soil and Rock Tests," Foundation Engineering: Current Principles and Practices: Proceedings of the Conference, edited by Fred H. Kulhawy, Evanston, IL, Vol. 2, pp. 1027-1039.

Sangong, M., Paik, K., & Kim, D. (2007) "A New Approach to Estimate Side Shear Resistance of Rock Socketed Drilled Shafts," Soil and Foundations, Japanese Geotechnical Society, Tokyo, Japan, Vol. 47, No. 2, pp. 415-421

Schmertmann, J. H, (1993) "The Bottom-Up, Osterberg Cell Method For Static Testing of Shafts and Piles," 13th Centeral PA Geotechnical Seminar, Hershey, PA pp. 1-7

Schmertmann, J. H., & Hayes, J. A. (1997), "The Osterberg Cell and Bored Pile Testing – A Symbiosis," Procedings: 3rd International Geotechnical Engineering Conference, Cairo University, Egypt, pp. 139-166.

Site – Blauvelt (2002) Unpublished Laboratory Test Results, Route 18, New Brunswick, NJ, Site– Blauvelt Engineers Inc., Mt. Laurel, NJ.

Turner, John, (2006) NCHRP Synthesis 360: Rock Socketed Shafts for Highway Structures Foundations, Transportation Research Board, National Research Council, Washington, D.C., 136 pp.

Wight, J. K., & MacGregor, J. G., (2009), "Reinforced Concrete", fifth edition Pearson Education inc., Upper Saddle River, New Jersey, 1112 pp.

Zuo, G., et al., (2004), "numerical Analysis of Drilled Shaft O-Cell Testing in Mica Shist", Proceedings, Geo-Support 2004 Conference, ASCE, GSP, No. 124, Orlando, Feburary 2004, pp. 778-789

Appendices

Appendix A

Example Calculations for Column Capacity

This appendix provides example calculations for shaft capacity as a column. Capacities are calculated only for the shaft diameters included in this study. Capacities for alternative diameters could be calculated in the same manner.

1 Meter Diameter

$A_g = \pi * 0.5^2\ m^2$

$A_g = 0.785\ m^2$

ASSUME

$A_{st} = 0.02 * Ag\ m^2$

$A_{st} = 0.016\ m^2$

$F'_c = 28{,}000{,}000$ Pa

$F_y = 414{,}000{,}000$ Pa

AASHTO LRFD Bridge Specifications

$P_n = 0.85\ [0.85 * F'_c * (A_g - A_{st}) + F_y * A_{st})$

$P_n = 2.11 \times 10^7$ N

$P_r = P_n * \phi = 21.1\ MN * 0.75 = 15.8\ MN$

2 Meter Diameter

$A_g = \pi * 1.0^2\ m^2$

$A_g = 3.14\ m^2$

ASSUME

$A_{st} = 0.02 * Ag\ m^2$

$A_{st} = 0.063\ m^2$

$F'_c = 28{,}000{,}000$ Pa

$F_y = 414{,}000{,}000$ Pa

AASHTO LRFD Bridge Specifications

$P_n = 0.85\ [0.85 * F'_c * (A_g - A_{st}) + F_y * A_{st})$

$P_n = 8.44 \times 10^7$ N

$P_r = P_n * \phi = 84.4\ MN * 0.75 = 63.3\ MN$

3 Meter Diameter

$A_g = \pi * 1.5^2 \text{ m}^2$

$A_g = 7.07 \text{ m}^2$

ASSUME

$A_{st} = 0.02 * Ag \text{ m}^2$

$A_{st} = 0.141 \text{ m}^2$

$F'_c = 28{,}000{,}000$ Pa

$F_y = 414{,}000{,}000$ Pa

AASHTO LRFD Bridge Specifications

$P_n = 0.85 [0.85 * F'_c * (A_g - A_{st}) + F_y * A_{st})$

$P_n = 18.98 \text{ x } 10^7$ N

$P_r = P_n * \phi = 189.8 \text{ MN} * 0.75 = 142.4 \text{ MN}$

3.5 Meter Diameter

$A_g = \pi * 1.75^2\ m^2$

$A_g = 9.62\ m^2$

ASSUME

$A_{st} = 0.02 * Ag\ m^2$

$A_{st} = 0.192$

$F'_c = 28{,}000{,}000$ Pa

$F_y = 414{,}000{,}000$ Pa

AASHTO LRFD Bridge Specifications

$P_n = 0.85\ [0.85 * F'_c * (A_g - A_{st}) + F_y * A_{st})$

$P_n = 25.8 \times 10^7$ N

$P_r = P_n * \phi = 258\ MN * 0.75 = 194\ MN$

Appendix B

Example Calculations Using Hard Rock Method

This appendix provides example calculations using the method developed in Chapter Five. There is an example for the case of not using a load test, an example for the case when a load test is used, and a case when the diameter and design load are specified.

Example 1 – No Load Test Conducted

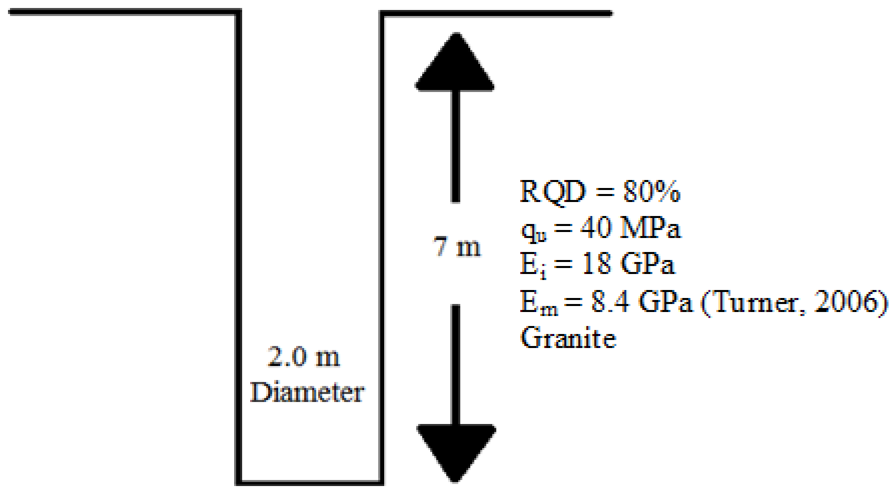

Find the capacity for this drilled shaft by current practice and by the proposed hard rock method at four tolerable displacements of 4, 8, 15, and 25 mm. Also find the column strength limit state resistance capacity (2.0 m assume no increase in shaft diameter above rock socket) directly above the shaft. Also, assume no Osterberg Test was conducted.

Summary of Findings

	Service Limit State Resistance, MN (tons)	**Strength Limit State Resistance, MN (tons)**	**Column Strength Limit State Resistance, MN (tons)**	**Design Resistance, MN (tons)**
Current Practice (Side only)	-	23.9 (2,690)	63.3 (7,080)	23.9 (2,690)
Hard Rock Method (4 mm)	72 (8,090)	111 (12,470)	63.3 (7,080)	63.3 (7,080)
Hard Rock Method (8 mm)	105 (11,800)	111 (12,470)	63.3 (7,080)	63.3 (7,080)
Hard Rock Method (15 mm)	155 (17,420)	111 (12,470)	63.3 (7,080)	63.3 (7,080)
Hard Rock Method (25 mm)	220 (24,720)	111 (12,470)	63.3 (7,080)	63.3 (7,080)

The design resistance from the "Hard Rock Method" is more than twice the current practice for the dimensions and rock properties used in this example. The design resistance in the "Hard Rock Method" is controlled by the column strength limit state resistance for the dimensions used in this example. By expanding the shaft diameter above the rock, a higher resistance could be attained.

Current Practice

Side Shear

$q_s = 0.65 * \alpha_E * p_a * (q_u / p_a)^{0.5} < 7.8 * p_a * (f'_c / p_a)^{0.5}$

$\alpha_E = 0.76$ (Table 2.2)

$p_a = 100,000$ Pa

$q_u = 40,000,000$ Pa

$f'_c = 28,000,000$ Pa

$q_s = 0.65 * 0.76 * 100,000 *(40,000,000 / 100,000)^{0.5} = 988,000$ Pa

988,000 Pa < $13,051,896 = 7.8 * p_a * (f'_c / p_a)^{0.5}$

Side Shear Area = $A_s = \pi * 2.0 \text{ m} * 7.0 \text{ m} = 43.98 \text{ m}^2$

Nominal Side Resistance = $R_s = 43.98 * 988,000 = 43,452,240$ N

Strength Limit State Side Resistance = 43.5 MN * 0.55 = 23.9 MN

Service Limit State Resistance (Tolerable Displacement)

4 mm

Service Limit State Resistance = 72 MN (Figure C.7)

8 mm

Service Limit State Resistance = 105 MN (Figure C.13)

15 mm

Service Limit State Resistance = 155 MN (Figure C.17)

25 mm

Service Limit State Resistance = 220 MN (Figure C.21)

Strength Limit State Resistance

Side Shear

Nominal Side Resistance = R_s = 40.24 * 988,000 = 39,757,120 N (see current practice)

End Bearing

$q_p = [\sqrt{s} + (m * \sqrt{s} + s)^{1/2}] * q_u$

s = 0.082 (Table 2.1)

m = 8.567 (Table 2.1)

q_u = 40,000,000 Pa

$q_p = [(\sqrt{0.082} + (8.567 * \sqrt{0.082} + 0.082)^{1/2}] * 40{,}000{,}000 = 75{,}143{,}696$ Pa

End Bearing Area = $A_p = \pi * 0.915^2 = 2.63\ m^2$

Nominal End Bearing = 2.63 * 75,000,000 = 184,100,000 N

Or

Nominal End Bearing = $q_{ult} = 3d \left[\frac{3+\frac{c_s}{D}}{10*\left(1+\frac{300t}{c_s}\right)^{0.5}}\right] q_u$

$$= 3*(1+0.4*7/1.83)*\left[\frac{3+\frac{1.0}{1.83}}{10*\left(1+\frac{300*.005}{1.0}\right)^{0.5}}\right]*28 = 47{,}000{,}000 \text{ N}$$

*assuming 1 meter spacing for discontinuities of thickness = 5 mm

Strength Limit State Resistance

Nominal Side Shear + End Bearing = 38 MN + 184 MN = 222 MN

Strength Limit State Resistance = 0.50 * 222 MN = 111 MN

Column Strength Limit State Resistance

2 Meter Diameter

$A_g = \pi * 1.0^2\ m^2$

$A_g = 3.14\ m^2$

Assume

$A_{st} = 0.02 * Ag\ m^2$

$A_{st} = 0.063\ m^2$

$F'_c = 28{,}000{,}000$ Pa

$F_y = 414{,}000{,}000$ Pa

AASHTO LRFD Bridge Specifications

$P_n = 0.85\ [0.85 * F'_c * (A_g - A_{st}) + F_y * A_{st})$

$P_n = 8.44 \times 10^7$ N

$P_r = P_n * \phi = 84.4\ MN * 0.75 = 63.3\ MN$

Example 2 – Osterberg Load Test Conducted

Find the capacity for the Bath 6C Shaft (section 4.1 of this report) when the top-down load curve from an Osterberg Test is given below.

Summary of Findings

In this example, the strength limit state resistance is found from the Osterberg Test conducted at the site.

	Service Limit State Resistance, MN (tons)	Osterberg Strength Limit State Resistance, MN (tons)	Column Strength Limit State Resistance, MN (tons)	Design Resistance, MN (tons)
Hard Rock Method (side or end only)	-	27.3 (3,070)	94.4 (10,600)	27.3 (3,070)
Hard Rock Method (4 mm)	16.0 (1,800)	50.4 (5,660)	94.4 (10,600)	16.0 (1,800)
Hard Rock Method (8 mm)	29.0 (3,260)	50.4 (5,660)	94.4 (10,600)	29.0 (3,260)
Hard Rock Method (15 mm)	46.0 (5,170)	50.4 (5,660)	94.4 (10,600)	46.0 (5,170)
Hard Rock Method (25 mm)	72.0 (8,090)	50.4 (5,660)	94.4 (10,600)	50.4 (5,660)

The design resistance from the “Hard Rock Method” exceeds present practice for tolerable displacements greater than 6 mm. For other shafts the tolerable displacement at which the “Hard Rock Method” has higher design resistance may change depending on shaft dimensions and rock properties.

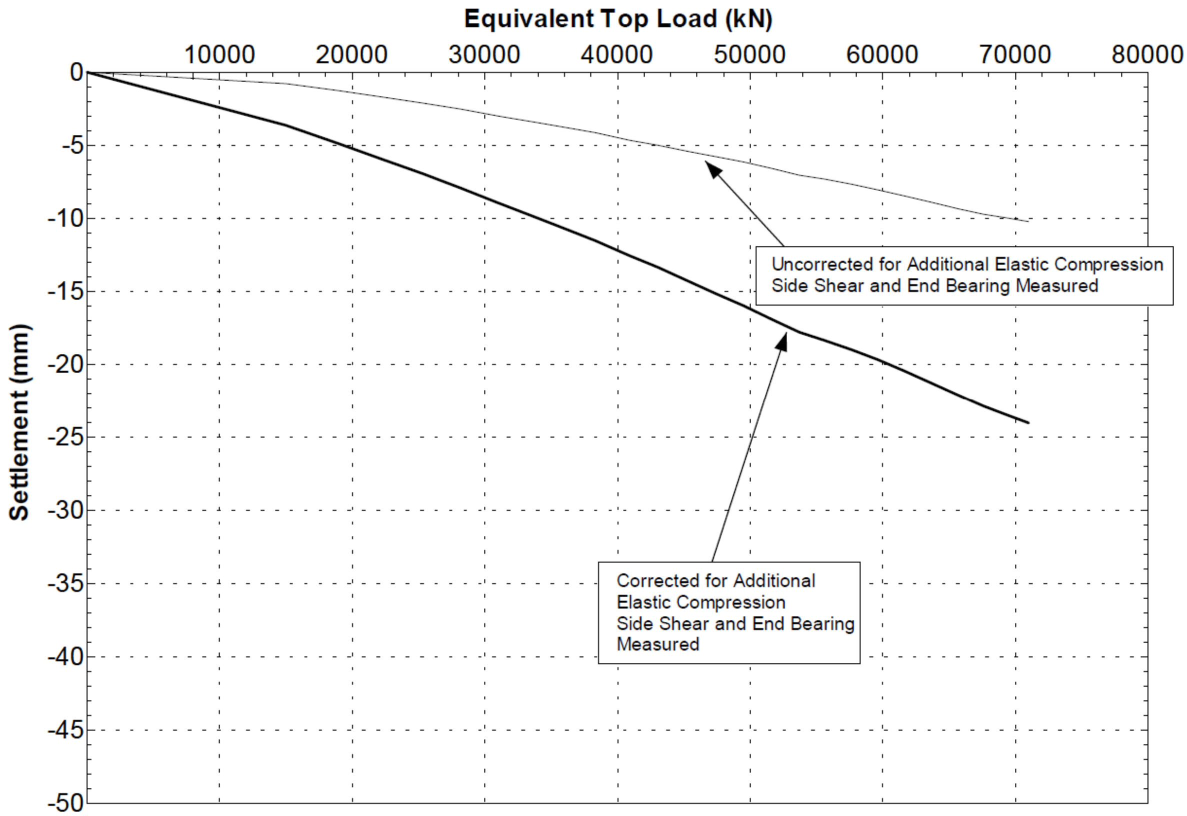

(LOADTEST, 1998a)

Maximum Side Shear + End Bearing Tested = 72 MN @ 10 mm Displacement

Maximum Side Shear Tested = 39 MN @13.5 mm Displacement

Maximum End Bearing Tested = 39 MN @ 10 mm Displacement

Current Practice

Osterberg Strength Limit State Resistance = 0.7 * 39 MN = 27.3 MN

Hard Rock Method

4 mm

Service Limit State Resistance = 16 MN (see LOADTEST, 1998a above)

Osterberg Strength Limit State Resistance = 0.7 * 72 MN = 50.4 MN

8 mm

Service Limit State Resistance = 29 MN (see LOADTEST, 1998a above)

Osterberg Strength Limit State Resistance = 0.7 * 72 MN = 50.4 MN

15 mm

Service Limit State Resistance = 46 MN (see LOADTEST, 1998a above)

Osterberg Strength Limit State Resistance = 0.7 * 72 MN = 50.4 MN

25 mm

Service Limit State Resistance = 16 MN (see LOADTEST, 1998a above)

Osterberg Strength Limit State Resistance = 0.7 * 72 MN = 50.4 MN

Strength Limit State Column Resistance

2.44 Meter Diameter

$A_g = \pi * 1.22^2 \text{ m}^2$

$A_g = 4.68 \text{ m}^2$

Assume

$A_{st} = 0.02 * Ag \text{ m}^2$

$A_{st} = 0.094 \text{ m}^2$

$F'_c = 28{,}000{,}000$ Pa

$F_y = 414{,}000{,}000$ Pa

AASHTO LRFD Bridge Specifications

$P_n = 0.85 [0.85 * F'_c * (A_g – A_{st}) + F_y * A_{st})$

$P_n = 125{,}853{,}380 \times 10^7$ N

$P_r = P_n * \phi = 125.9 \text{ MN} * 0.75 = 94.4 \text{ MN}$

Example 3 – Specified Resistance and Socket Diameter

Find the depth of socket for a specified column diameter of 3.0 m (9.8 ft) (having a socket diameter equal to the column diameter) and a specified strength limit state load of 75 MN (8,430 tons) and a service limit state load of 60 MN (6,744 tons) given. The rock properties are given on the following diagram. A shaft depth is determined using common design practice as well as the "Hard Rock Method" at 4, 8, 15, and 25 mm top of shaft displacements.

Summary of Findings

Method	**Length of Socket, m (ft)**
Current Practice (side shear only)	14.7 (48)
Hard Rock Method (4 mm)	0.0 (0.0)
Hard Rock Method (8 mm)	0.0 (0.0)
Hard Rock Method (15 mm)	0.0 (0.0)
Hard Rock Method (25 mm)	0.0 (0.0)

Given

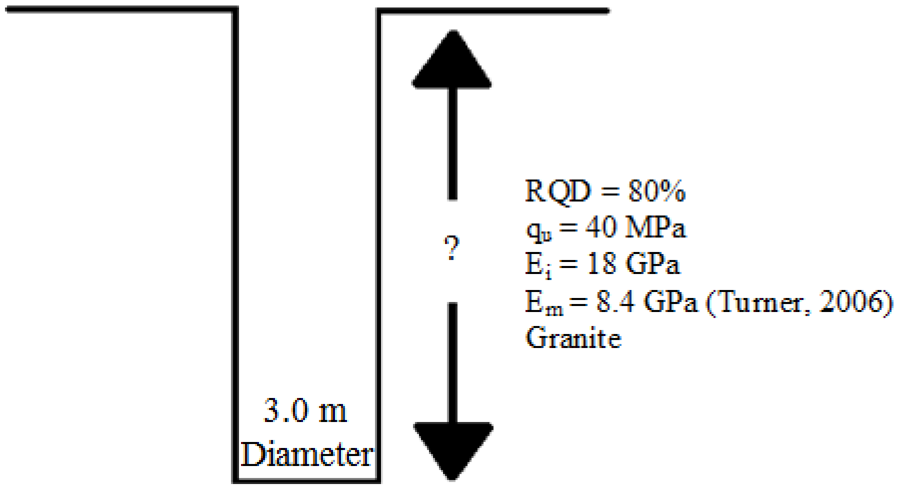

Strength Limit State Axial Resistance = 75 MN

Shaft Diameter = Socket Diameter = 3.0 m

Current Practice

Side Shear

$q_s = 0.65 * \alpha_E * p_a * (q_u / p_a)^{0.5} < 7.8 * p_a * (f'_c / p_a)^{0.5}$

$\alpha_E = 0.76$ (Table 2.2)

$p_a = 100{,}000$ Pa

$q_u = 40{,}000{,}000$ Pa

$f'_c = 28{,}000{,}000$ Pa

$q_s = 0.65 * 0.76 * 100{,}000 *(40{,}000{,}000 / 100{,}000)^{0.5} = 988{,}000$ Pa

$988{,}000 \text{ Pa} < 13{,}051{,}896 = 7.8 * p_a * (f'_c / p_a)^{0.5}$

Side Shear Area = $A_s = \pi * 3.0 \text{ m} * \text{h m} = 9.4\text{h m}^2$ (h = socket depth)

Nominal Side Resistance = R_s = 9.4h * 988,000 = 9,287,200h N

Strength Limit State Side Resistance = 9.3h MN * 0.55 = 5.1h MN

Find necessary height – 75 MN = 5.1h   Height = 14.7 m

Hard Rock Method

4 mm

Design Charts

Height = 0.0 m (Figure C.7)

(height required to meet service limit state resistance of 60 MN if diameter=3.0 m)

Check Strength Limit State Resistance

End Bearing

$q_p = [\ \sqrt{s} + (m * \sqrt{s} + s)^{1/2}] * q_u$

$s = 0.082$ (Table 2.1)

$m = 8.567$ (Table 2.1)

$q_u = 40{,}000{,}000$ Pa

$q_p = [(\sqrt{0.082} + (8.567 * \sqrt{0.082} + 0.082)^{1/2}] * 40{,}000{,}000 = 75{,}143{,}696$ Pa

End Bearing Area = $A_p = \pi * 1.5^2 = 7.07\ m^2$

Nominal End Bearing Resistance = 7.07 * 75,000,000 = 530,250,000 N

End Bearing Strength Limit State Resistance = 530 MN * 0.5 = 265 MN

*note – no need to check side shear limit. End bearing has sufficient resistance

8 mm

Design Charts

Height = 0 m (Figure C.7)

(height required to meet resistance of 60 MN if diameter=3.0 m)

15 mm

Design Charts

Height = 0 m (Figure C.7)

(height required to meet resistance of 60 MN if diameter=3.0 m)

25 mm

Design Charts

Height = 0 m (Figure C.7)

(height required to meet resistance of 60 MN if diameter=3.0 m)

Appendix C

Service Limit State Charts

This appendix contains a complete set of Service Limit State charts for Rock Socketed Drilled Shafts. Charts provide the service limit state resistance, as well as percent side shear at a certain service limit state criteria for shafts of different depths, diameters, and rock conditions. Charts are only to be used for hard rock where the socket can be well cleaned. They are intended primarily for Metamorphic or igneous rock formations, but certain hard sedimentary rocks may also be considered if clean sockets are possible.

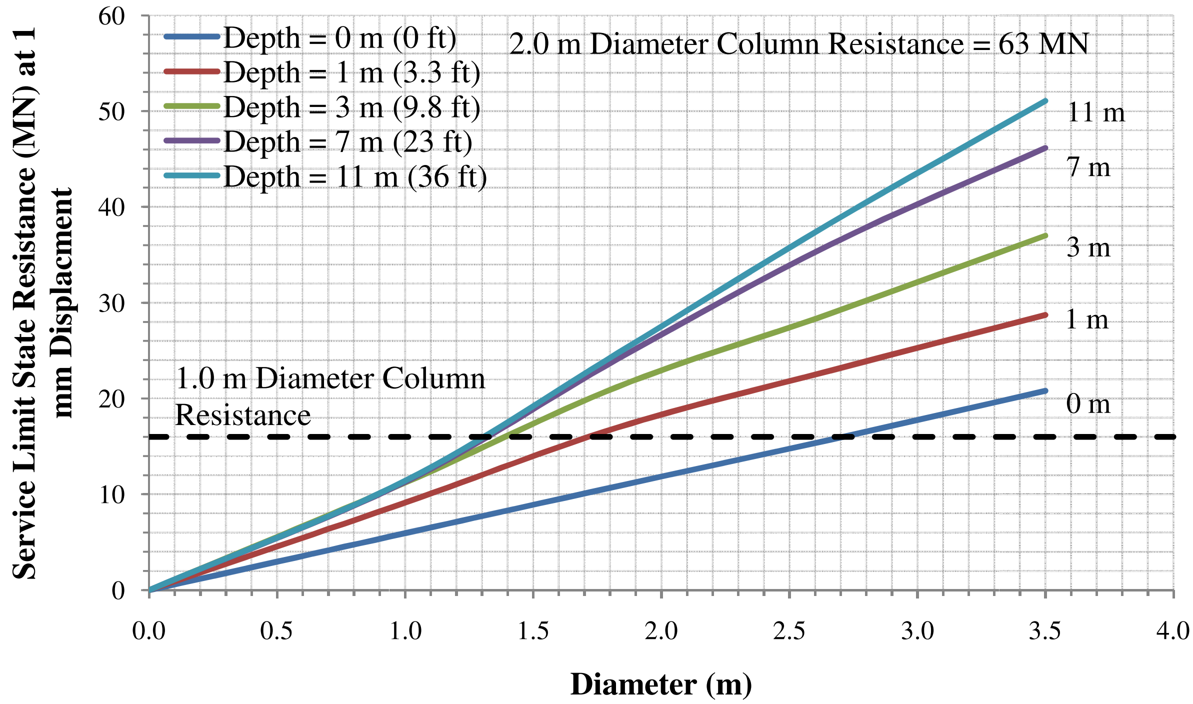

Figure C.1 Service Limit State Resistance at 1 mm (0.04 inch) Displacement for RQD = 80%

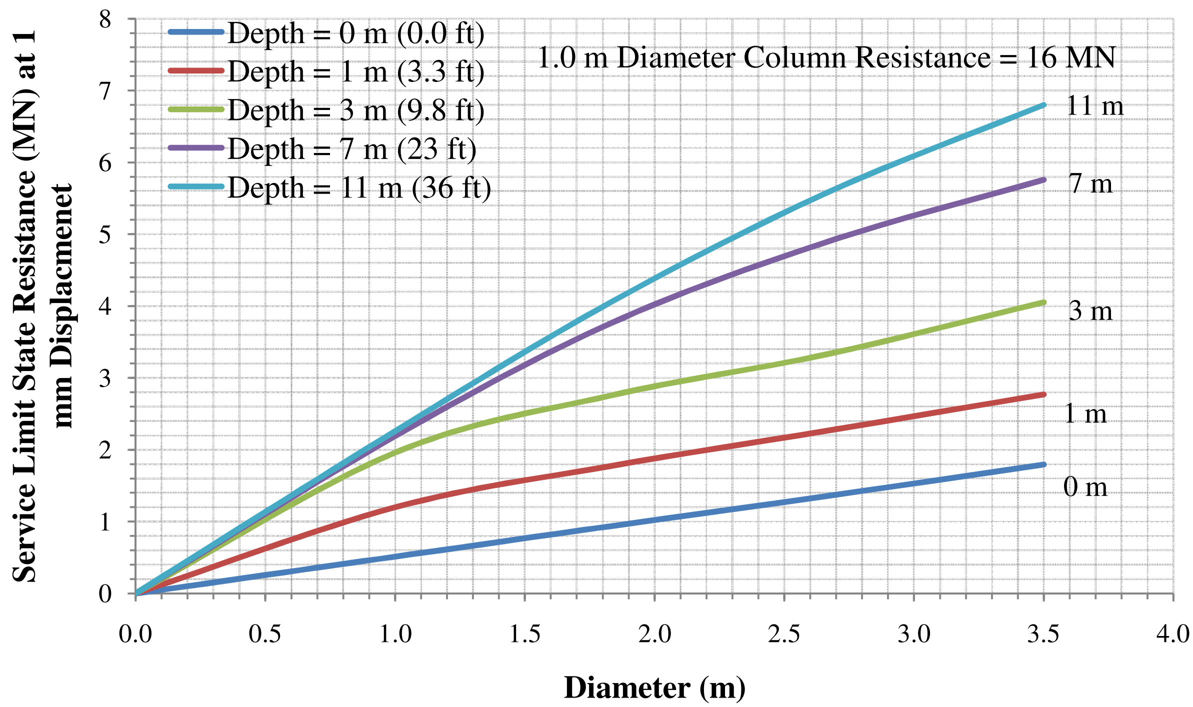

Figure C.2 Service Limit State Resistance at 1 mm (0.04 inch) Displacement for RQD = 50%

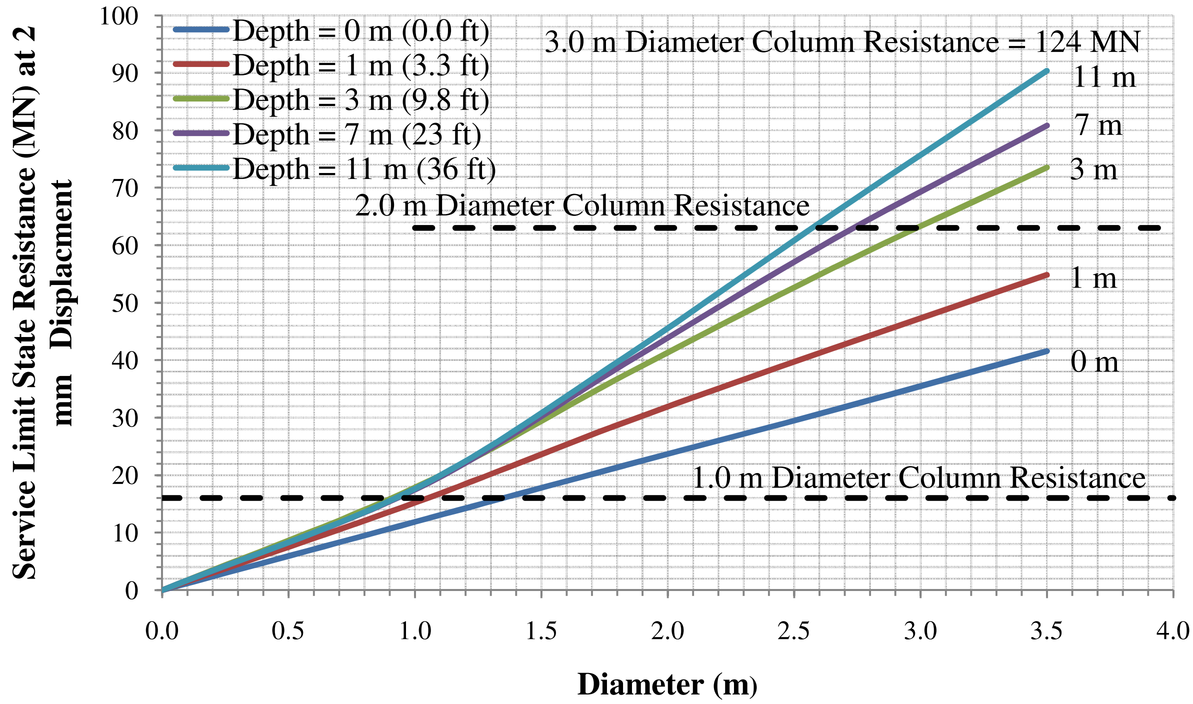

Figure C.3 Service Limit State Resistance at 2 mm (0.08 inch) Displacement for RQD = 80%

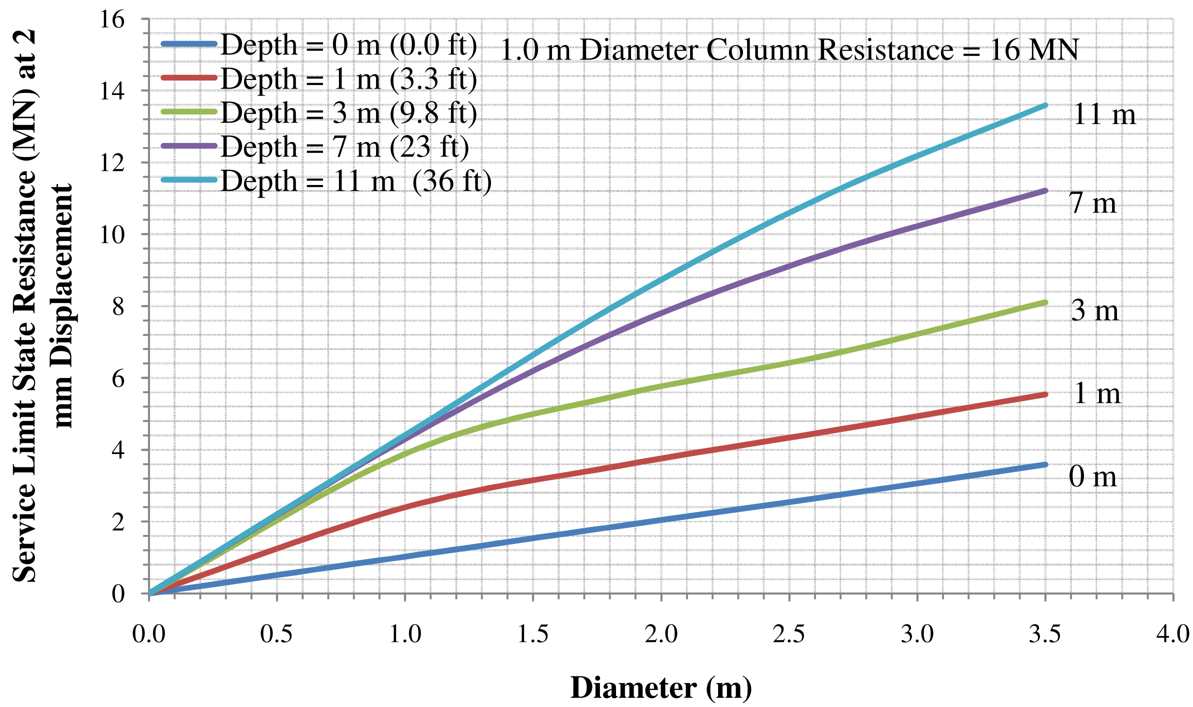

Figure C.4 Service Limit State Resistance at 2 mm (0.08 inch) Displacement for RQD = 50%

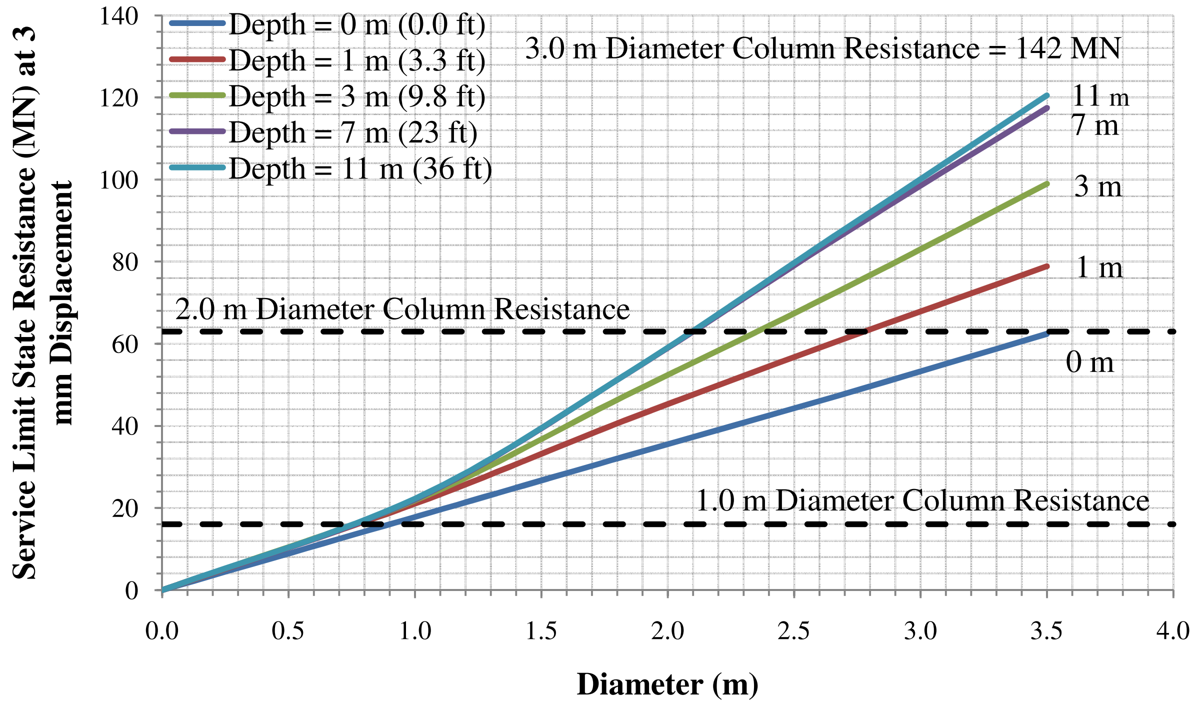

Figure C.5 Service Limit State Resistance at 3 mm (0.12 inch) Displacement for RQD = 80%

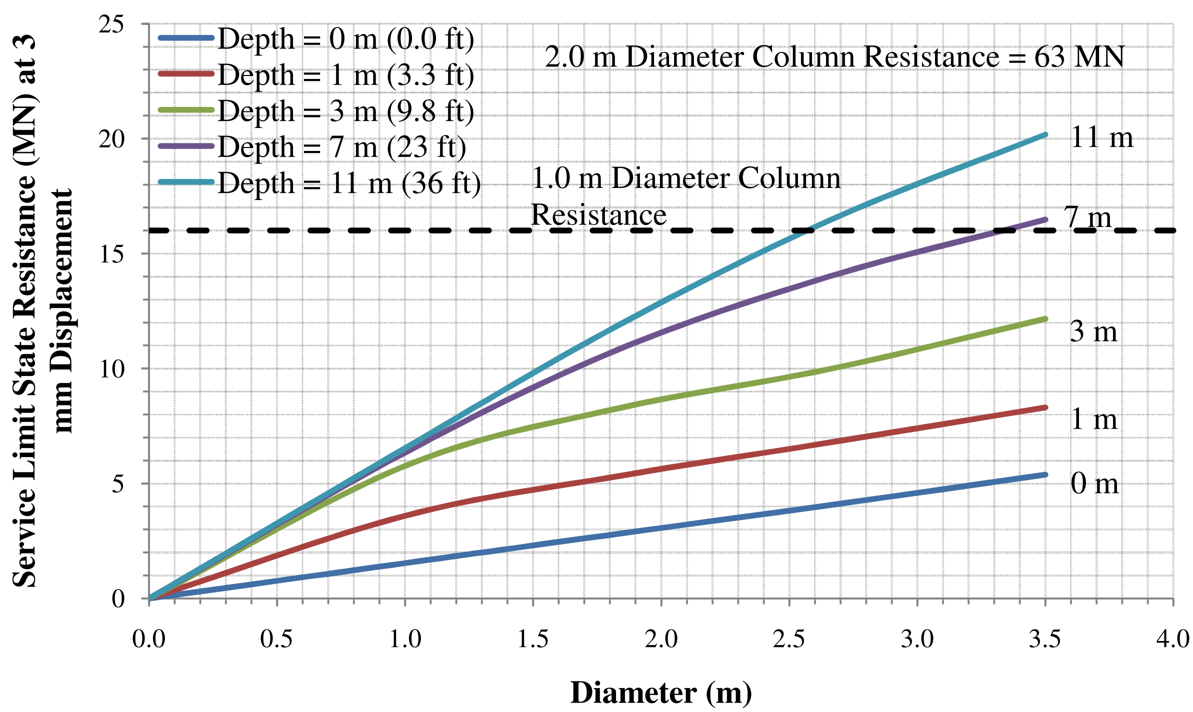

Figure C.6 Service Limit State Resistance at 3 mm (0.12 inch) Displacement for RQD = 50%

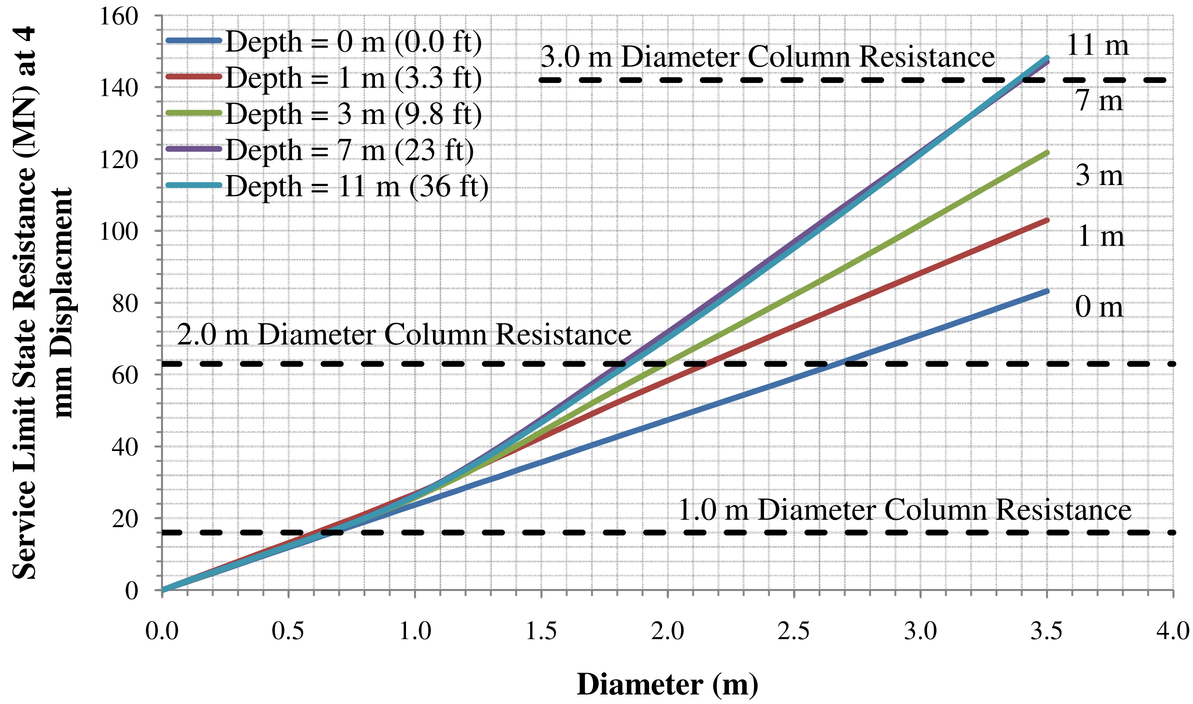

Figure C.7 Service Limit State Resistance at 4 mm (0.16 inch) Displacement for RQD = 80%

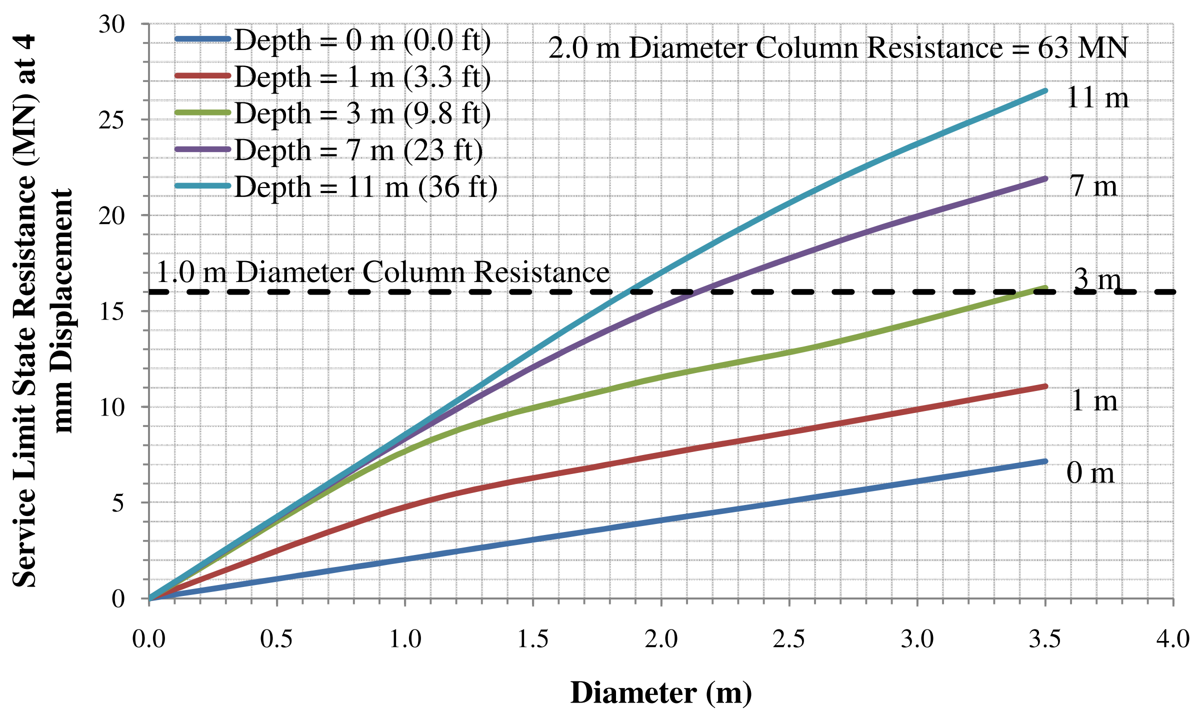

Figure C.8 Service Limit State Resistance at 4 mm (0.16 inch) Displacement for RQD = 50%

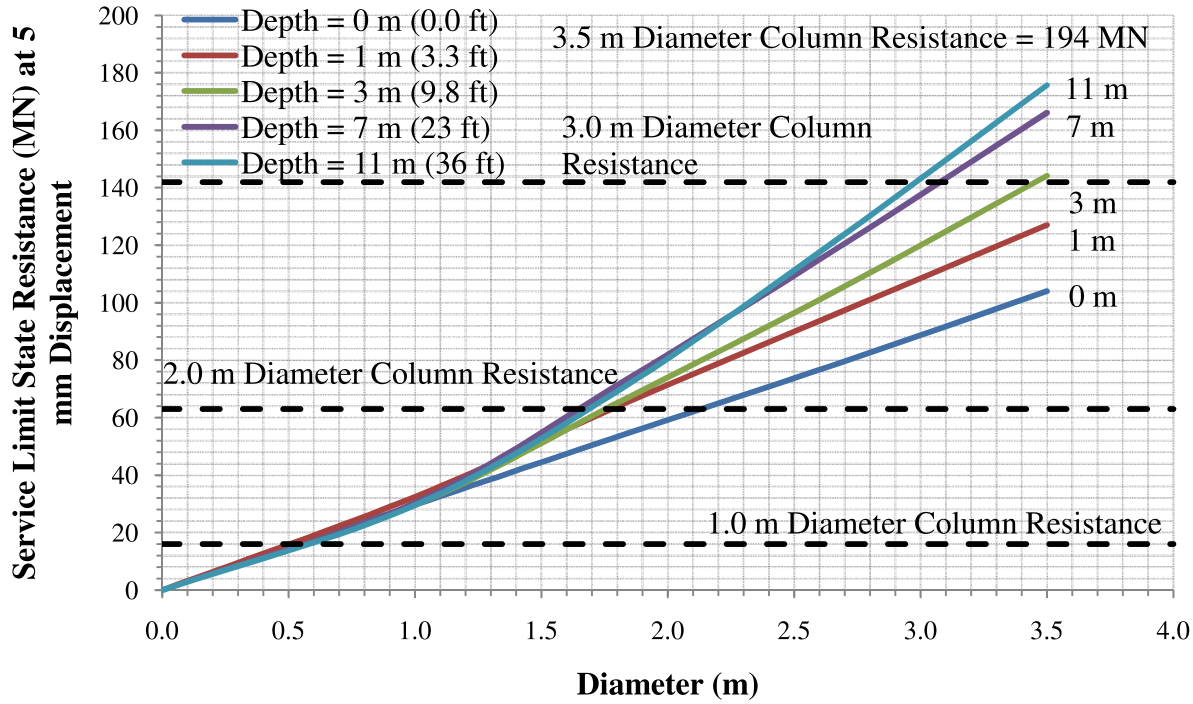

Figure C.9 Service Limit State Resistance at 5 mm (0.20 inch) Displacement for RQD = 80%

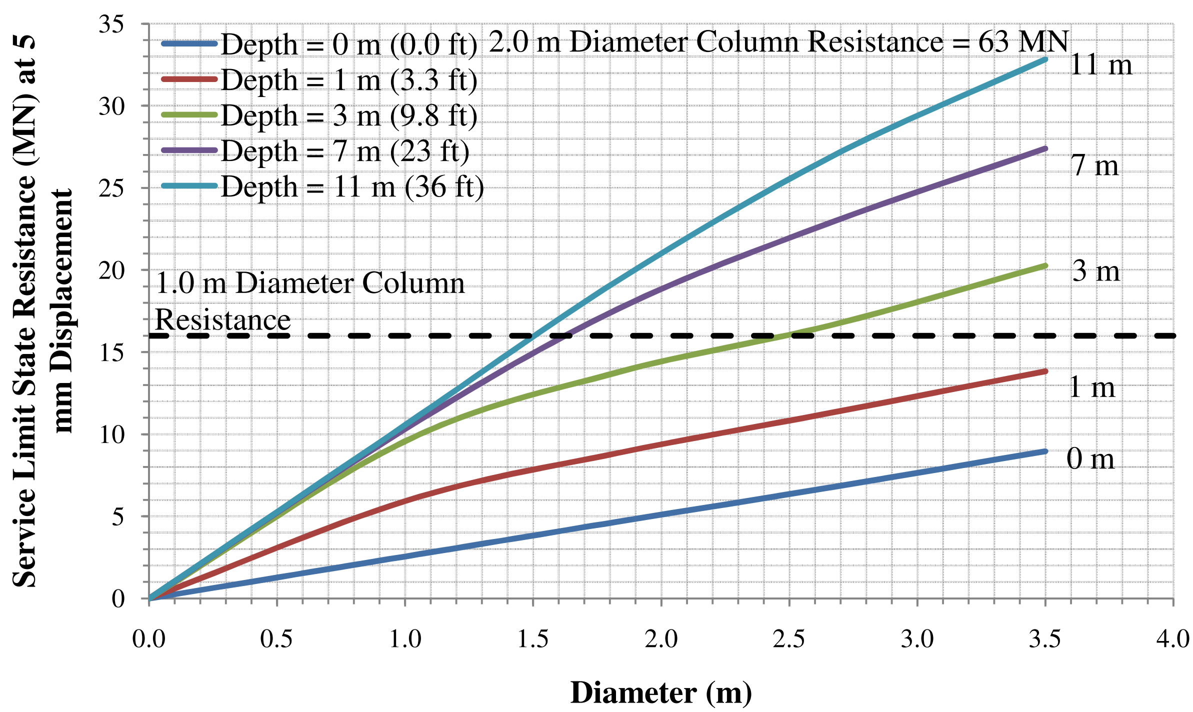

Figure C.10 Service Limit State Resistance at 5 mm (0.20 inch) Displacement for RQD = 50%

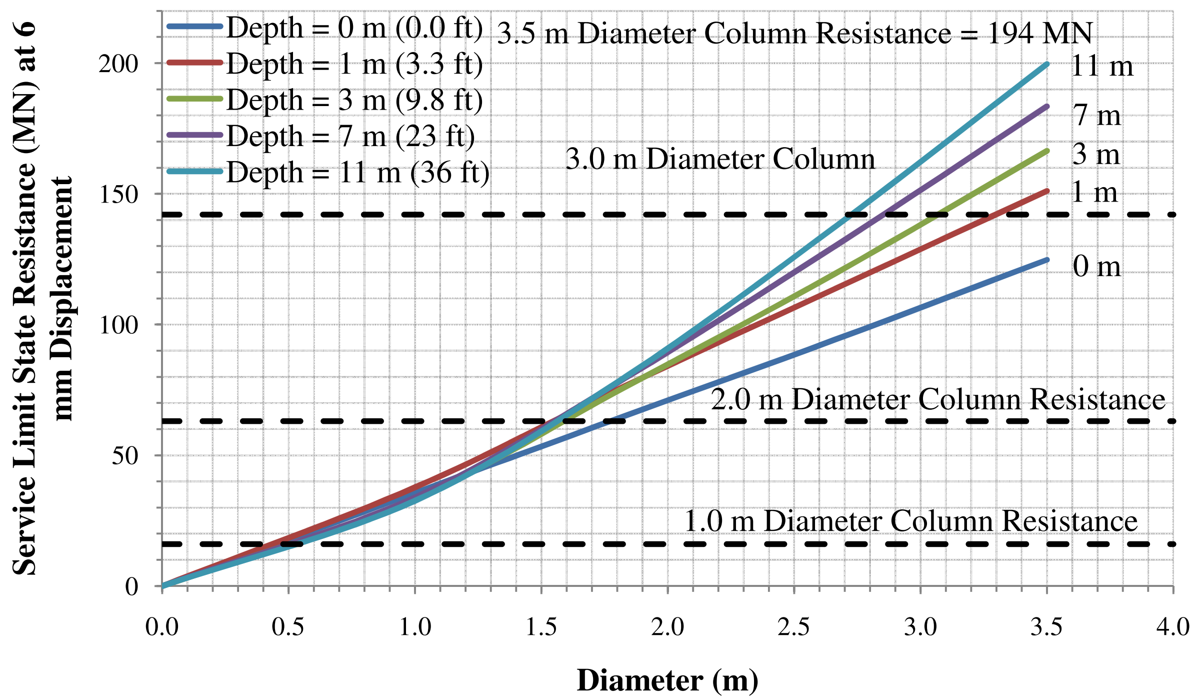

Figure C.11 Service Limit State Resistance at 6 mm (0.24 inch) Displacement for RQD = 80%

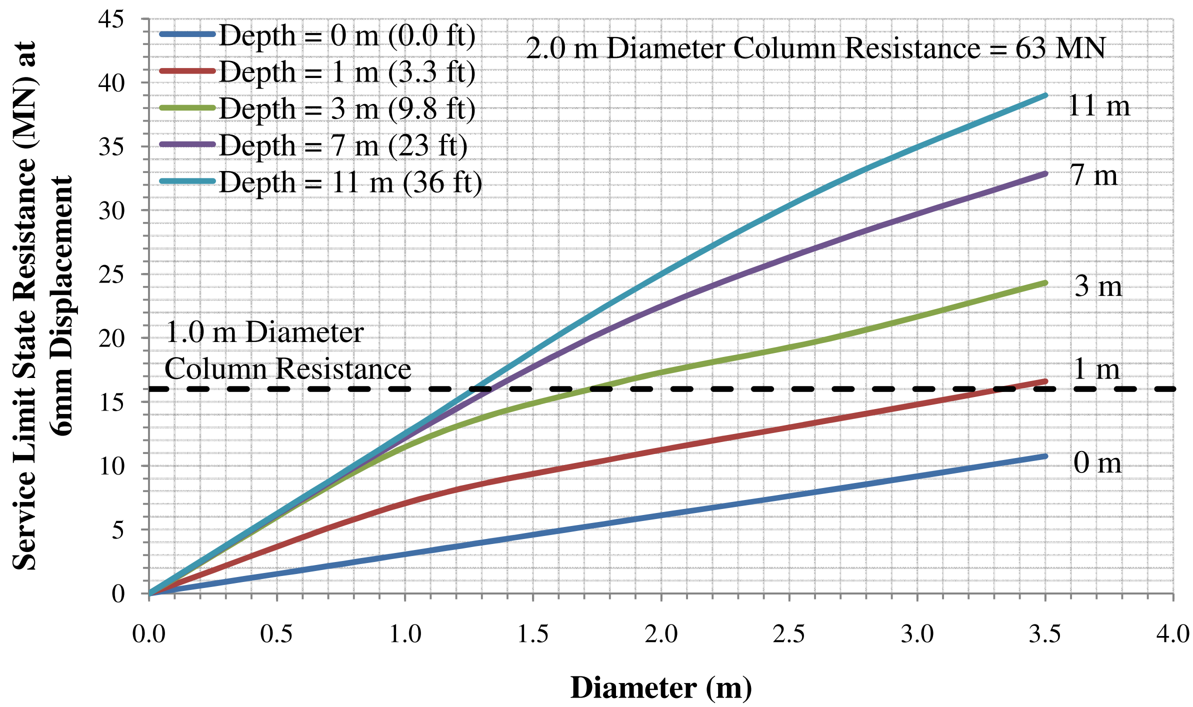

Figure C.12 Service Limit State Resistance at 6 mm (0.24 inch) Displacement for RQD = 50%

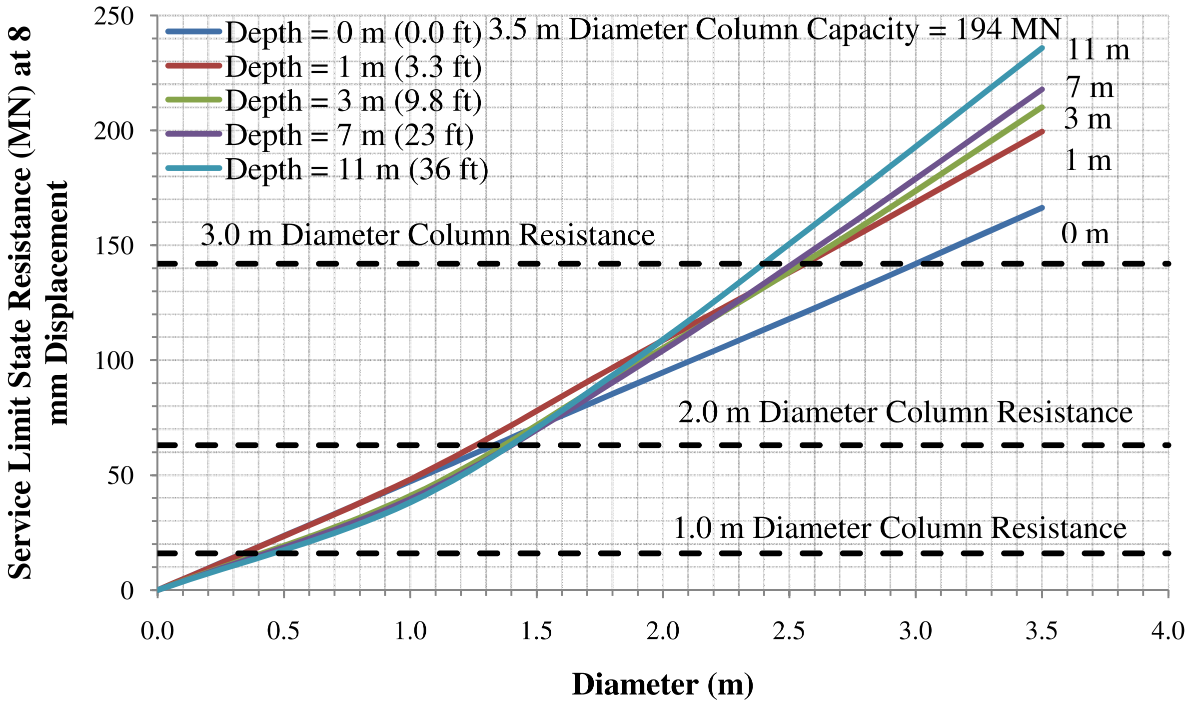

Figure C.13 Service Limit State Resistance at 8 mm (0.32 inch) Displacement for RQD = 80%

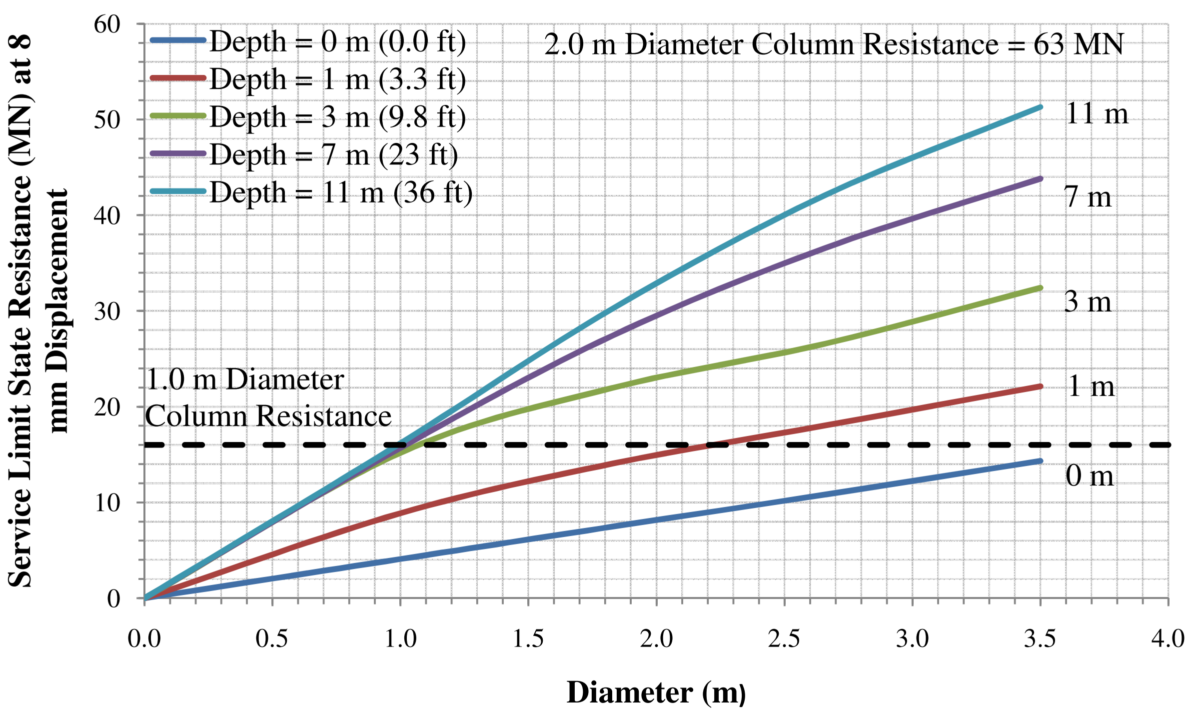

Figure C.14 Service Limit State Resistance at 8 mm (0.32 inch) Displacement for RQD = 50%

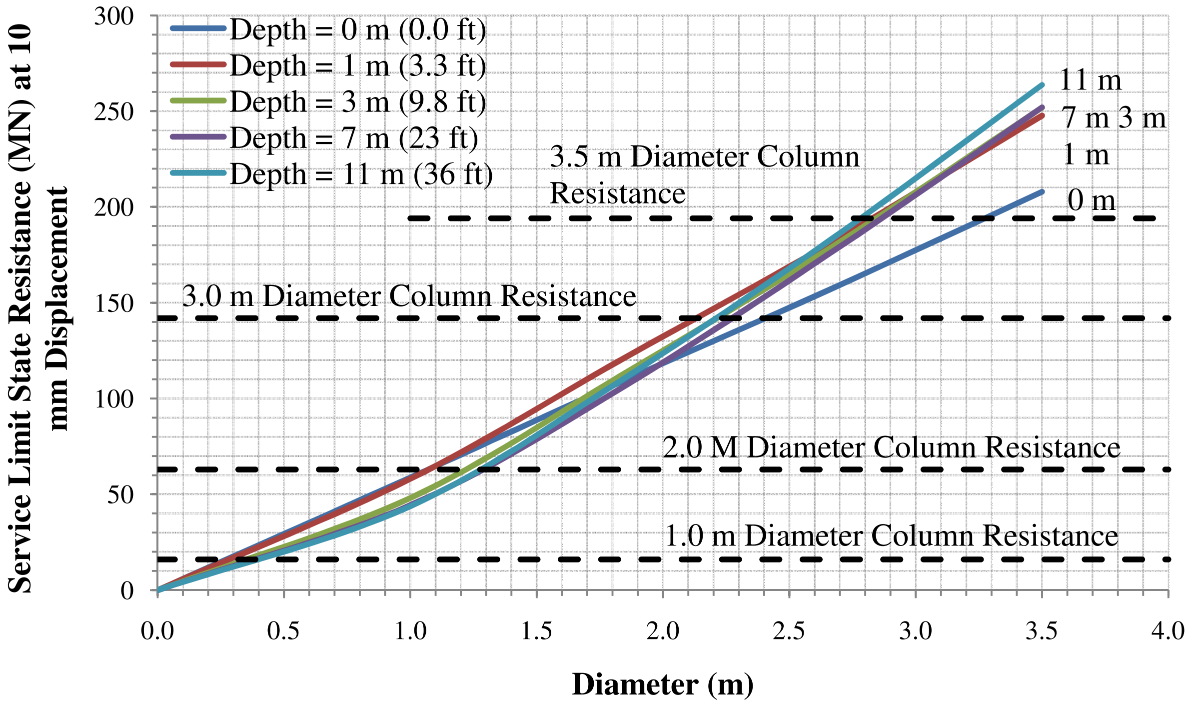

Figure C.15 Service Limit State Resistance at 10 mm (0.39 inch) Displacement for RQD = 80%

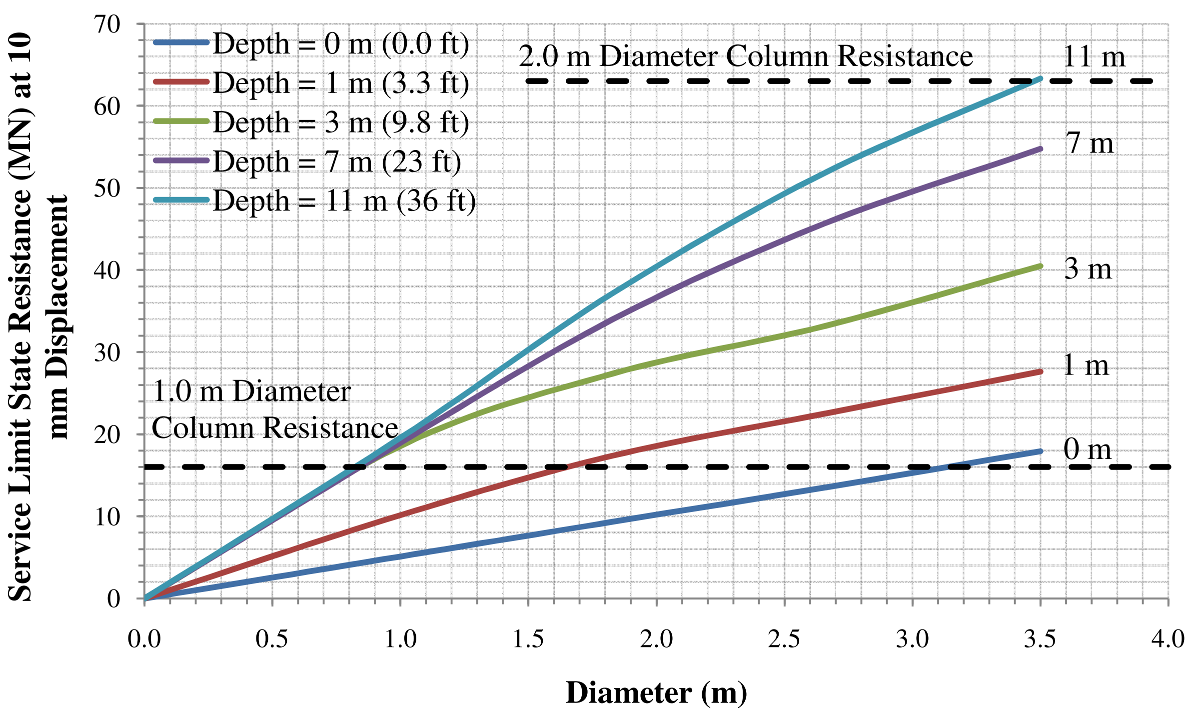

Figure C.16 Service Limit State Resistance at 10 mm (0.39 inch) Displacement for RQD = 50%

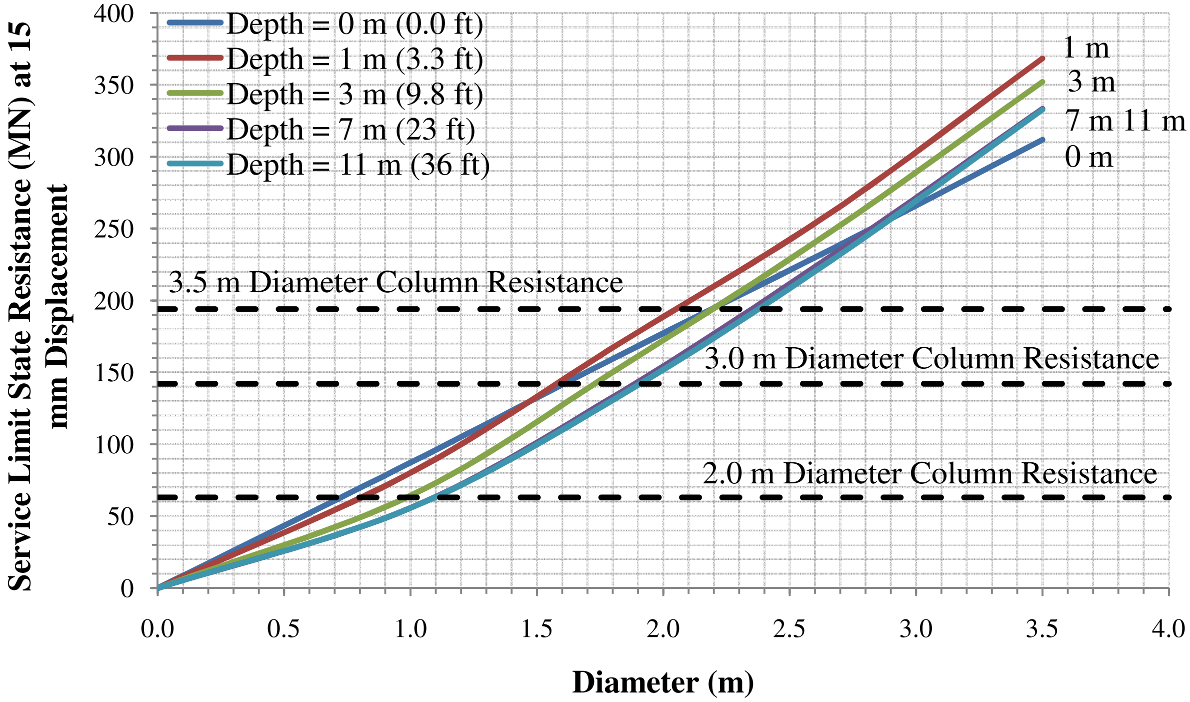

Figure C.17 Service Limit State Resistance at 15 mm (0.59 inch) Displacement for RQD = 80%

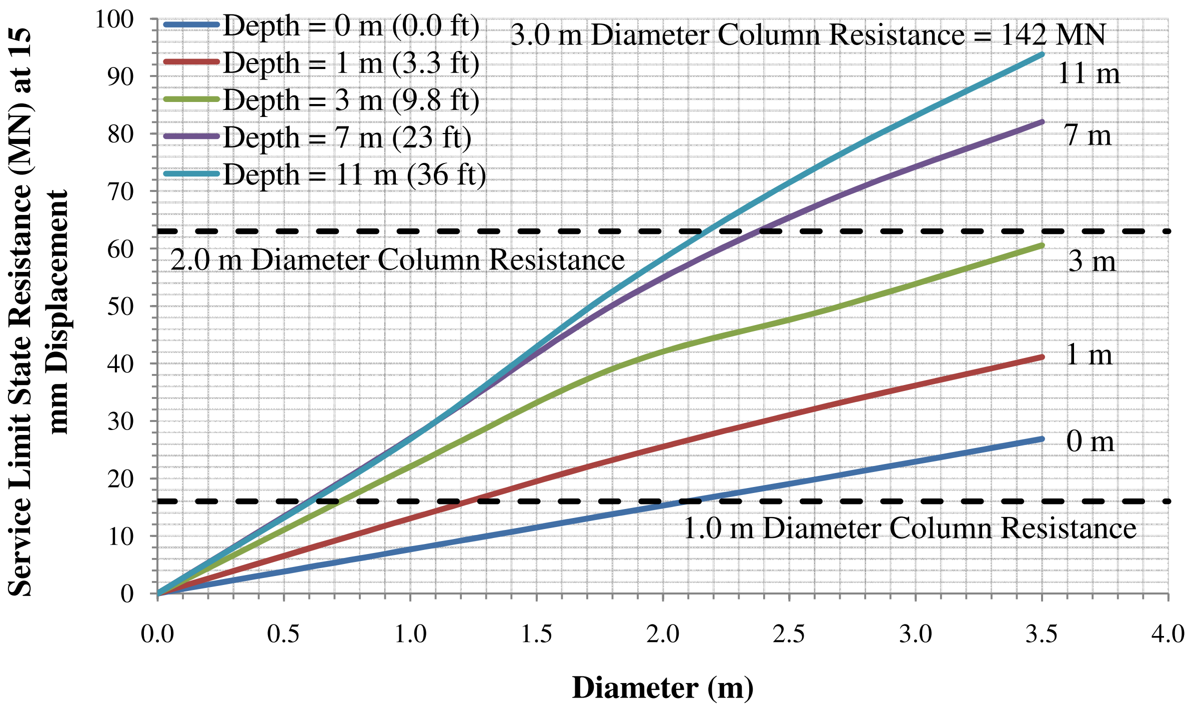

Figure C.18 Service Limit State Resistance at 15 mm (0.59 inch) Displacement for RQD = 50%

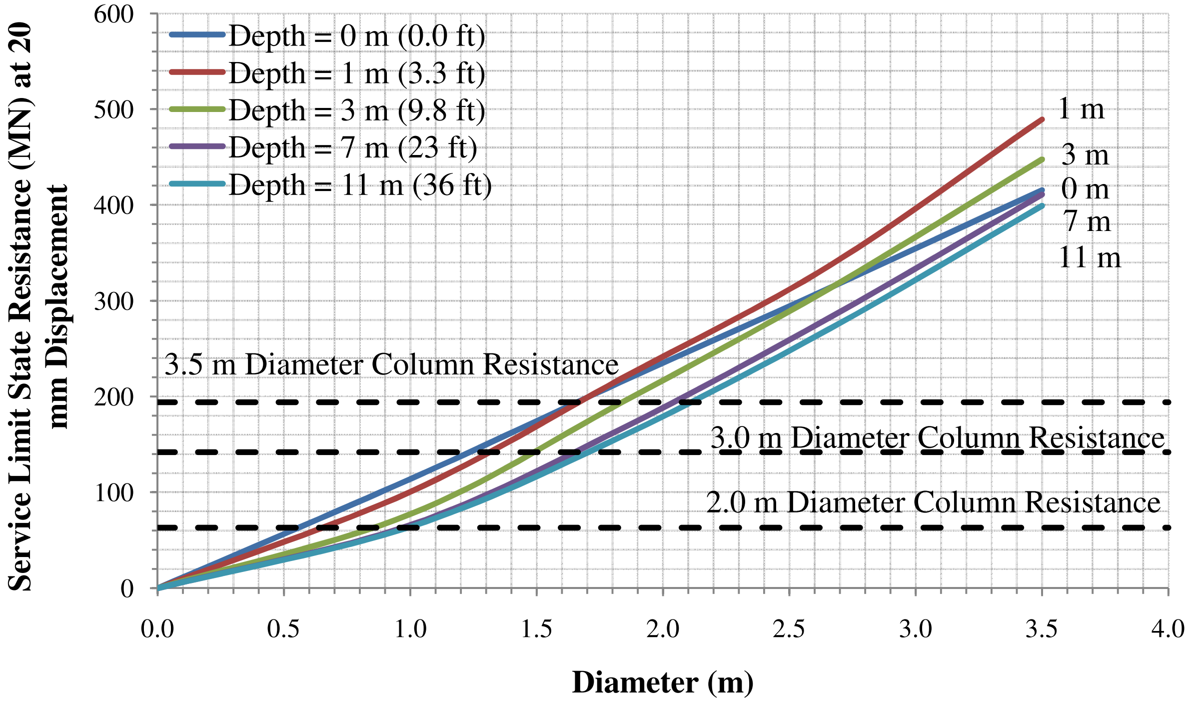

Figure C.19 Service Limit State Resistance at 20 mm (0.79 inch) Displacement for RQD = 80%

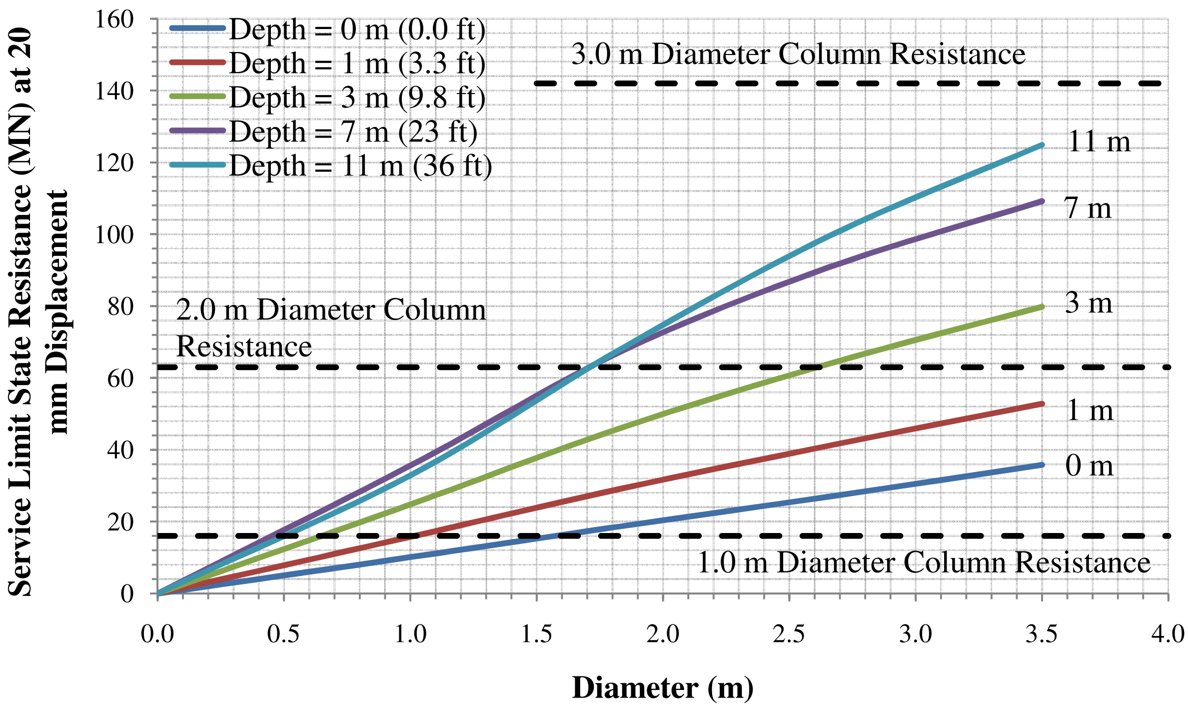

Figure C.20 Service Limit State Resistance at 20 mm (0.79 inch) Displacement for RQD = 50%

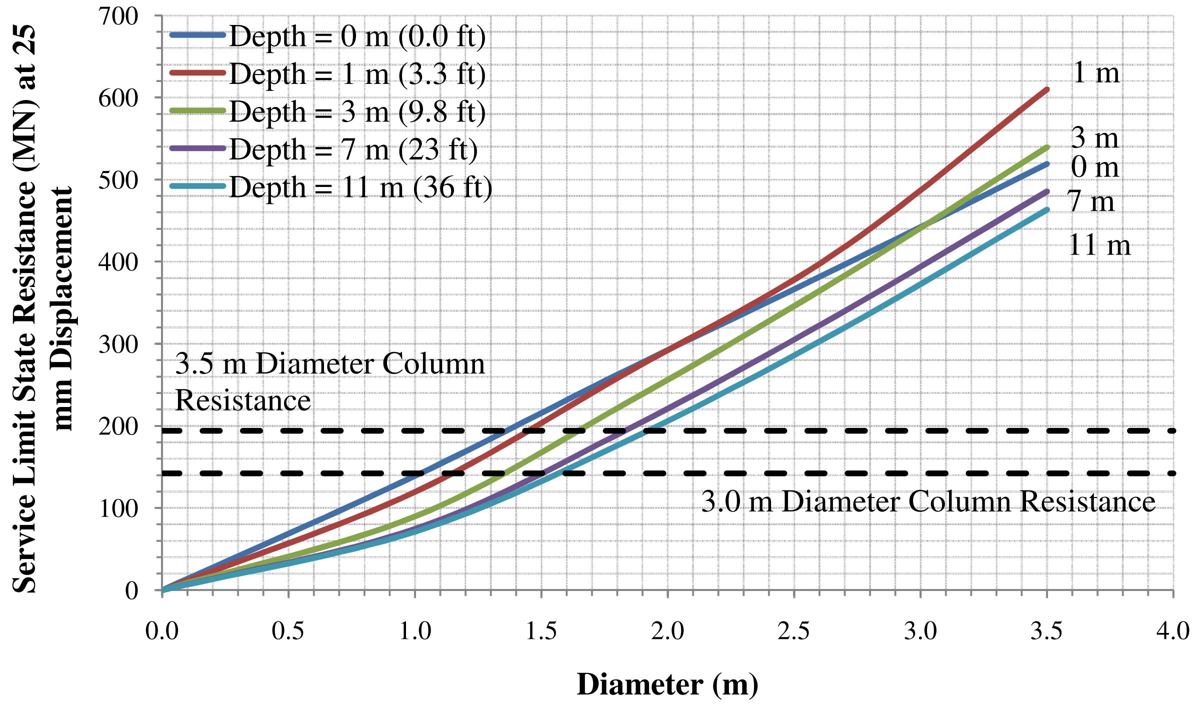

Figure C.21 Service Limit State Resistance at 25 mm (0.98 inch) Displacement for RQD = 80%

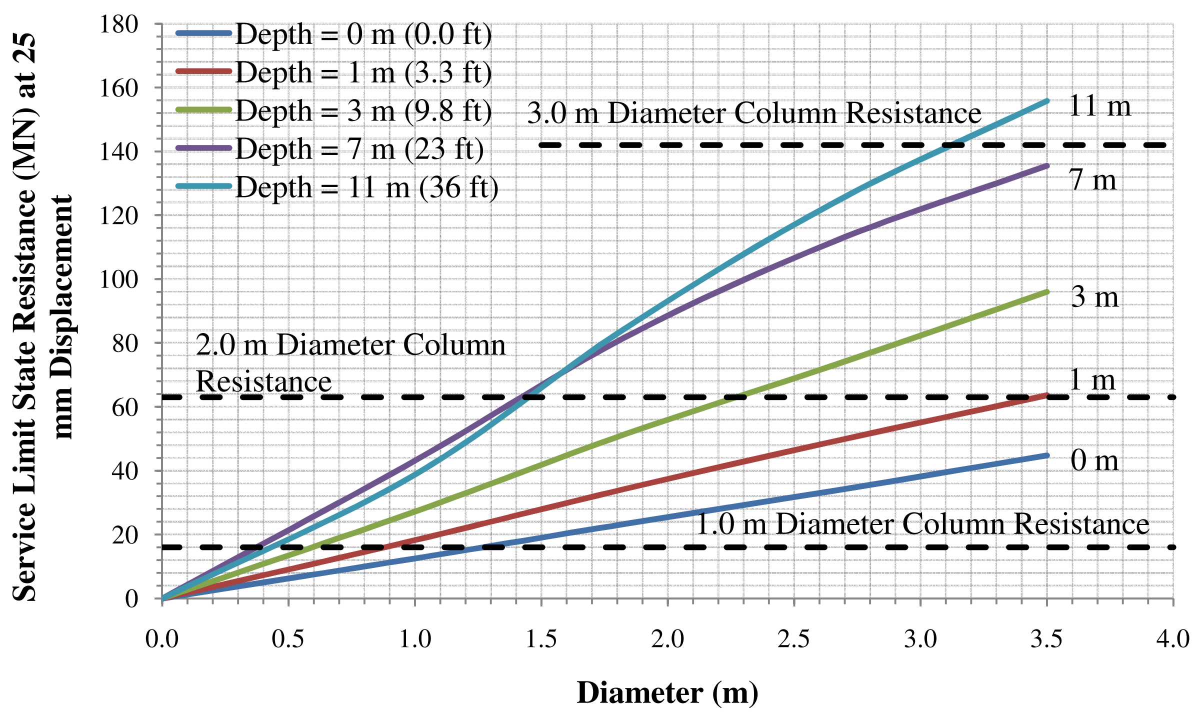

Figure C.22 Service Limit State Resistance at 25 mm (0.98 inch) Displacement for RQD = 50%

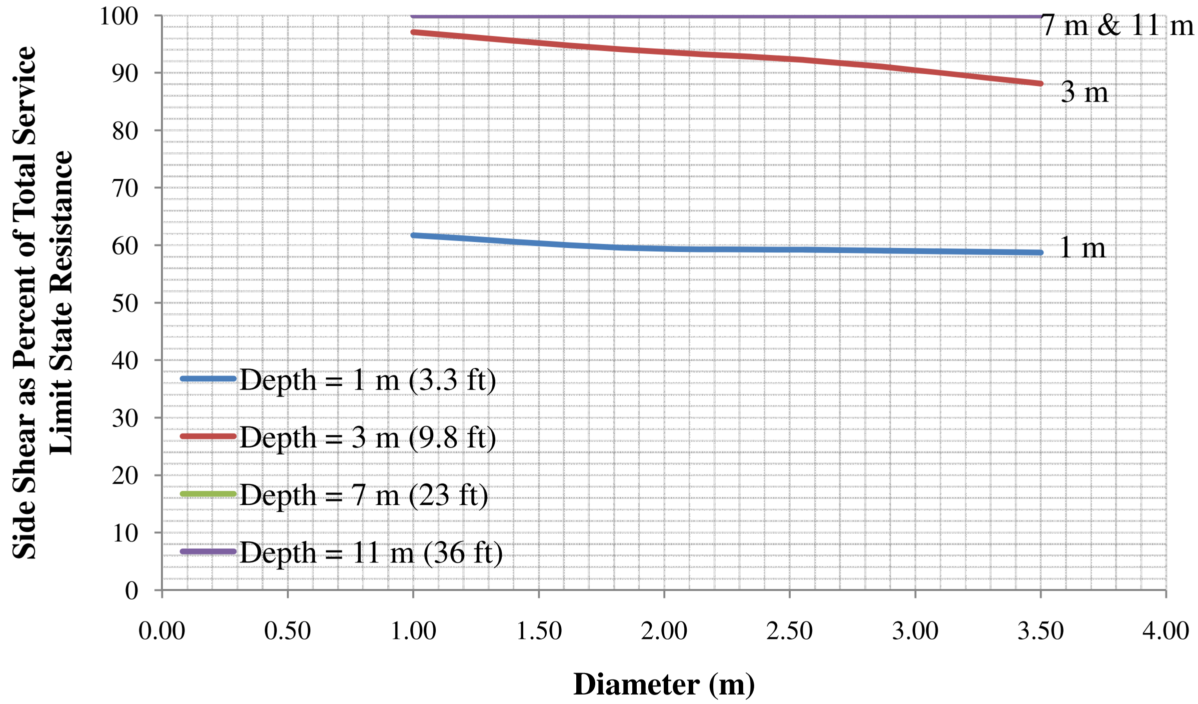

Figure C.23 Percent Side Shear at 1 mm (0.04 inch) Top of Shaft Displacement RQD = 80%

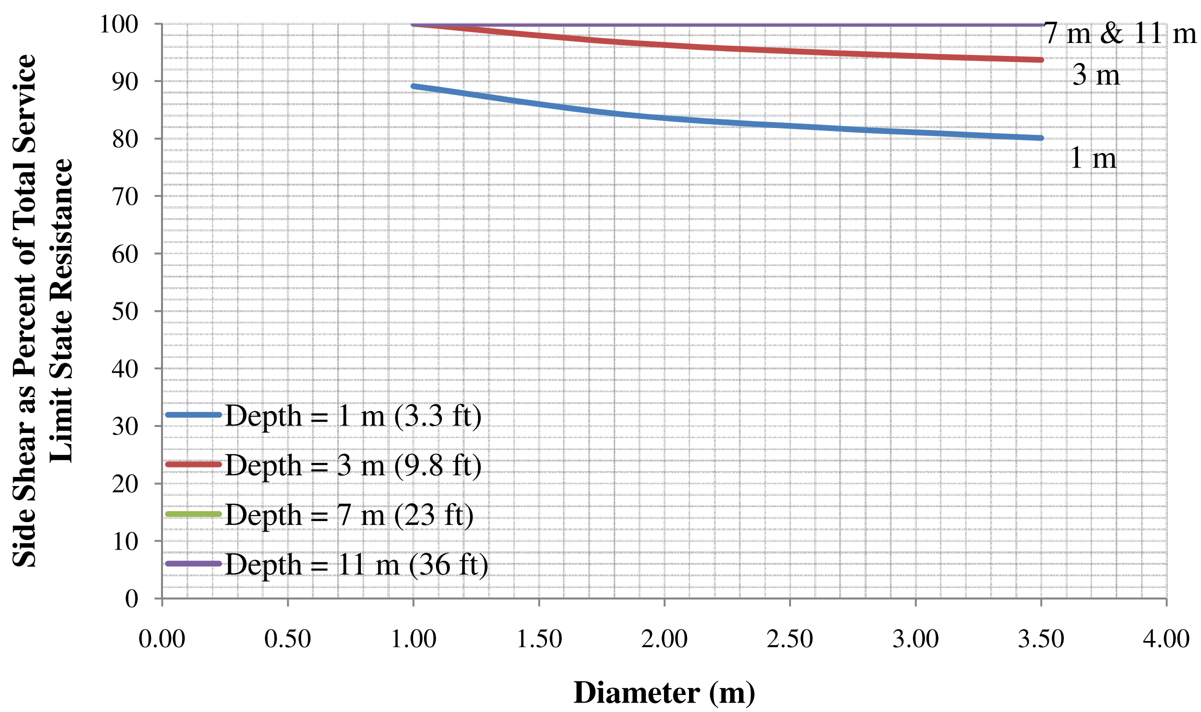

Figure C.24 Percent Side Shear at 1 mm (0.04 inch) Top of Shaft Displacement RQD = 50%

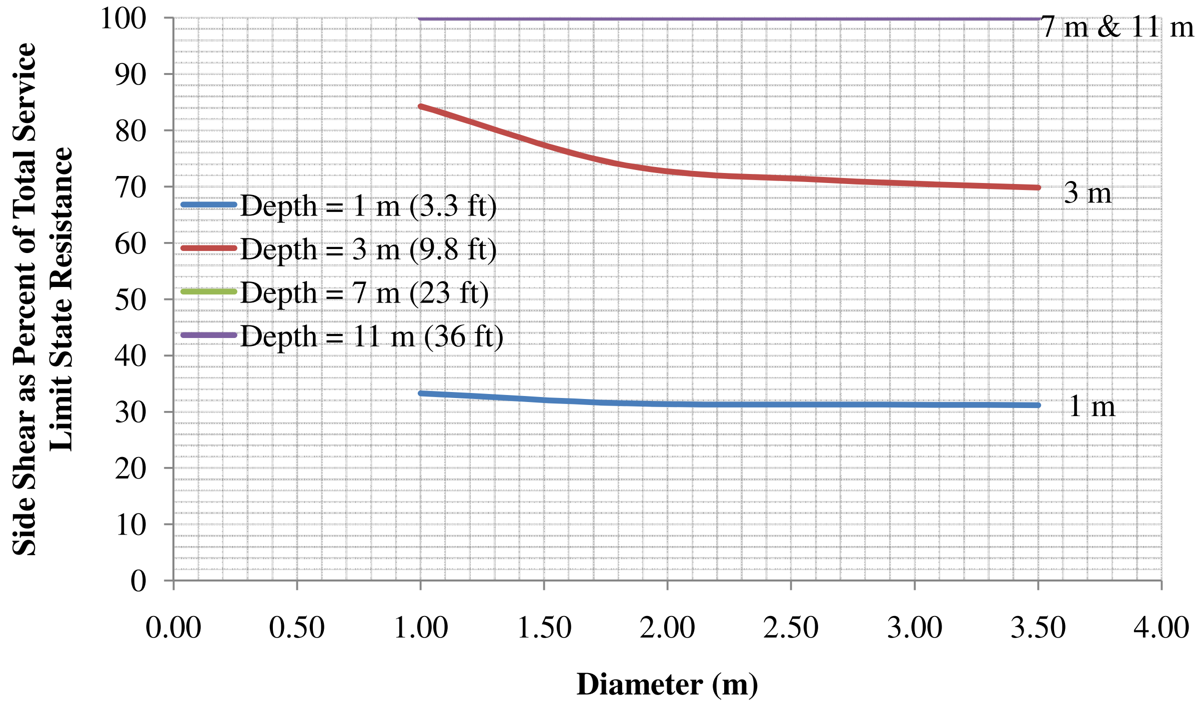

Figure C.25 Percent Side Shear at 2 mm (0.08 inch) Top of Shaft Displacement RQD = 80%

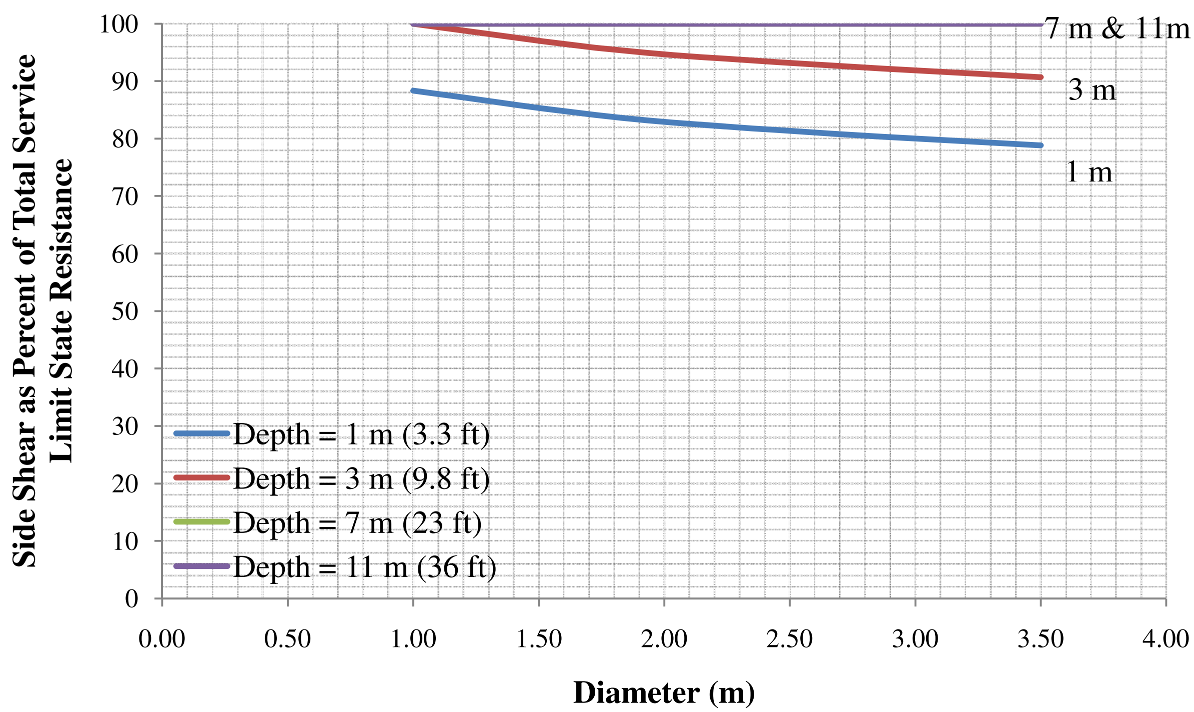

Figure C.26 Percent Side Shear at 2 mm (0.08 inch) Top of Shaft Displacement RQD = 50%

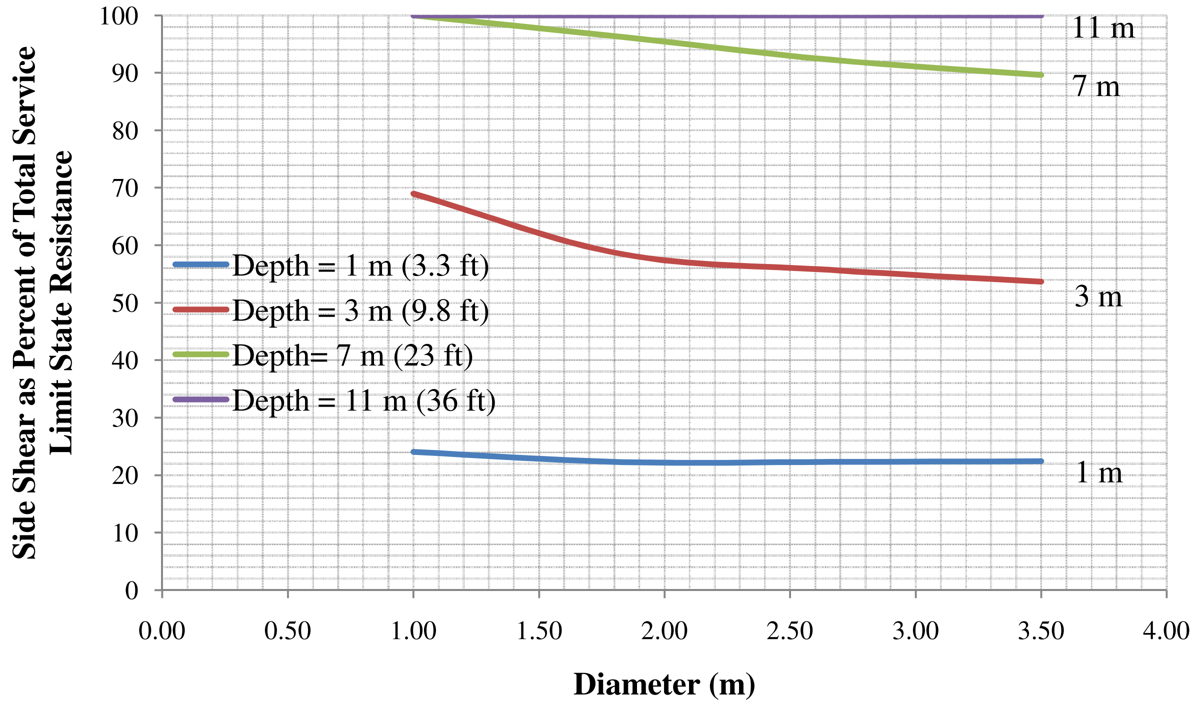

Figure C.27 Percent Side Shear at 3 mm (0.12 inch) Top of Shaft Displacement RQD = 80%

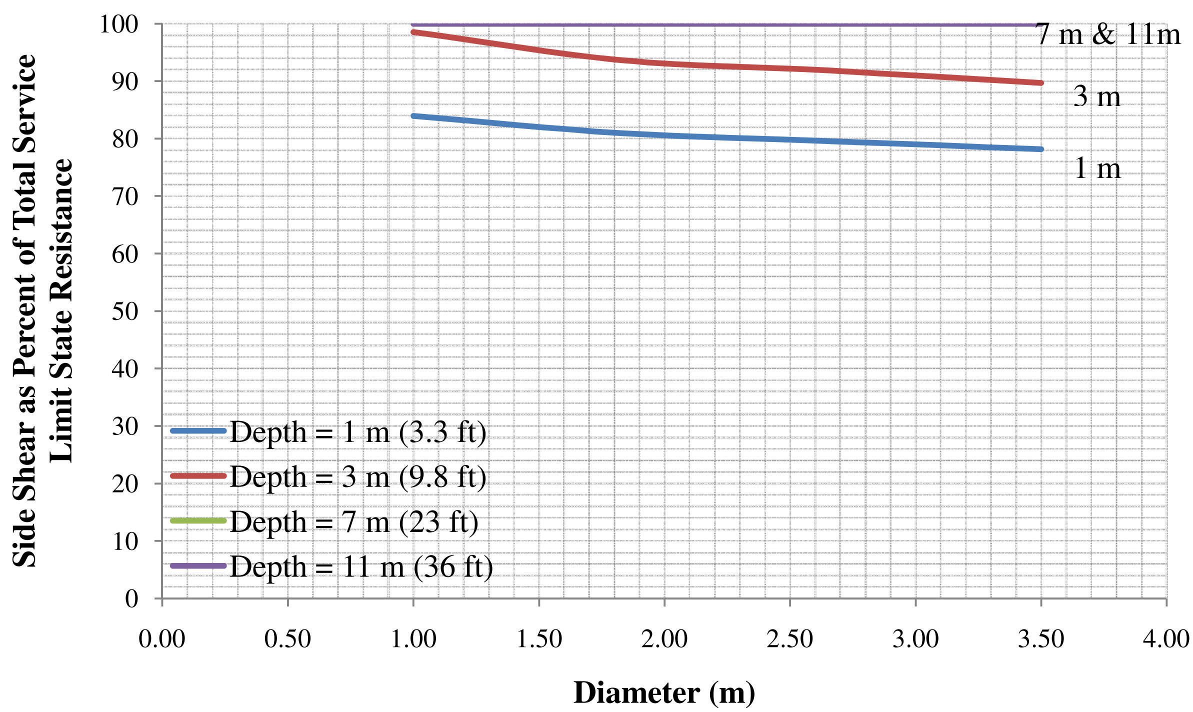

Figure C.28 Percent Side Shear at 3 mm (0.12 inch) Top of Shaft Displacement RQD = 50%

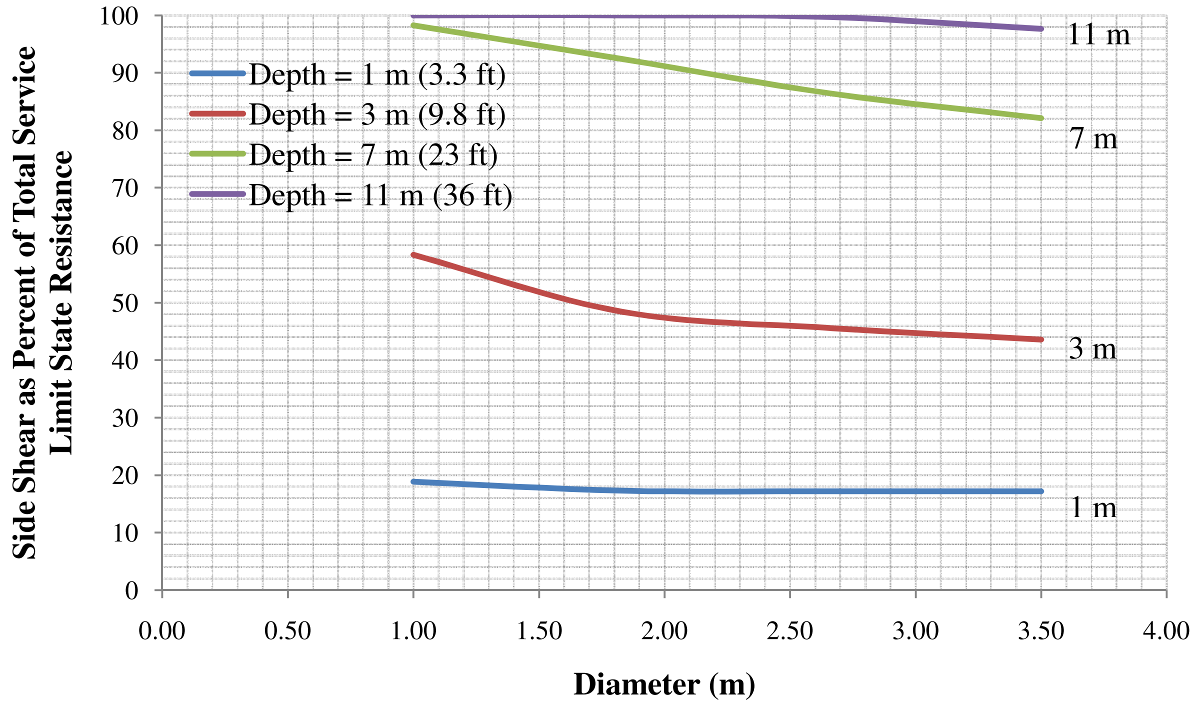

Figure C.29 Percent Side Shear at 4 mm (0.16 inch) Top of Shaft Displacement RQD = 80%

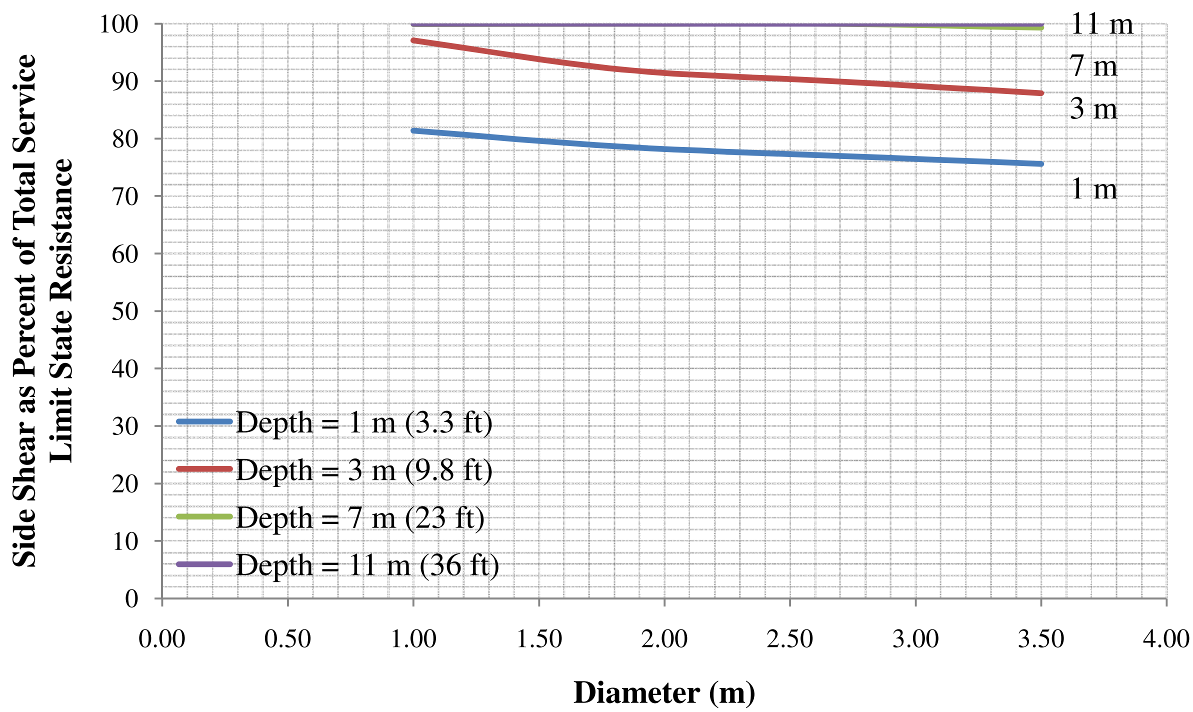

Figure C.30 Percent Side Shear at 4 mm (0.16 inch) Top of Shaft Displacement RQD = 50%

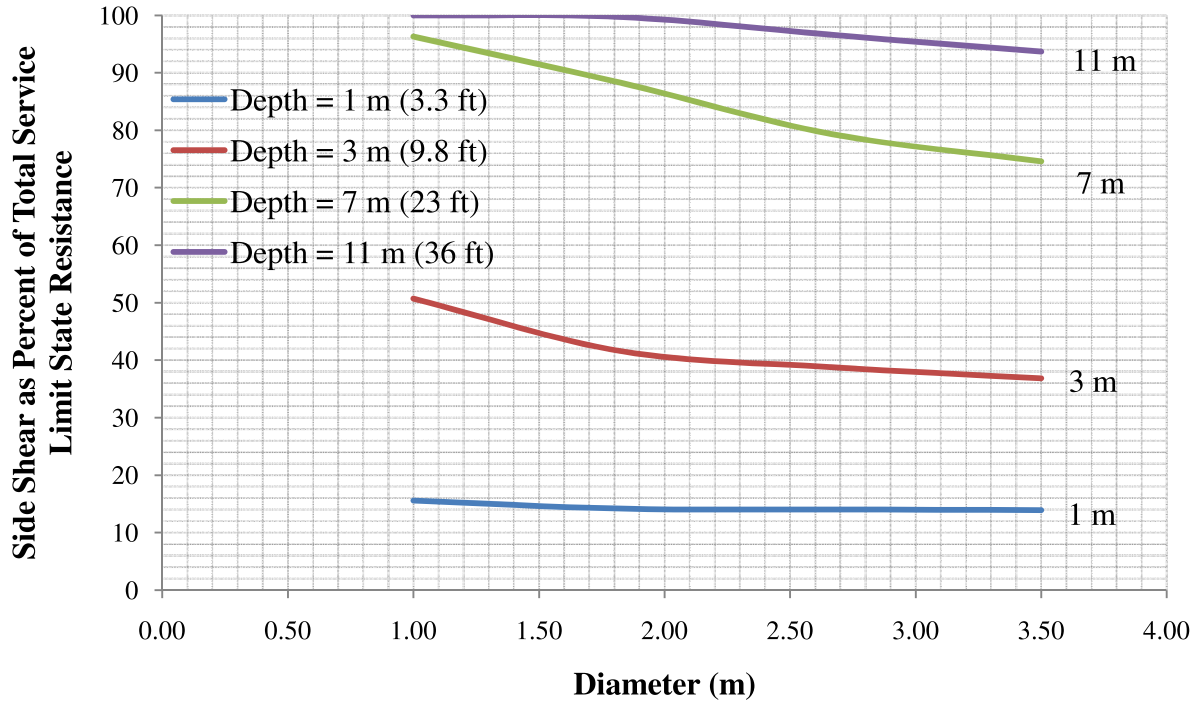

Figure C.31 Percent Side Shear at 5 mm (0.20 inch) Top of Shaft Displacement RQD = 80%

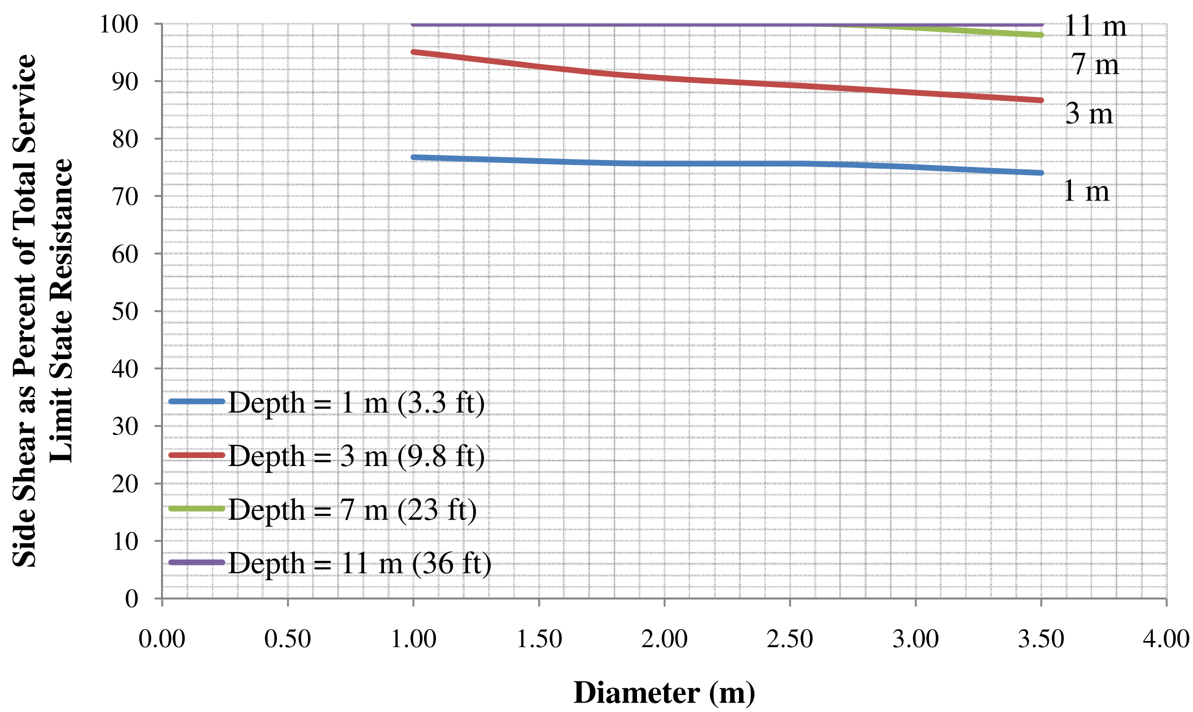

Figure C.32 Percent Side Shear at 5 mm (0.20 inch) Top of Shaft Displacement RQD = 50%

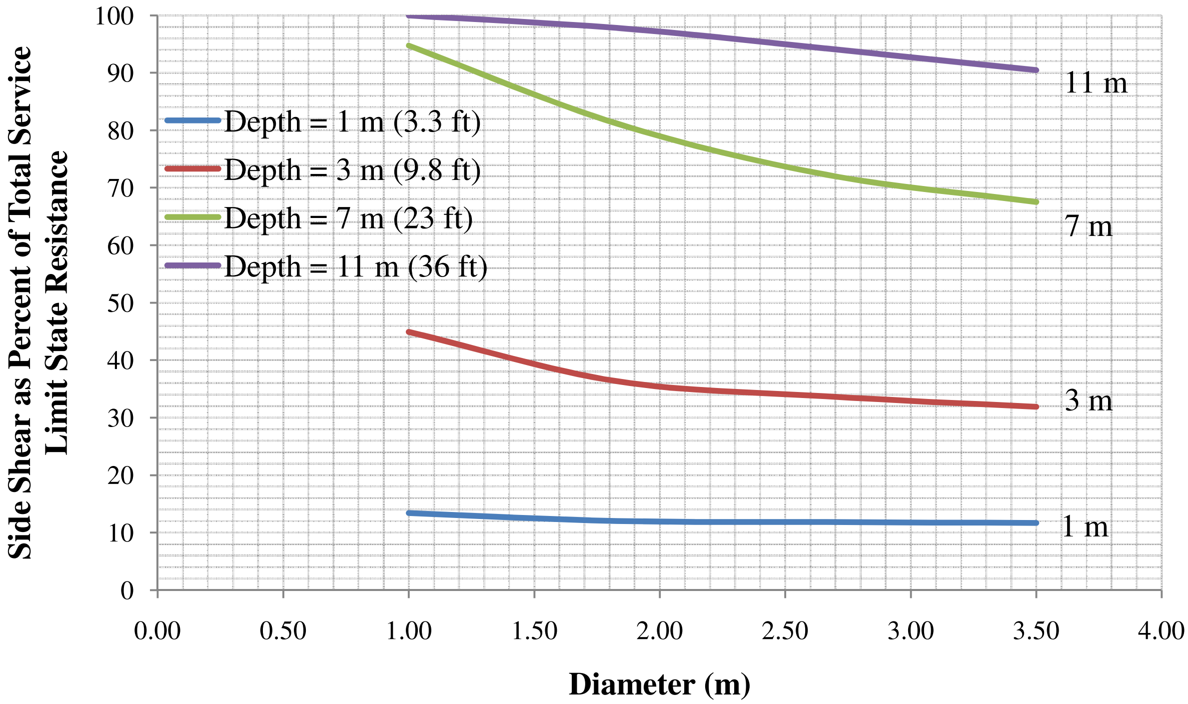

Figure C.33 Percent Side Shear at 6 mm (0.24 inch) Top of Shaft Displacement RQD = 80%

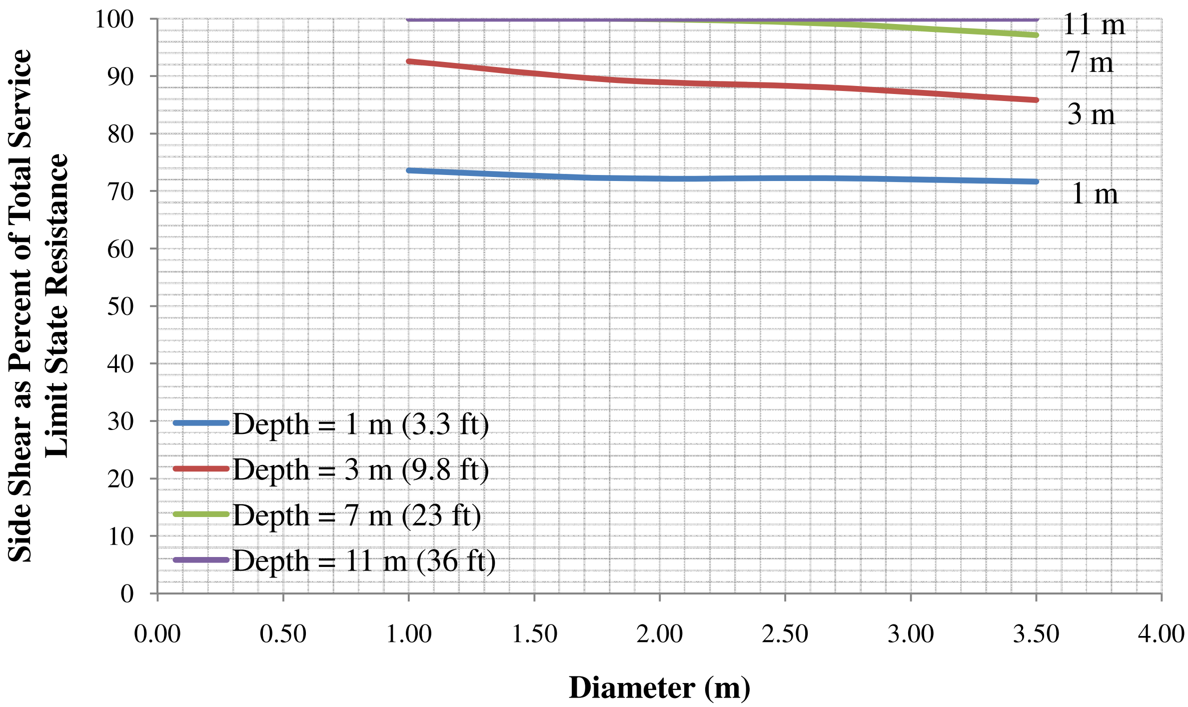

Figure C.34 Percent Side Shear at 6 mm (0.24 inch) Top of Shaft Displacement RQD = 50%

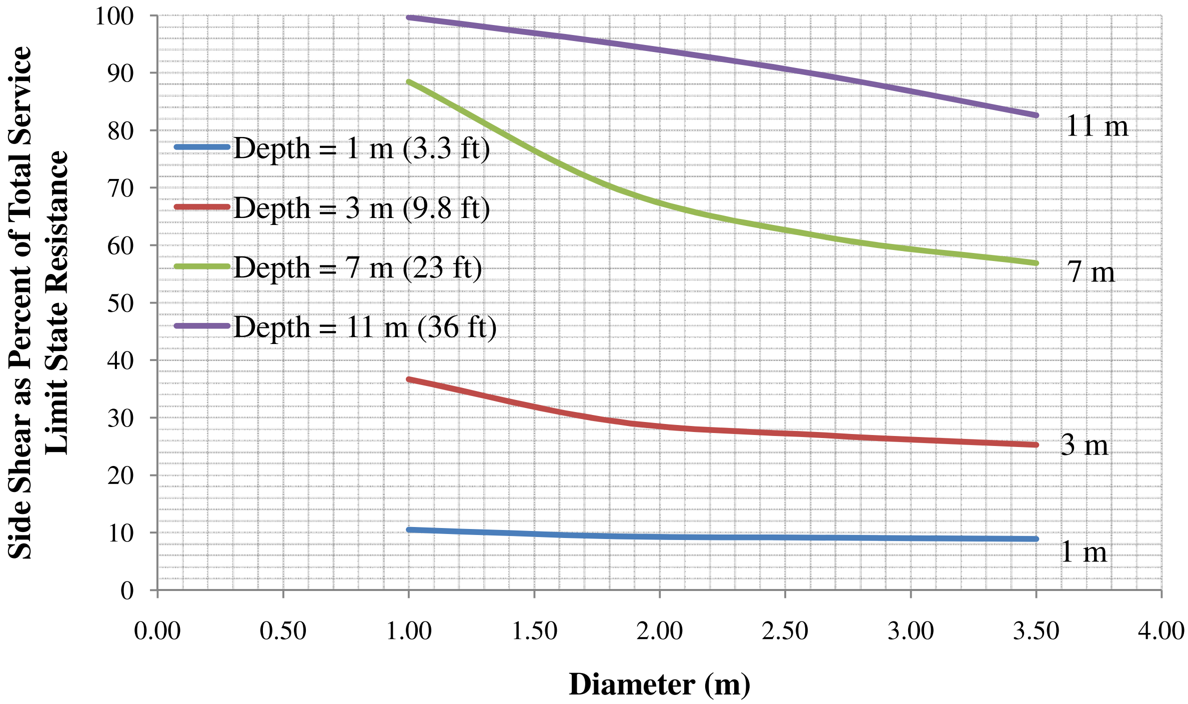

Figure C.35 Percent Side Shear at 8 mm (0.32 inch) Top of Shaft Displacement RQD = 80%

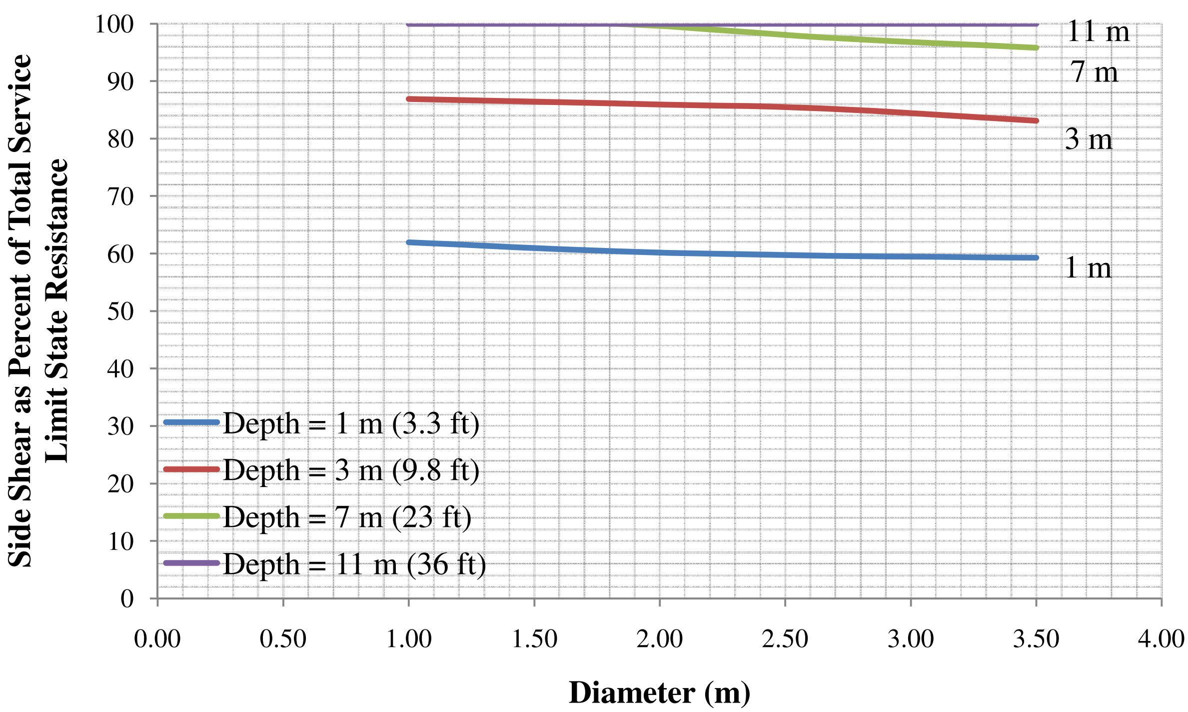

Figure C.36 Percent Side Shear at 8 mm (0.32 inch) Top of Shaft Displacement RQD = 50%

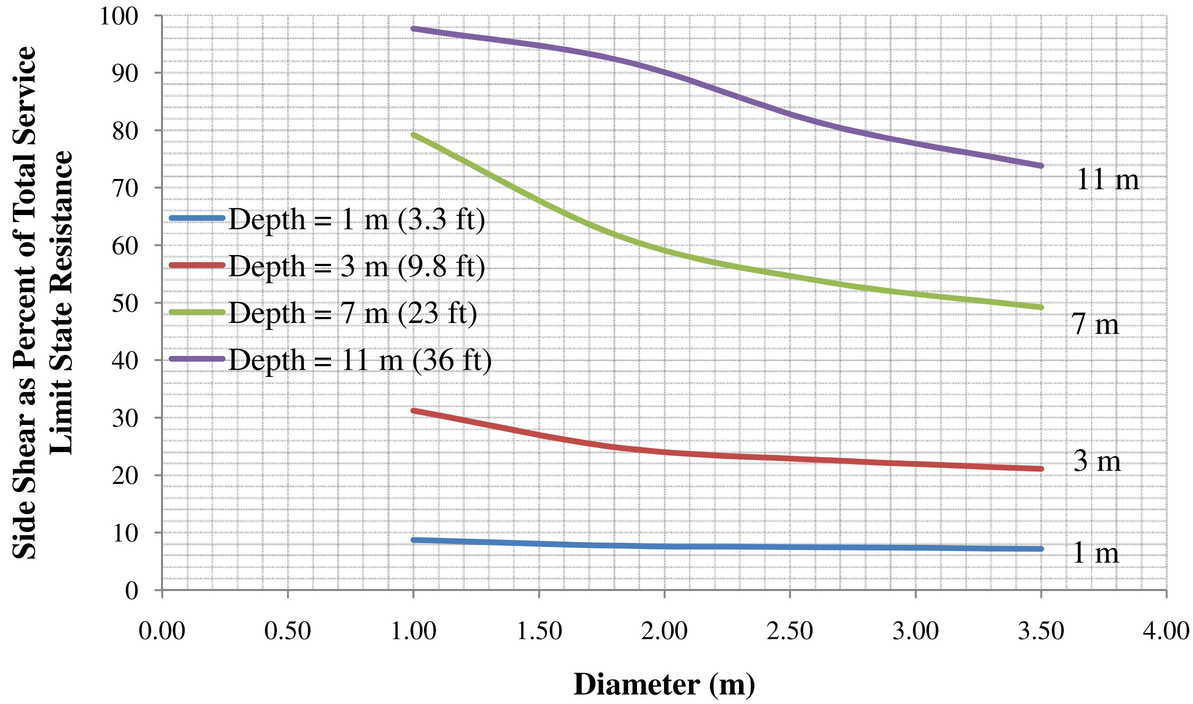

Figure C.37 Percent Side Shear at 10 mm (0.39 inch) Top of Shaft Displacement RQD = 80%

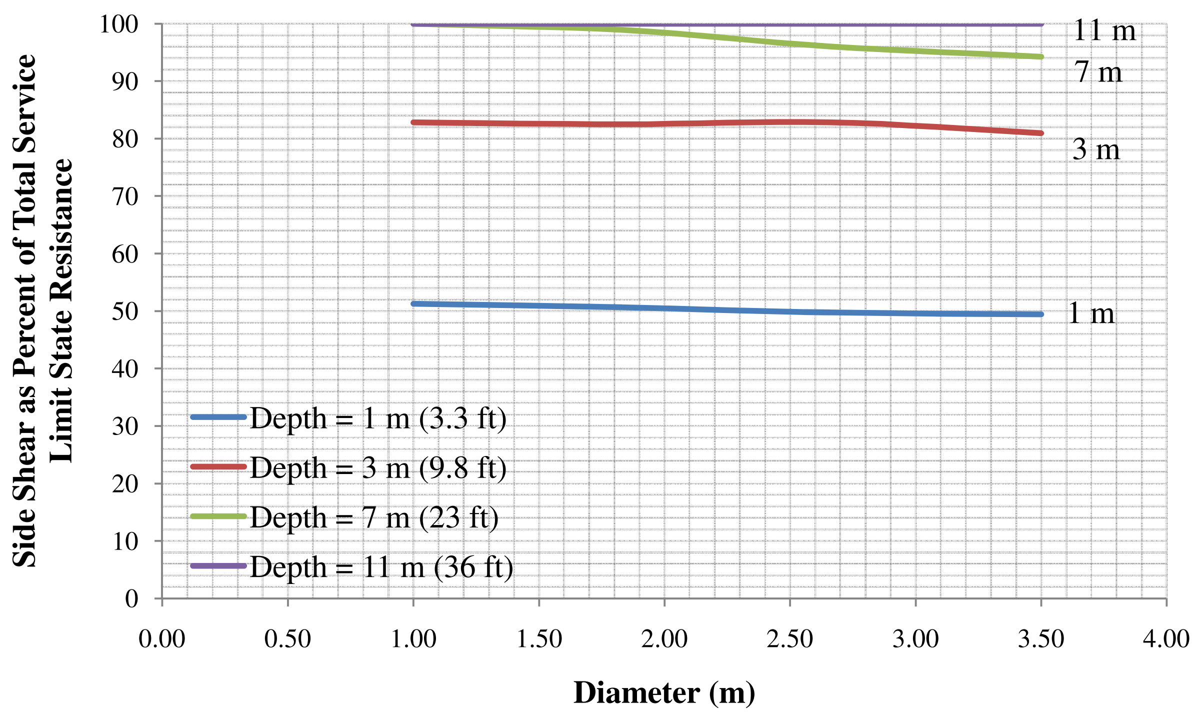

Figure C.38 Percent Side Shear at 10 mm (0.39 inch) Top of Shaft Displacement RQD = 50%

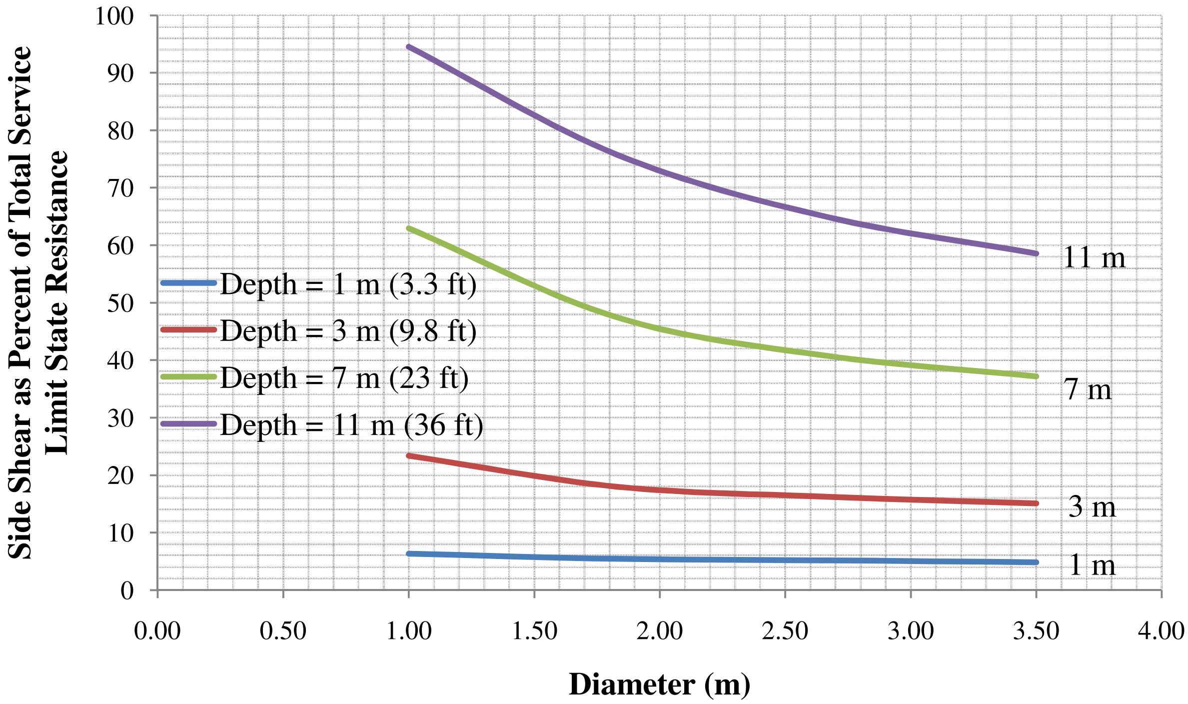

Figure C.39 Percent Side Shear at 15 mm (0.59 inch) Top of Shaft Displacement RQD = 80%

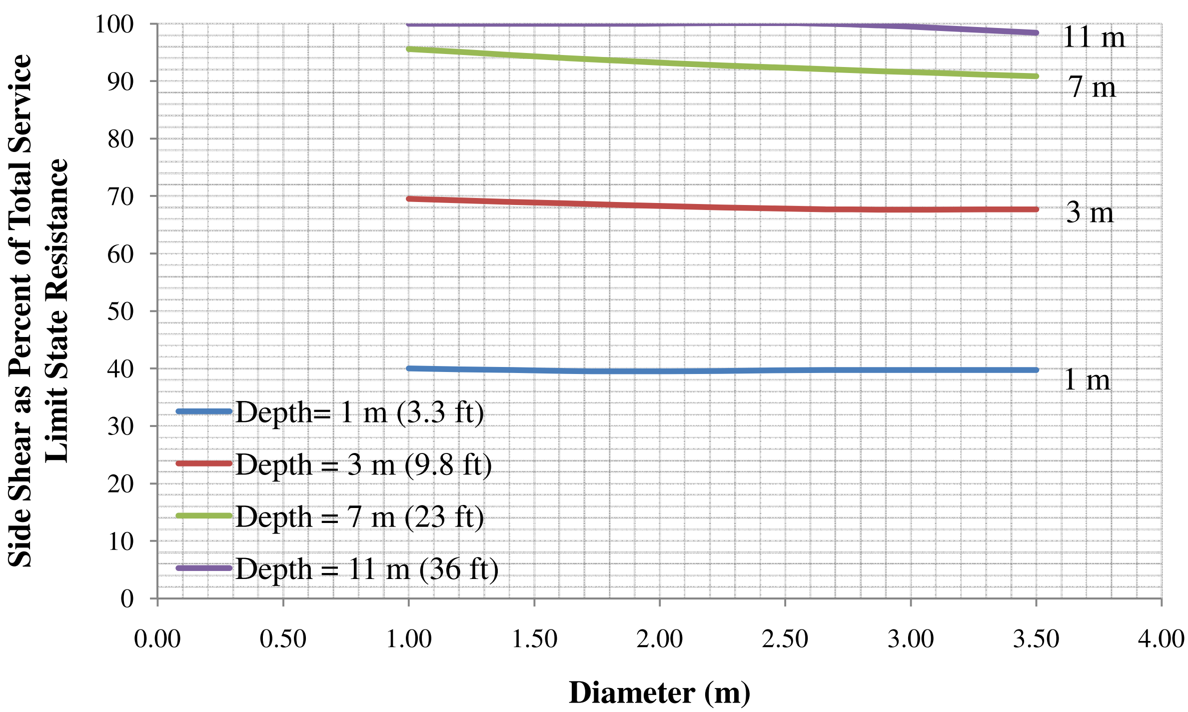

Figure C.40 Percent Side Shear at 15 mm (0.59 inch) Top of Shaft Displacement RQD = 50%

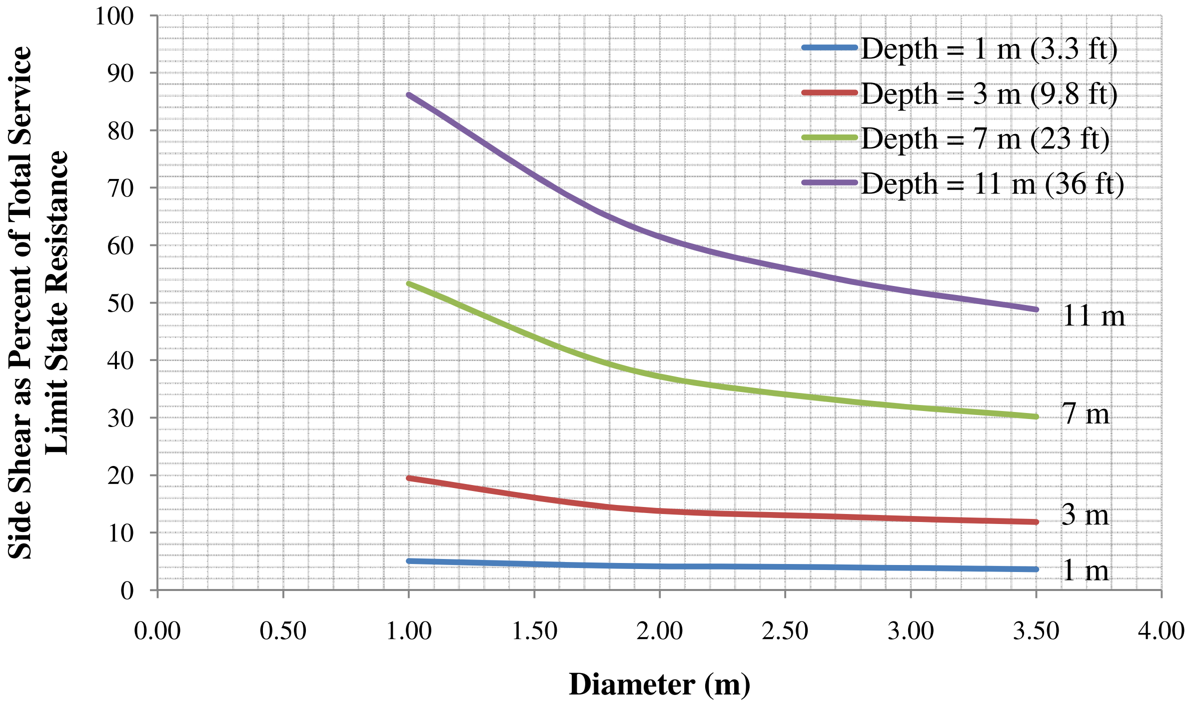

Figure C.41 Percent Side Shear at 20 mm (0.79 inch) Top of Shaft Displacement RQD = 80%

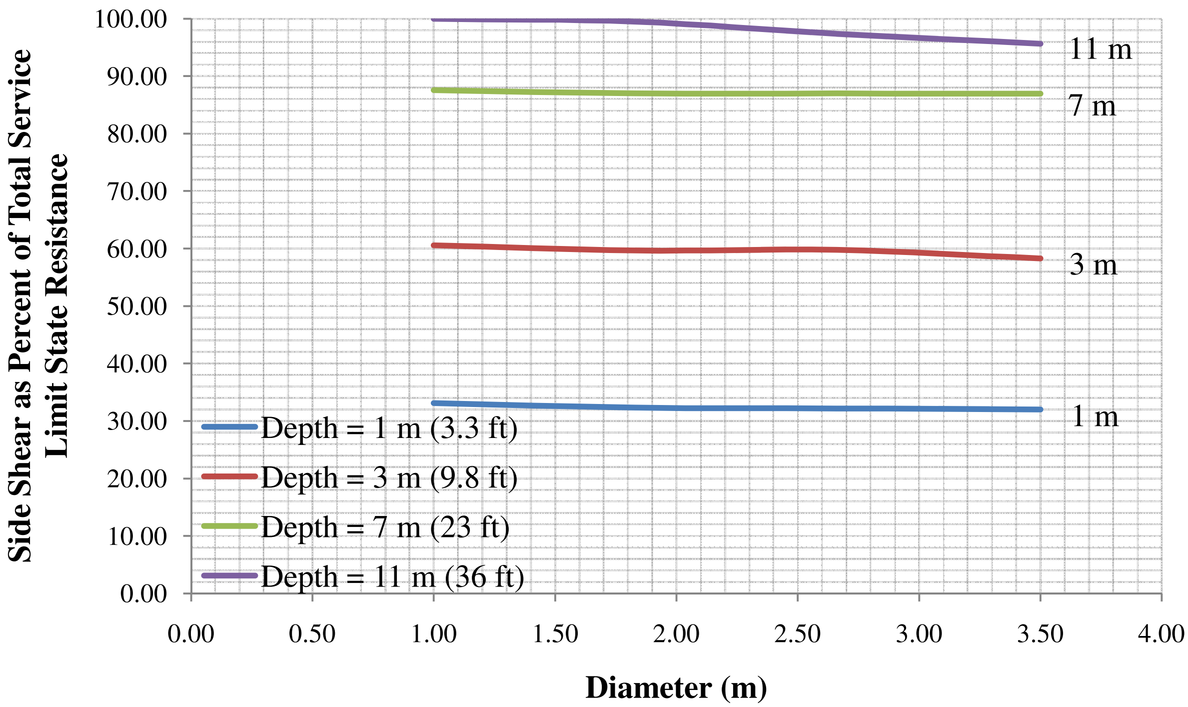

Figure C.42 Percent Side Shear at 20 mm (0.79 inch) Top of Shaft Displacement RQD = 50%

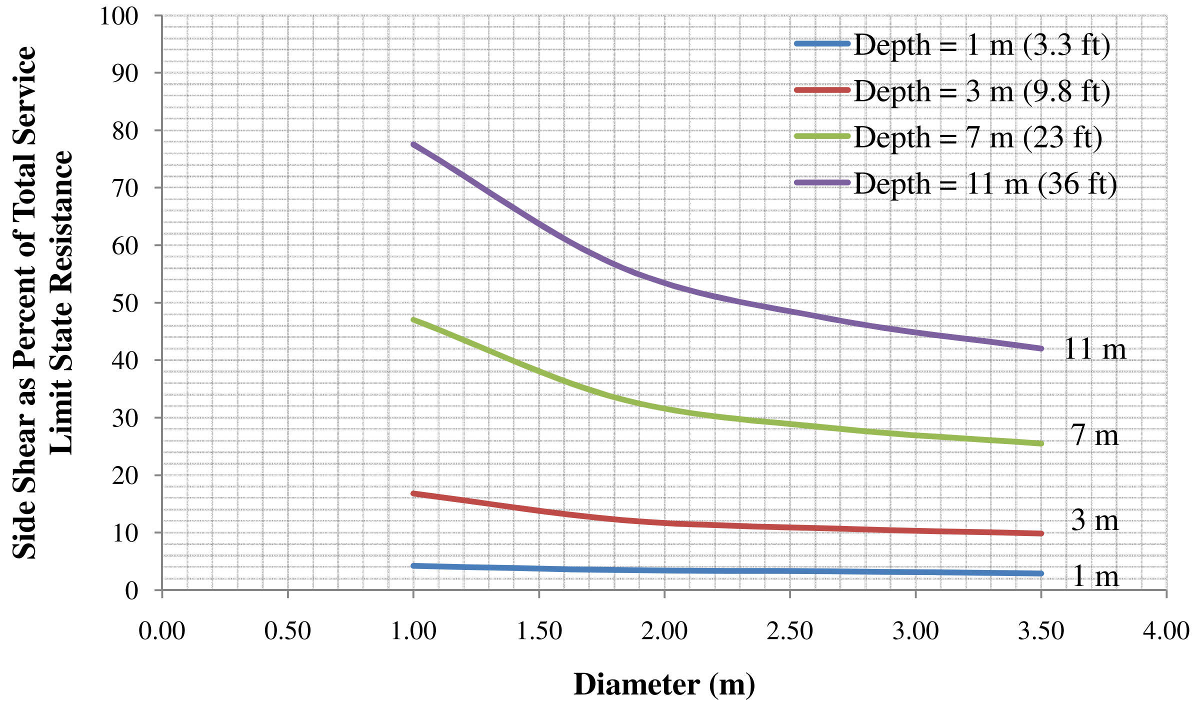

Figure C.43 Percent Side Shear at 25 mm (0.98 inch) Top of Shaft Displacement RQD = 80%

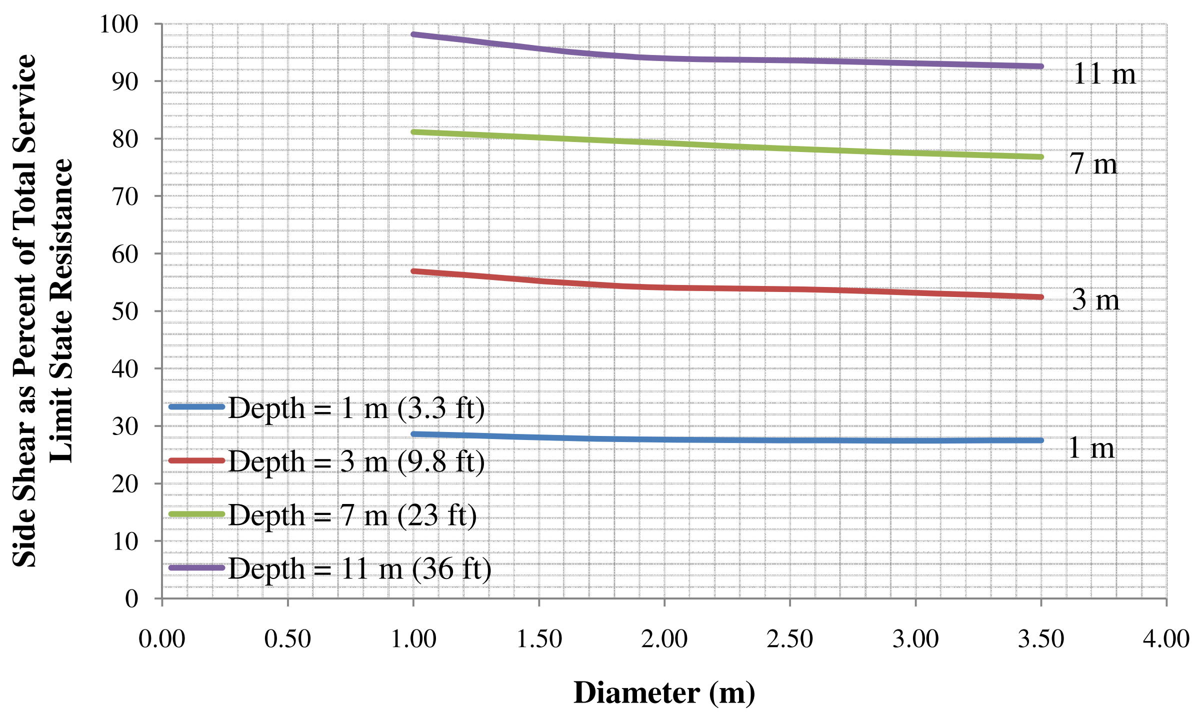

Figure C.44 Percent Side Shear at 25 mm (0.98 inch) Top of Shaft Displacement RQD = 50%